Defence Research and Development Canada
Recherche et développement pour la défense Canada

DRDC | RDDC
technologyscienceetechnologie

Analysis of planar array of 64 monopoles for over-the-horizon radar

Manifold calculations and null-steering performance study

Simon Henault
DRDC – Ottawa Research Centre

Defence Research and Development Canada
Scientific Report
DRDC-RDDC-2018-R233
January 2019

Canada

IMPORTANT INFORMATIVE STATEMENTS

Abstract

The particular challenges of a 64 planar monopole antenna array used in an over-the-horizon radar (OTHR) and error mechanisms leading to auroral clutter suppression deterioration are evaluated. A comprehensive methodology is presented to calculate the array manifold for arbitrary azimuth, elevation and polarization. The calculated manifold is then available to calibrate the experimental array, and is used in this report to analyze null-steering performance for different ground types and signal scenarios. Clutter rejections exceeding 40 dB are found to be possible in transmission at all frequencies, and increase with frequency, but require a highly accurate manifold. The manifold and performance are found to be very sensitive to ground properties, and techniques are proposed to mitigate the impact of manifold uncertainties. Adaptive array processing is also considered with an emphasis on the presence and strength of the target signal in the training data as well as correlation between the target signal and auroral clutter. Practical considerations relative to power handling and nonlinear effects in high power amplifiers are studied.

Significance for defence and security

The OTHR research program evaluates possibilities for expanding Arctic surveillance to areas beyond current capabilities, and perhaps replace some of the existing line-of-sight radar capabilities in the Arctic. The outcome of this research is highly dependent on the way experimental systems are designed and operated. A significant challenge for OTHR at higher latitudes is the auroral clutter, which we attempt to reject in this report using null-steering techniques. Particular attention to electromagnetic interactions between antennas and the ground is required, otherwise auroral clutter rejection can fail and the conclusions of the research program may be incorrect. This report is a preliminary step to ensure that the best research results are ultimately obtained.

Résumé

Les défis particuliers d'un réseau d'antennes de 64 monopoles utilisé dans un radar trans-horizon (OTHR) et les mécanismes d'erreur entraînant une détérioration de la suppression du fouillis auroral sont évalués. Une méthodologie complète est présentée pour calculer les diagrammes de rayonnement pour des azimuth, élevation et polarisation arbitraires. Les diagrammes calculés sont ensuite disponibles pour calibrer le réseau expérimental, et sont utilisés dans ce rapport pour analyser la performance dans la formation de nuls pour différents types de sol et scénarios de signaux. Des rejets du fouillis excédant 40 dB sont déterminés être possibles, et augmente avec la fréquence, mais nécessitent des diagrammes de rayonnement très précis. Les diagrammes et la performance sont très sensibles aux propriétes du sol, et des techniques sont proposées pour réduire les impacts de l'incertitude au sujet des diagrammes de rayonnement. Le traitement réseau adaptatif est aussi considéré avec une attention particulière à la présence et l'amplitude du signal de la cible dans les données d'entraînement, ainsi que la corrélation entre le signal de la cible et le fouillis auroral. Des considérations pratiques relatives à la gestion de la puissance et aux effets non linéaires des amplificateurs à haute puissance sont étudiées.

Importance pour la défense et la sécurité

Le programme de recherche OTHR évalue les possibilités d'étendre la surveillance de l'Arctique au-delà des capacités existantes, et peut-être de remplacer certains des dispositifs existants limités à leur ligne de mire dans l'Arctique. Les résultats de cette recherche dépendent grandement de la conception et l'opération des systèmes expérimentaux. Un défi significatif du OTHR dans les latitudes nordiques est le fouillis auroral que l'on tente de rejeter dans ce rapport en utilisant des techniques de formation de nuls. Une attention particulière aux intéractions entre les antennes et le sol est requise, autrement le rejet du fouillis auroral peut échouer et les conclusions de ce programme de recherche peuvent être incorrectes. Ce rapport est une étape préliminaire afin d'assurer que les meilleurs résultats de recherche soient obtenus.

Table of contents

List of figures

1 Introduction

Planar arrays of monopoles are being considered by Defence Research and Development Canada (DRDC) as potential antennas as part of the over-the-horizon radar (OTHR) research program. Their simplicity and small horizontal dimensions make them ideally suited for radar applications where radiation must be maximized toward targets and minimized toward interference and clutter sources, which is typical in radar. OTHR at higher latitudes are particularly affected by auroral clutter resulting from significant plasma irregularities in the earth's auroral ionosphere. This has historically limited the use of OTHR in the Canadian North, but due to major technological improvements it may now be possible to mitigate adverse effects of auroral clutter [1].

Using a planar array of monopoles, it is possible to suppress the auroral clutter to levels acceptable for the use of OTHR in the Canadian North. However, significant challenges exist in the use of monopole antennas located very close to the ground. The purpose of this report is to document these challenges, theoretically determine the achievable performance in suppressing the auroral clutter, and study possible error mechanisms leading to quantifiable performance deterioration. Although various array dimensions are being considered by DRDC, the scope of this report is limited to the 64 monopole regular planar array.

The results of this report can be used for calibrating the 64 monopole array, in the absence of other measurements. Measurements are also planned as part of this research program, but they will not necessarily yield more accurate results than the theoretical calculations. Significant challenges exist in performing antenna measurements at OTHR operating frequencies. Very large distances are involved, and both azimuth and elevation operation needs to be considered. This can necessitate the use of aircraft or drones.

This report is organized as follows. The methodology for characterizing the monopole array is first presented in Section 2 and the impact of different ground types on clutter suppression is examined. While Section 2 focuses on vertically polarized signals, Section 3 studies the unavoidable horizontal signal polarization that is due to the finite ground system dimensions, and describes how to correctly take it into account and still obtain reasonable performance. Section 4 evaluates the use of robust beamforming techniques to mitigate the effects of calibration model uncertainties. Although most of this research is focused on a transmit array in which no signal statistics are available, adaptive array processing is studied in Section 5. This provides some insight on the performance on the receive side and of promising technologies such as the multiple-input-multiple-output (MIMO) radar. It can also be useful in case a radar system is implemented where the receiver would also be able to transmit a signal to help the transmitter adapt its transmission. In Section 6, the required high power amplifier backoff is calculated. This is a mandatory reduction in transmit power to keep the amplifiers operating normally. This reduction is highly dependent on electromagnetic coupling between the monopoles. Finally, conclusions are presented in Section 7.

2 Manifold determination methodology and analysis

In order to perform beamforming using the OTHR antenna arrays, accurate electromagnetic characterization is generally necessary. This characterization is commonly known as the array manifold and essentially consists of the individual complex radiation patterns of the array elements over a set of azimuth angles, elevation angles and frequencies. These are then used for correcting the non-ideal behavior of the array elements, including mutual coupling, in a procedure generally known as calibration. The radiation patterns can be measured in a controlled environment as to eliminate potential sources of errors. Unfortunately, in the case of an OTHR, operating wavelengths are in the order of tens of meters which preclude the possibility of performing measurements in a laboratory environment. Outdoor test ranges for this type of measurement are also problematic due to the required dimensions and potential multipath sources which can significantly degrade the results. Numerical modeling could be the best approach to obtain more accurate array manifolds. Modern electromagnetic numerical codes are viable alternatives and could potentially give the best results.

While it is possible in a receive array to adaptively reject interference without a priori knowledge of the manifold[1] [2], it is different in a transmit array where null-steering must be performed deterministically. Therefore the transmit array needs careful attention to optimize the overall OTHR performance. The intent is to reduce radiation as much as possible in the direction of the auroral clutter to improve the radar signal-to-clutter ratio (SCR) [1, 2].

The manifold determination methodology used here is based on [3]. Instead of calculating the individual element patterns and recording them for a finite set of azimuth and elevation angles, a coupling matrix is formed and can be used for calculating the array manifold for an arbitrary angle. This approach minimizes the number of parameters that need to be stored and provides the best interpolation possible. Knowing this coupling matrix, radiated fields can be calculated using the following equation:

$$\mathbf{E}(\theta, \phi) = C\mathbf{v}_{ideal}(\theta, \phi) \tag{1}$$

where C is the coupling matrix, $\mathbf{E}(\theta, \phi)$ is a column vector containing the radiated electric fields by each of the array elements, and $\mathbf{v}_{ideal}(\theta, \phi)$ is the idealized steering vector that is only based on the relative positions of the elements and the azimuth and elevation angles ϕ and θ respectively. Note that the matrix C is effectively independent of ϕ and θ and is frequency dependent, i.e. it needs to be recorded for a set of frequencies spanning the OTHR operating band. In special cases involving azimuth-only arrays of vertical thin wires, C is a square matrix with dimensions equal to the number of array elements, but in the context of the OTHR, operation over various elevation angles is required and unless the array elements can be considered electrically small, the matrix has a non-square structure

[1] Note that under conditions of strong mutual coupling, even receive arrays may suffer from inaccuracies in their main beam steering.

with a number of columns larger than the number of rows. This is to account for phase shifts over the entire length of the elements.

With an array of vertical thin wire elements, the vector $\mathbf{v}_{ideal}(\theta, \phi)$ takes the form:

$$\mathbf{v}_{ideal}(\theta, \phi) = \sin\theta \begin{bmatrix} e^{j\frac{2\pi}{\lambda}(\sin\theta(x_1\cos\phi + y_1\sin\phi) + z_1\cos\theta)} \\ e^{j\frac{2\pi}{\lambda}(\sin\theta(x_2\cos\phi + y_2\sin\phi) + z_2\cos\theta)} \\ \vdots \\ e^{j\frac{2\pi}{\lambda}(\sin\theta(x_K\cos\phi + y_K\sin\phi) + z_K\cos\theta)} \end{bmatrix} \tag{2}$$

where λ is the signal wavelength, and $x_1, \cdots, x_K$, $y_1, \cdots, y_K$ and $z_1, \cdots, z_K$ are the physical locations of the K wire segments in cartesian coordinates. Each array element is discretized into several segments and the total number of segments is equal to K.

The coupling matrix C is determined numerically by solving Maxwell's equations and using the resulting current distributions on all segments in this equation:

$$C = -\Delta z Z_L \left(Z_L + Z\right)^{-1} Z \begin{bmatrix} I_{11} & I_{12} & \cdots & I_{1N} \\ I_{21} & I_{22} & \cdots & I_{2N} \\ \vdots & \vdots & \ddots & \vdots \\ I_{K1} & I_{K2} & \cdots & I_{KN} \end{bmatrix}^T \tag{3}$$

where N is the number of array elements, $[\cdot]^T$ denotes the transpose operation, I_{kn} is the current on segment k when element n is excited in transmit-mode by a voltage (or current source) when all other elements are short-circuited (or open-circuited), Z is the mutual impedance matrix of the array, Z_L is a diagonal matrix whose entries are the transmitter load impedances, and Δz is the segment length when all segments have the same length. For simplicity, the receive-mode formulation of [3] (Table 1, Rx mode, 3rd line) was used here, which is identical to the transmit-mode formulation (Table 1, Tx mode, 3rd line) except for a scalar scaling factor.

This approach results into a $N \times K$ matrix that needs to be stored for different frequencies, along with the physical locations of the K segments. Substituting (2)-(3) into (1) should provide the array manifold for an arbitrary direction defined by θ and ϕ. In comparison, if we were to record radiation patterns of every array element with an angular resolution of one degree in the upper radiation hemisphere, 90 elevation and 360 azimuth angles would need to be considered and $90 \times 360 \times N = 32,400 \times N$ complex numbers would have to be stored for each frequency. This is in general orders of magnitude more than $N \times K$, and in addition is only accurate at discrete values of angles θ and ϕ.

2.1 Assumption of infinite perfect conductor ground

In this section, the 8×8 planar monopole array is modeled over an infinite perfect electrical conductor (PEC) ground using 4NEC2 [4], a NEC2-based [5] graphical user freeware. NEC2

is an open-source electromagnetics code based on the method of moments and developed by the Lawrence Livermore National Laboratory. The monopoles are modeled as perfect wire conductors, nine meter high with a radius of 3.81 cm, and uniformly separated by eight meters. It was found that only five segments were necessary for good accuracy over the frequency range considered of $3 - 18$ MHz, for a total of 320 segments, as shown in Figure 1. The load impedances in this array are 200Ω, so the matrix Z_L in (3) is given

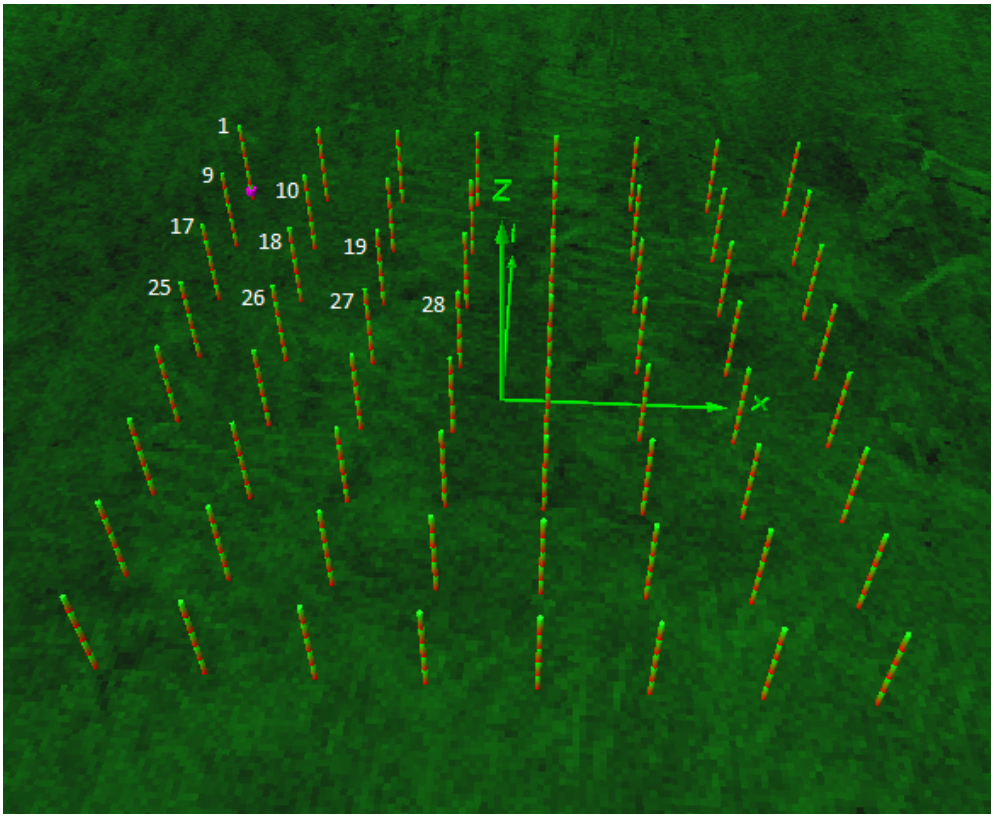

Figure 1: *8×8 planar array model in 4NEC2 [4]. Each Monopole is discretized into 5 segments and element 1 is excited by a voltage source in this figure while the other elements are short-circuited. By symmetry, only 10 elements (1, 9, 10, 17, 18, 19, 25, 26, 27 and 28) need to be separately excited to determine the entire array manifold.*

by $200I$ where I is a 64×64 identity matrix. By symmetry, it is possible to reduce the number of numerical calculations required to determine the array manifold. For example, the excitation of element 1 at the top-left corner of the array yields a current distribution that can be used to determine the current distributions produced by the other three corner elements. This way, four columns of the current distribution matrix on the right side of (3) can be filled using a single numerical calculation. Using similar considerations, only ten numerical calculations are required to fill this matrix completely and compute the coupling matrix, as illustrated in Figure 1.

An example of a NEC2 input file used in this model is available in Annex A.1. The resulting coupling matrix has $64 \times 320 = 20,480$ complex parameters which are significantly less than the $32,400 \times 64 = 2,073,600$ needed when recording all radiation patterns with one degree angular resolution. In addition, numerical calculations were carried out at every MHz from 3 to 18 MHz, so the total number of stored parameters is $20,480 \times 16 = 327,680$ instead of $2,073,600 \times 16 = 33,177,600$. This represents a 99% reduction while also providing superior interpolation.

Due to the presence of the PEC infinite ground plane, image theory needs to be invoked in the determination of the manifold. This is done in a straightforward manner by introducing a vector similar to (2) that includes the imaged segments under the ground plane ($z < 0$):

$$\mathbf{v}_{ideal}(\theta, \phi)' = \sin\theta \begin{bmatrix} e^{j\frac{2\pi}{\lambda}(\sin\theta(x_1\cos\phi + y_1\sin\phi) - z_1\cos\theta)} \\ e^{j\frac{2\pi}{\lambda}(\sin\theta(x_2\cos\phi + y_2\sin\phi) - z_2\cos\theta)} \\ \vdots \\ e^{j\frac{2\pi}{\lambda}(\sin\theta(x_K\cos\phi + y_K\sin\phi) - z_K\cos\theta)} \end{bmatrix} \tag{4}$$

Then the array manifold is obtained using:

$$\mathbf{E}(\theta, \phi) = C\left(\mathbf{v}_{ideal}(\theta, \phi) + \mathbf{v}_{ideal}(\theta, \phi)'\right) \tag{5}$$

2.1.1 Model validation

A useful way to verify whether the numerical model with five segments per monopole is adequate is to perform a simulation in the receive-mode using the same model and compare the results. The NEC2 input file in receive-mode used for this validation is available in Annex A.2 where a test plane-wave signal of unitary electric field magnitude arriving from $(\theta, \phi) = (60°, 60°)$ is considered.

Using the formulation of (5), the predicted manifold for $(\theta, \phi) = (60°, 60°)$ is compared against the receive-mode simulation over the $3 - 18$ MHz range in Figure 2. The results are in good agreement and suggest that the numerical model and coupling matrix are suitable for the determination of the manifold.

2.1.2 Beamforming

A simple way to perform beamforming in the transmit-mode is to compute an array correlation matrix using the array manifold for directions in which nulls are desired. This can be done using:

$$R_{xx} = \sum_{l=1}^{L} \mathbf{E}(\theta_l, \phi_l)\mathbf{E}(\theta_l, \phi_l)^H + \sigma_o^2 I \tag{6}$$

where $(\cdot)^H$ denotes the Hermitian transpose operation, L is the number of desired nulls, $\mathbf{E}(\theta_l, \phi_l)$ is the manifold in desired null directions (θ_l, ϕ_l), I is the identity matrix, and σ_o^2 is

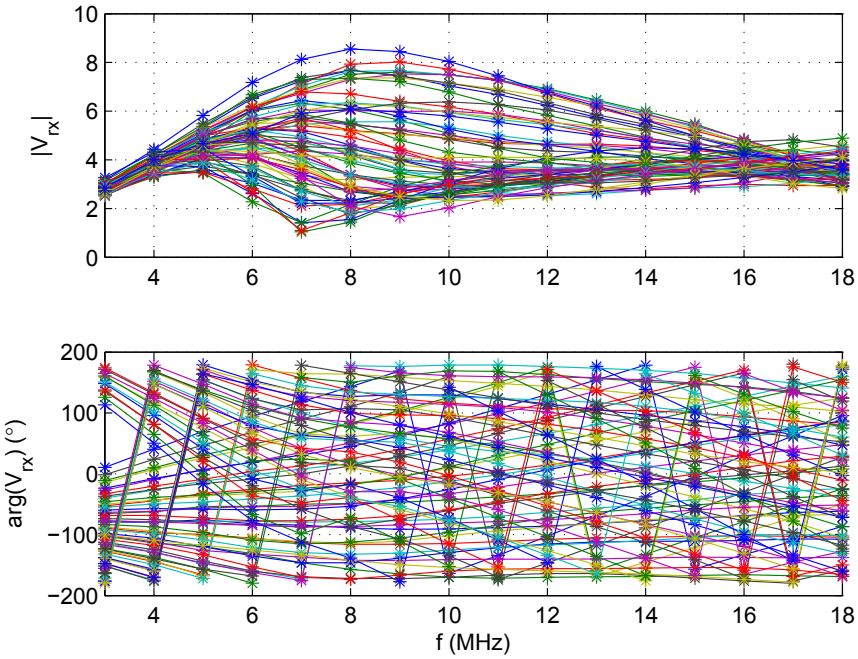

Figure 2: *Validation of numerical model and coupling matrix by comparison with receive-mode numerical simulation. The predicted array manifold (*) is compared with the receive-mode results (solid) for a signal arriving from* $(\theta, \phi) = (60°, 60°)$ *in amplitude (top) and phase (bottom) for the* 64 *monopoles on an infinite PEC ground.*

fictitious noise employed here to load the diagonal of the correlation matrix R_{xx} and ensure a good condition number for the matrix. A value of $\sigma_o^2 = 10^{-6}$ is used in this report. The required weights to steer a main beam towards (θ_s, ϕ_s) are obtained using:

$$\mathbf{w} = {R_{xx}}^{-1}\mathbf{E}(\theta_s, \phi_s) \tag{7}$$

In the transmit array, the complex conjugates of these weights are the open-circuit voltages of the sources connected to each of the array elements. The total radiated fields are given by:

$$E(\theta, \phi) = \mathbf{w}^H\mathbf{E}(\theta, \phi) \tag{8}$$

An example involving the formation of a main beam at $(\theta_s, \phi_s) = (45°, 60°)$ and 15 nulls equally spaced by 10° over $60° \leq \theta \leq 80°$ and $-20° \leq \phi \leq 20°$ at 18 MHz is presented in Figure 3. The corresponding radiation pattern in 4NEC2 is shown in Figure 4. The

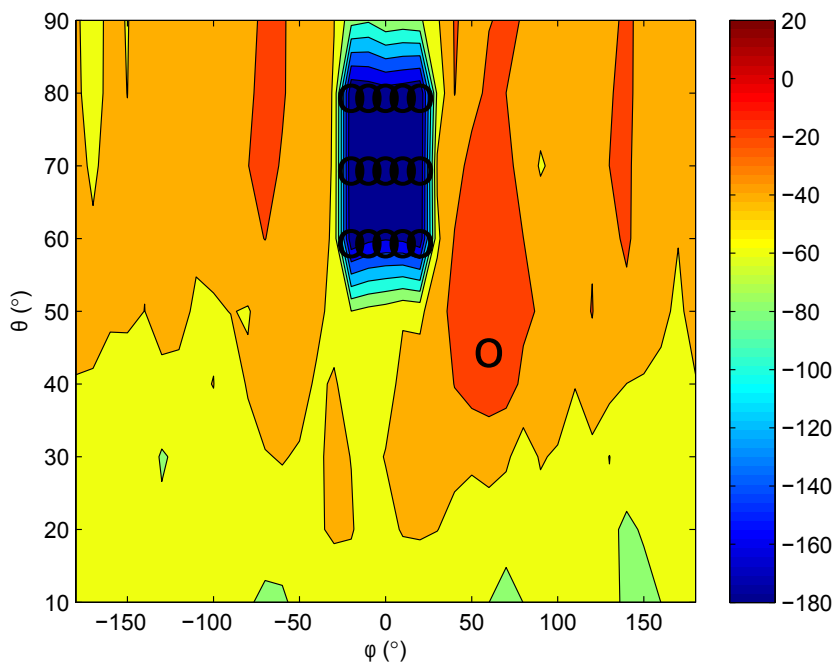

Figure 3: *Beamforming example at 18 MHz for desired radiation at $(\theta, \phi) = (45°, 60°)$ and 15 nulls equally spaced over $60° \leq \theta \leq 80°$ and $-20° \leq \phi \leq 20°$ for the 8×8 monopole array on infinite PEC ground plane. These directions are indicated by circles and the color scale is in decibels.*

NEC2 input file used for generating this radiation pattern is available in Annex A.3. It is seen in Figures 3-4 that extremely deep nulls are formed as desired and most of the radiation is directed towards (θ_s, ϕ_s). Note that the amplitudes in Figure 3 are relative to

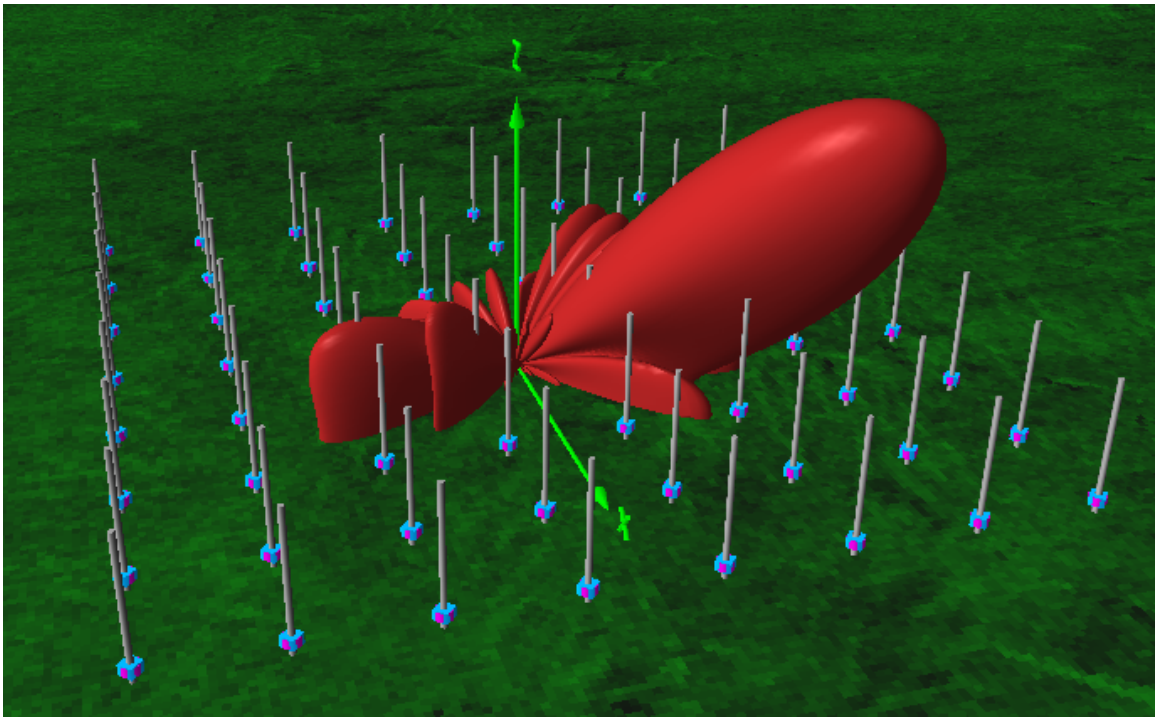

Figure 4: *Radiation pattern calculated by 4NEC2 [4] for the beamforming example of Figure 3. Maximum radiation is observed around* $(\theta, \phi) = (45°, 60°)$ *and minimum radiation is observed at low elevations around the positive* x*-axis as desired.*

those of an idealized beamformer of point sources with the same number of elements and planar array geometry. The same amplitude normalization scheme is used throughout the remainder of this report, and quantifies the radiation efficiency of the beamformer. Other relevant quantities such as effective isotropic radiated power (EIRP) and signal-to-noise ratio (SNR) can be derived from amplitude results presented in this report based on power and noise sources specific to an application.

It is important to note that the excellent beamforming performance observed in Figures 3-4 is due to the accurate determination of the array manifold which allows proper array calibration to be implemented. To gain a better appreciation for the importance of accurate calibration, the uncalibrated results are shown in Figure 5(a) where the array weights of (7) are determined by assuming that the array consists of ideal point sources. It is clear that the nulling performance of the uncalibrated array is severely degraded with much shallower nulls.

A popular approach for calibrating antenna arrays in the literature is the simple use of the mutual impedance matrix, but unlike (3) the coupling matrix ignores the full current distributions and takes the following simplified form:

$$C = Z_L \left(Z_L + Z\right)^{-1} \tag{9}$$

where Z is the mutual impedance matrix. As discussed in [3], this approach cannot be expected to be accurate in general and this is confirmed in Figure 5(b) where the resulting performance appears to be similar to the uncalibrated case.

2.2 Finite ground modeling

So far in this report, the ground under the monopole array elements was assumed to be perfect, i.e. perfectly conducting and infinite in extent. In reality, some tradeoffs need to be made due to the large physical dimensions of antennas operating at HF frequencies and the resulting requirement on the amount of material needed to build a proper ground. A common implementation of a ground system under a monopole antenna is to use several wires, known as radials, all intersecting at the base of the monopole and directed away from it with uniform angular distribution. When each monopole is placed on such a ground system, the overall structure has a geometry such as that of Figure 6.

The number of radials and their dimensions are still debated today [6]. The early work of [7] has established a popular guideline of 120 radials per monopole and a radial length equal to a quarter of a wavelength, but other studies have determined that these numbers could be a little conservative, and could be reduced depending on frequency, monopole dimensions and soil properties [7, 8]. The study of [8] evaluated the optimal number of radials for a given total available wire length, and this has guided our choice for the design of the monopole array elements. The initial design evaluated here is for monopoles using ground systems comprised of 32 radials each 9.75 meter long. These 64 monopoles are shown in Figure 6. It

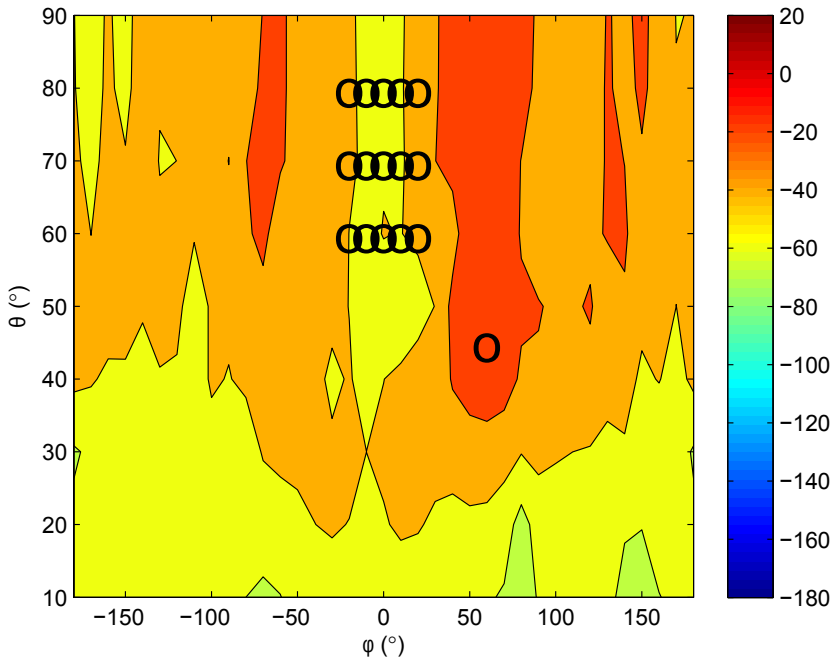

(a)

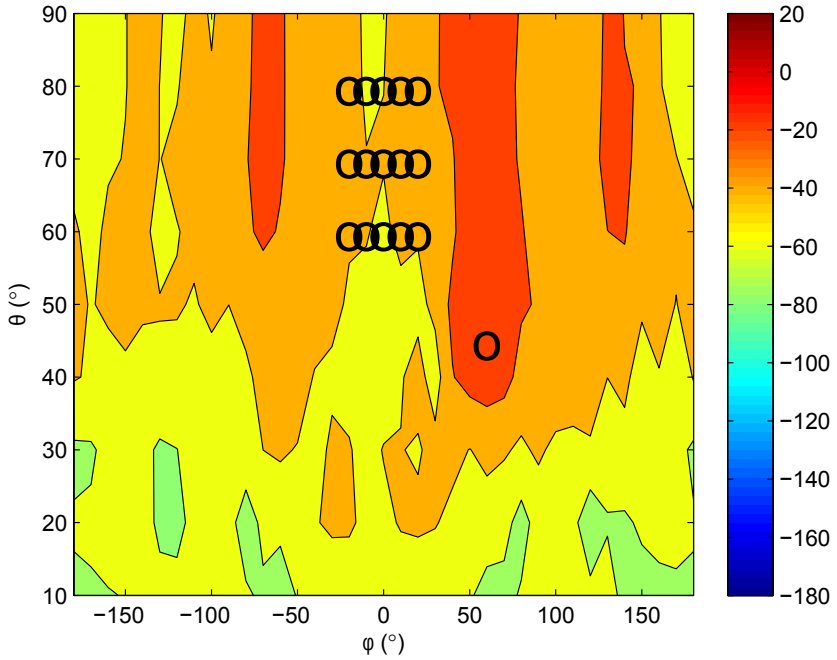

(b)

Figure 5: *Radiation patterns for beamforming example of Figure 3 (a) without any calibration and (b) with mutual impedance matrix calibration.*

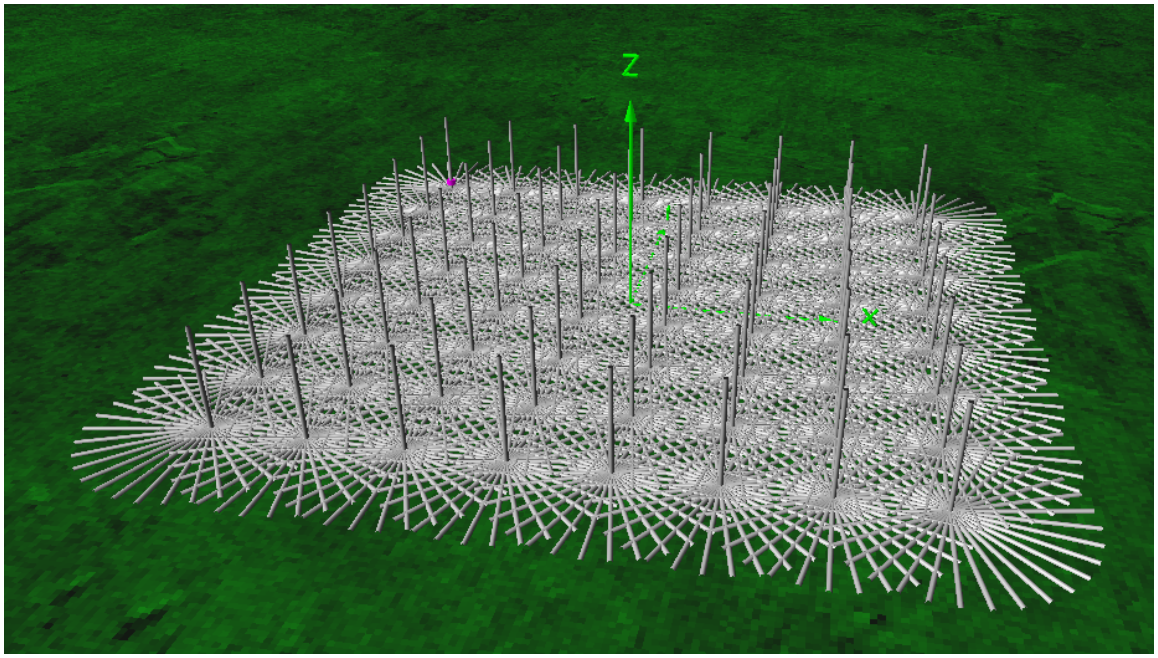

Figure 6: *8×8 planar array with 32 radials per monopole. The monopoles are 9 meter high and the radials are 9.75 meter long.*

is important to note that for practical reasons, the radials are insulated from each other due to their dielectric coatings except at the intersection points at the base of each monopole.

A significant complication of a finite ground plane is the presence of horizontal currents on the radials that need to be taken into account in the determination of the manifold. Unlike (3) where only z-directed currents were considered, the coupling matrix here takes the following form:

$$C = -Z_L \left(Z_L + Z\right)^{-1} Z \begin{bmatrix} \Delta r \begin{bmatrix} I_{x11} & \cdots & I_{x1N} \\ \vdots & \ddots & \vdots \\ I_{xM1} & \cdots & I_{xMN} \end{bmatrix} \\ \Delta r \begin{bmatrix} I_{y11} & \cdots & I_{y1N} \\ \vdots & \ddots & \vdots \\ I_{yM1} & \cdots & I_{yMN} \end{bmatrix} \\ \Delta z \begin{bmatrix} I_{z11} & \cdots & I_{z1N} \\ \vdots & \ddots & \vdots \\ I_{zK1} & \cdots & I_{zKN} \end{bmatrix} \end{bmatrix}^T \tag{10}$$

where Δr is the segment size for the radials assuming it is kept constant and M is the number of radial segments. It is seen in (10) that the matrix is partitioned into three submatrices,

the first accounting for x-directed currents on the radials, the second accounting for y-directed currents on the radials, and the third accounting for z-directed currents on the monopoles. The column vector on the right side of (1) then takes the following form:

$$\mathbf{v}_{ideal}(\theta,\phi) = \begin{bmatrix} -\cos\theta\cos\phi \begin{bmatrix} e^{j\frac{2\pi}{\lambda}(\sin\theta(x_1\cos\phi+y_1\sin\phi)+z_1\cos\theta)} \\ \vdots \\ e^{j\frac{2\pi}{\lambda}(\sin\theta(x_M\cos\phi+y_M\sin\phi)+z_M\cos\theta)} \end{bmatrix} \\ -\cos\theta\sin\phi \begin{bmatrix} e^{j\frac{2\pi}{\lambda}(\sin\theta(x_1\cos\phi+y_1\sin\phi)+z_1\cos\theta)} \\ \vdots \\ e^{j\frac{2\pi}{\lambda}(\sin\theta(x_M\cos\phi+y_M\sin\phi)+z_M\cos\theta)} \end{bmatrix} \\ \sin\theta \begin{bmatrix} e^{j\frac{2\pi}{\lambda}(\sin\theta(x_1\cos\phi+y_1\sin\phi)+z_1\cos\theta)} \\ \vdots \\ e^{j\frac{2\pi}{\lambda}(\sin\theta(x_K\cos\phi+y_K\sin\phi)+z_K\cos\theta)} \end{bmatrix} \end{bmatrix} \tag{11}$$

Using this formulation, the performance of the 8×8 array of monopoles with ground systems made of 32 radials and modeled using the software package FEKO [9] is evaluated at different frequencies in Figure 7 for a target at $(\theta, \phi) = (60°, 90°)$ and 15 nulls equally spaced over $30° \leq \theta \leq 50°$ and $-20° \leq \phi \leq 20°$. This is the best achievable performance for this particular antenna system and it requires the perfect knowledge of the array manifold. Since the ground systems are meant to act as perfect ground planes, it is worthwhile evaluating performance using the manifold of Section 2.1 where a perfect ground plane was considered. It is seen in Figure 8 that performance is severely degraded when the perfect ground plane is assumed, in particular at lower frequencies. Hence the finite dimensions of the ground plane have to be carefully considered to optimize performance of the array.

2.3 Effects of soil variations on array manifold

Since the ground plane cannot be approximated as being perfect, it becomes important to consider the soil on which the array is installed. This is generally done in numerical electromagnetic codes by making the approximation that the soil is uniform and described by its constant conductivity and permittivity. In FEKO, calculations involving antennas close to the ground are handled using Sommerfeld's exact integrals [10–12]. Once current distributions are calculated with this formulation, far-field calculations can use the well-known reflection coefficient method. This is implemented here by determining the vertical and horizontal reflection coefficients at the ground interface. The propagation constant of a medium is given by:

$$\gamma = \sqrt{j\omega\mu\left(\sigma + j\omega\epsilon\right)} \tag{12}$$

where ω is the angular frequency in rad/s, σ is the medium conductivity in S/m, μ is the medium permeability in H/m and ϵ is the medium permittivity in F/m. The intrinsic impedance of the medium is given by:

$$\eta = \frac{j\omega\mu}{\gamma} \tag{13}$$

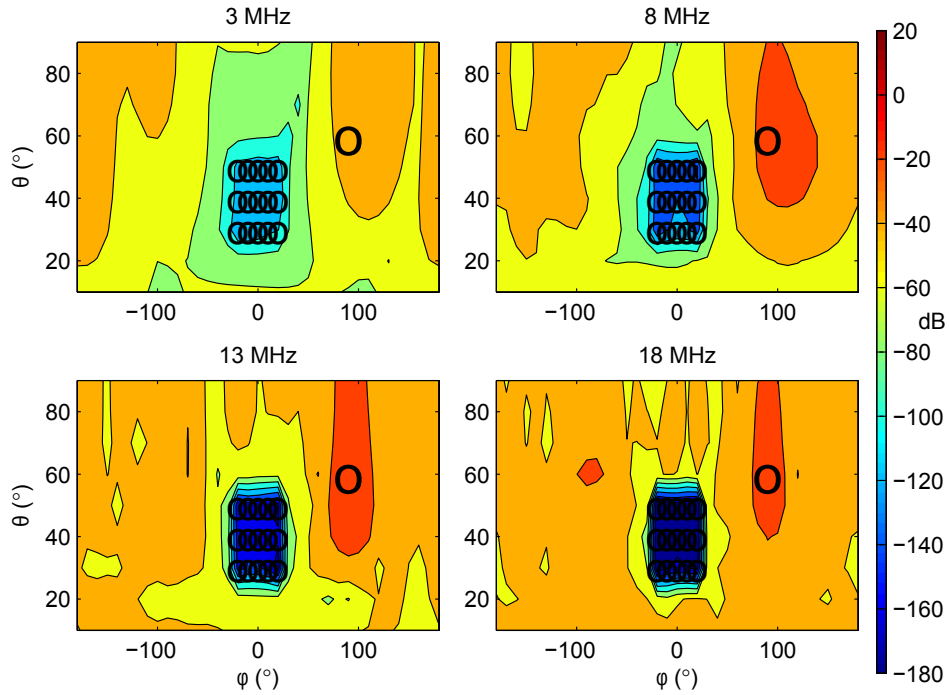

Figure 7: *Radiation patterns for desired radiation at* $(\theta, \phi) = (60°, 90°)$ *and* 15 *nulls equally spaced over* $30° \leq \theta \leq 50°$ *and* $-20° \leq \phi \leq 20°$ *with a 32 radial ground system for each element. The main beam direction is indicated by a large circle and null directions by smaller circles.*

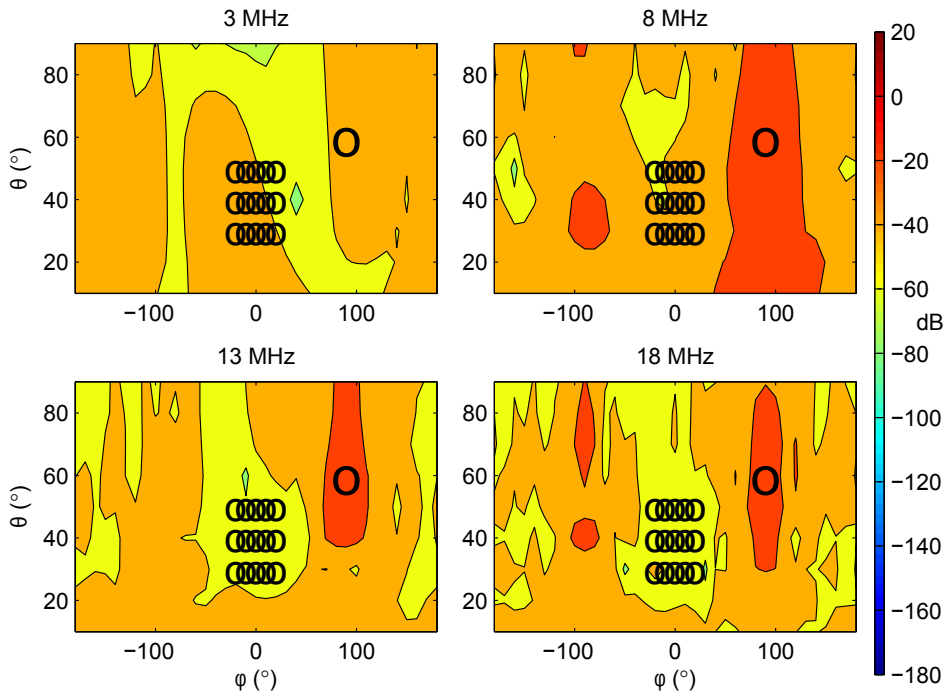

Figure 8: *Radiation patterns for beamforming example of Figure 7 calibrated with the model of Section 2.1 (assuming perfect infinite PEC ground).*

The refracted angle in the ground is governed by Snell's law:

$$\theta_t = \sin^{-1}\left(\frac{\gamma_o}{\gamma_1}\sin\theta\right) \tag{14}$$

where γ_o and γ_1 are the propagation constant of free-space and the ground respectively, and θ is the elevation angle. The vertical and horizontal reflection coefficients are obtained using:

$$\Gamma_v = \frac{\eta_o\cos\theta - \eta_1\cos\theta_t}{\eta_o\cos\theta + \eta_1\cos\theta_t} \tag{15}$$

$$\Gamma_h = \frac{\eta_1\cos\theta_t - \eta_0\cos\theta}{\eta_o\cos\theta + \eta_1\cos\theta_t} \tag{16}$$

where η_o and η_1 are the intrinsic impedances of free-space and the ground respectively. It is observed that $\Gamma = \Gamma_v = -\Gamma_h$, and the manifold can be expressed as:

$$\mathbf{E}(\theta,\phi) = C\left(\mathbf{v}_{ideal}(\theta,\phi) + \Gamma\mathbf{v}_{ideal}(\theta,\phi)'\right) \tag{17}$$

where

$$\mathbf{v}_{ideal}(\theta,\phi)' = \begin{bmatrix} \cos\theta\cos\phi \begin{bmatrix} e^{j\frac{2\pi}{\lambda}(\sin\theta(x_1\cos\phi+y_1\sin\phi)-z_1\cos\theta)} \\ \vdots \\ e^{j\frac{2\pi}{\lambda}(\sin\theta(x_M\cos\phi+y_M\sin\phi)-z_M\cos\theta)} \end{bmatrix} \\ \cos\theta\sin\phi \begin{bmatrix} e^{j\frac{2\pi}{\lambda}(\sin\theta(x_1\cos\phi+y_1\sin\phi)-z_1\cos\theta)} \\ \vdots \\ e^{j\frac{2\pi}{\lambda}(\sin\theta(x_M\cos\phi+y_M\sin\phi)-z_M\cos\theta)} \end{bmatrix} \\ \sin\theta \begin{bmatrix} e^{j\frac{2\pi}{\lambda}(\sin\theta(x_1\cos\phi+y_1\sin\phi)-z_1\cos\theta)} \\ \vdots \\ e^{j\frac{2\pi}{\lambda}(\sin\theta(x_K\cos\phi+y_K\sin\phi)-z_K\cos\theta)} \end{bmatrix} \end{bmatrix} \tag{18}$$

2.3.1 Array on average soil

The operation of the array over an average soil with $\sigma = 0.005$ S/m and $\epsilon = 13\epsilon_o$ is considered in this section. A more realistic auroral clutter scenario based on [13] is evaluated with a target at $(\theta,\phi) = (50°, 40°)$ and 21 nulls equally spaced over $60° \leq \theta \leq 80°$ and $-30° \leq \phi \leq 30°$. Using (11) and (18) in (17) for this signal scenario, the performance of the 8×8 planar monopole array with the 32 radials considered in Section 2.2, but this time modeled over an average soil, is shown in Figure 9. Again, this is the best achievable performance for this particular antenna system and depends on the accurate modeling of the ground, assumed to be of constant conductivity and permittivity.

To help evaluate performance, the signal-to-clutter ratio is indicated in brackets at each of the different frequencies. This measure is given by:

$$SCR = \frac{\mathbf{w}^H\mathbf{E}\left(\theta_s,\phi_s\right)\mathbf{E}\left(\theta_s,\phi_s\right)^H\mathbf{w}}{\frac{1}{L}\sum_{l=1}^{L}\mathbf{w}^H\mathbf{E}\left(\theta_l,\phi_l\right)\mathbf{E}\left(\theta_l,\phi_l\right)^H\mathbf{w}} \tag{19}$$

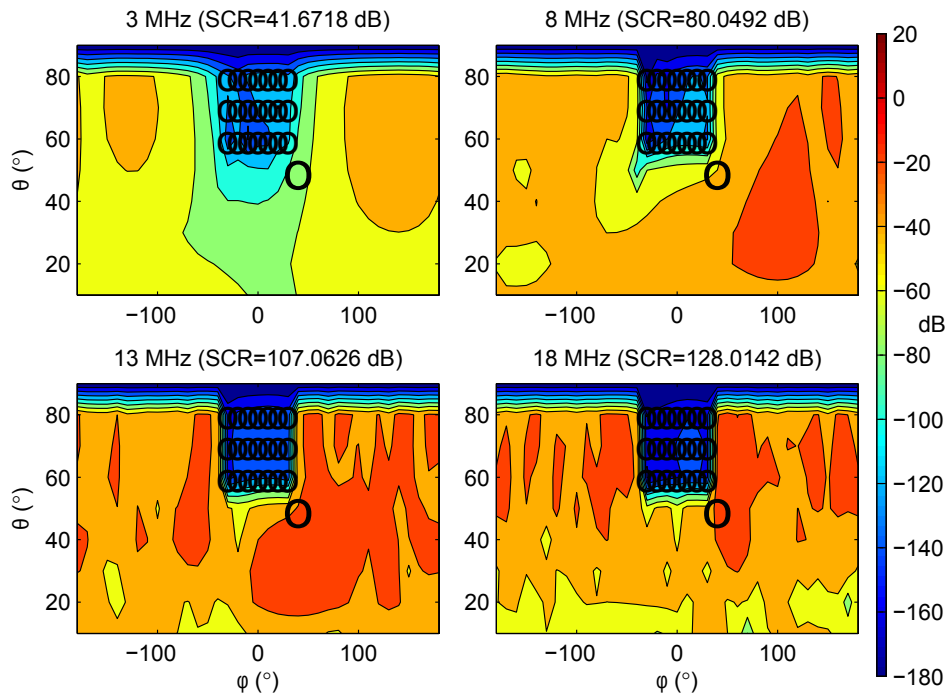

Figure 9: *Radiation patterns for desired radiation at* $(\theta, \phi) = (50°, 40°)$ *and* 21 *nulls equally spaced over* $60° \leq \theta \leq 80°$ *and* $-30° \leq \phi \leq 30°$ *with a 32 radial ground system for each element over average soil.*

where the weight vector $\mathbf{w}$ is obtained using (7). In other words, this is the ratio of the power in the desired direction to the average power towards the L nulls. Due to the very small angular separation between the target and clutter, it is observed that the maximum radiation does not always occur in the target direction, but nevertheless acceptable SCR values are achieved.

The impact of ignoring the soil by using the model of Section 2.2 for the determination of the weight vector $\mathbf{w}$ is evaluated in Figure 10(a). The performance obtained assuming the perfect ground plane model of Section 2.1 is shown in Figure 10(b) and only improves performance at 8 MHz compared to Figure 10(a). The other three frequencies turn out to have poorer performance. Both Figures 10(a)-(b) show SCR degradations of over 33 dB for each of the different frequencies compared to the accurate calibration results presented in Figure 9.

This motivates the use of the full model including the soil and radials in the calibration of the antenna system. A disadvantage compared to the use of the perfect ground plane model of Section 2.1 is the size of the matrix C that needs to be stored at each frequency. Another issue is that the full model involves an important assumption with respect to the soil in that it has a uniform conductivity and permittivity. This can be a crude approximation in practice.

2.3.2 Array on arctic land

The best achievable performance over arctic land, a poor conductor soil with $\sigma = 0.0005$ S/m and $\epsilon = 3\epsilon_o$ is presented in Figure 11(a). Given accurate modeling of the soil, it is seen that good performance is possible similar to Figure 9. However, Figure 11(b) evaluates the impact of a ground model mismatch where the actual soil is arctic land and the weight vector $\mathbf{w}$ is obtained using the average soil manifold. It is seen that the nulls are very sensitive to the soil properties and the performance of Figure 11(a) can be very difficult to achieve in practice when a theoretical manifold is used. It becomes worthwhile to determine whether a full theoretical model that includes the soil and radials is necessary for the calibration of the system. The performance over arctic land but calibrated ignoring the soil and using the perfect ground model is evaluated in Figure 12. In both cases, the resulting SCR is seen to degrade at 3 MHz and 18 MHz. However, the perfect ground model gives better performance at 8 MHz and ignoring the soil gives better performance at 13 MHz. The average soil model appears to be a good tradeoff to maintain an acceptable balance across all frequencies. This suggests that using the full theoretical model for calibration can be beneficial.

It is important to note that an alternative to using the theoretical model is to perform on-site measurements of the individual array element radiation patterns and use these measurements as the manifold for calibrating the system. However, such a measurement procedure is a significant challenge due to the physical distances involved in the far-field and the two-dimensional operation of the system which requires measurements to be performed in both azimuth and elevation. In addition, sources of multipath propagation can significantly

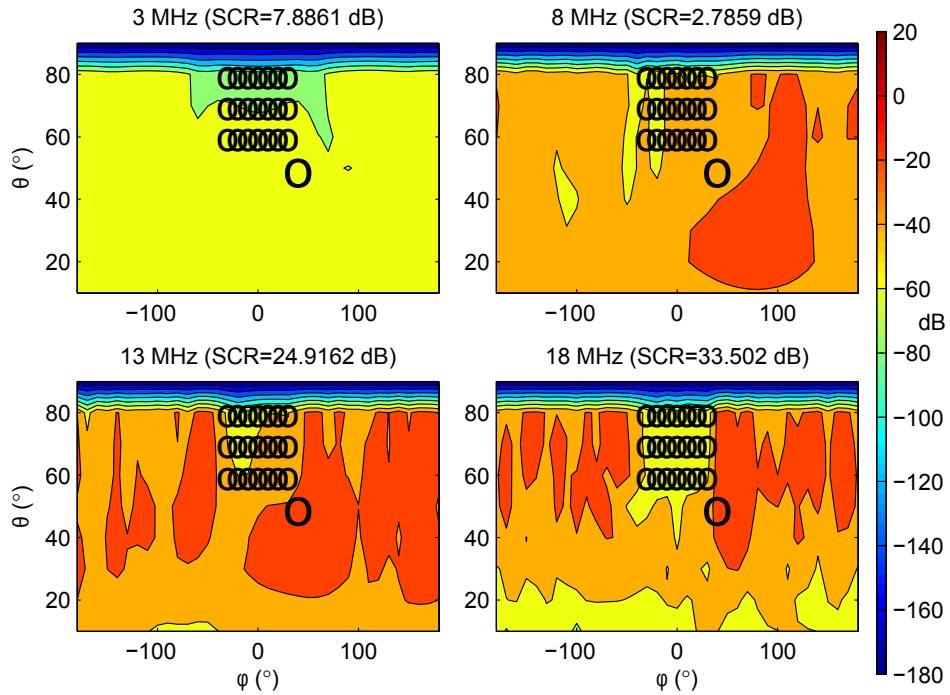

(a)

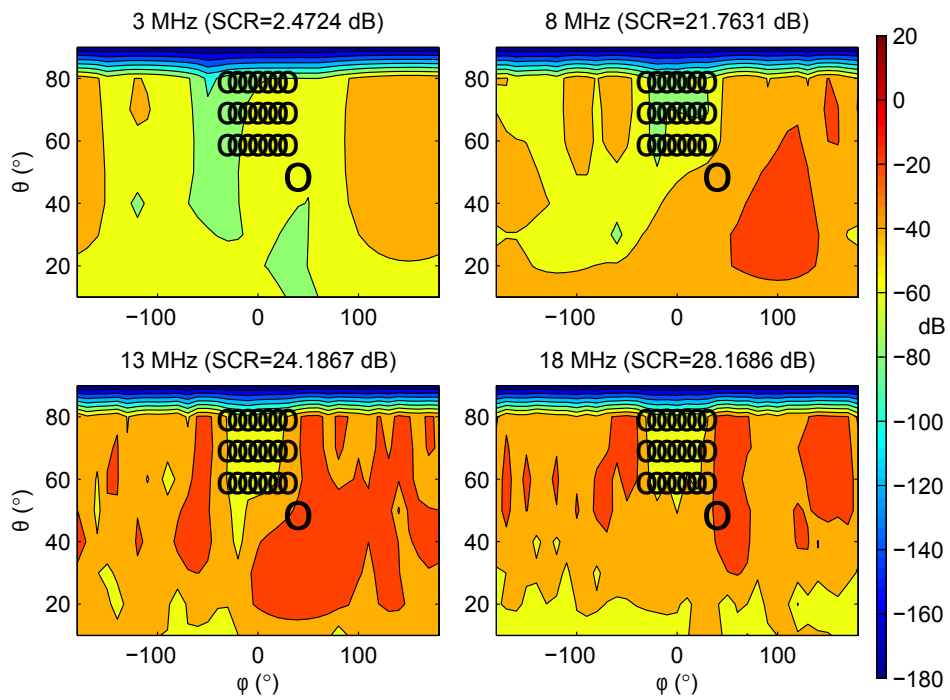

(b)

Figure 10: *Radiation patterns for the beamforming example of Figure 9 calibrated with (a) the model of Section 2.2 (ignoring the soil) and (b) the model of Section 2.1 (assuming perfect infinite PEC ground).*

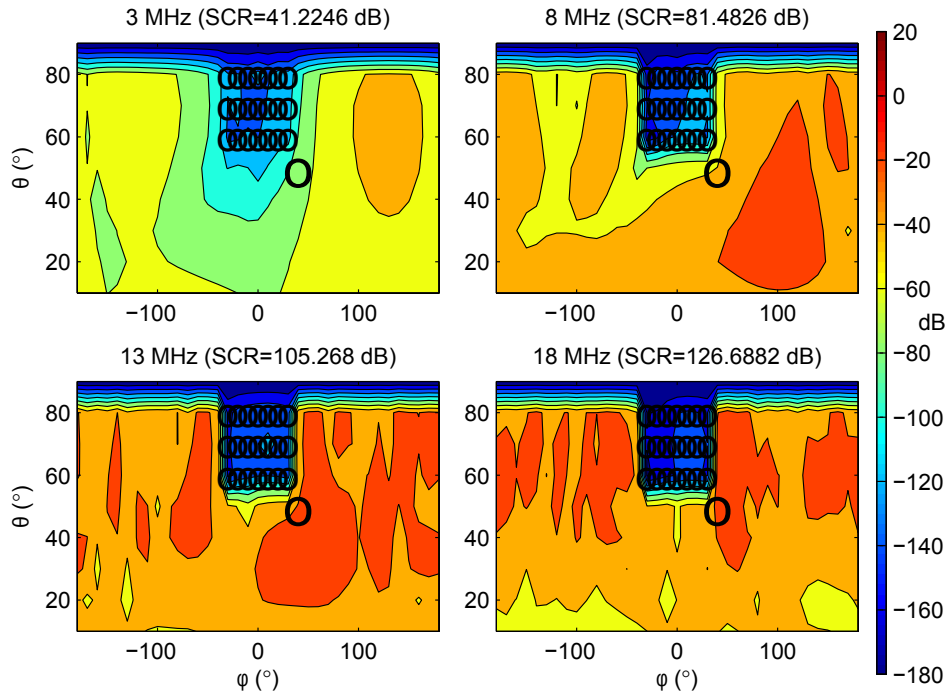

(a)

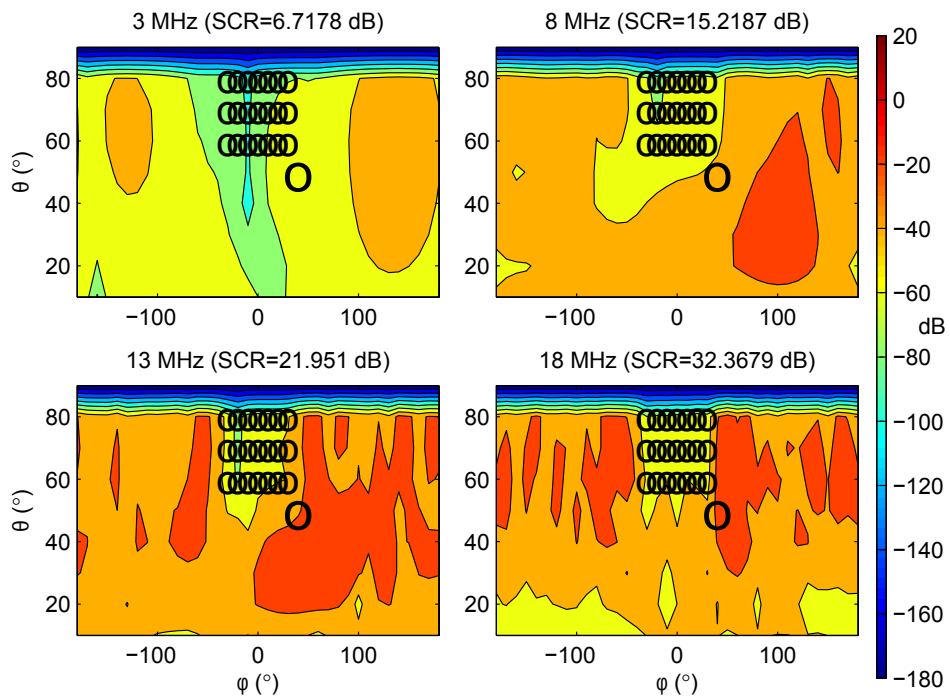

(b)

Figure 11: *Radiation patterns with the 32 radial ground system for each element over arctic land calibrated with (a) accurate manifold and (b) average soil manifold.*

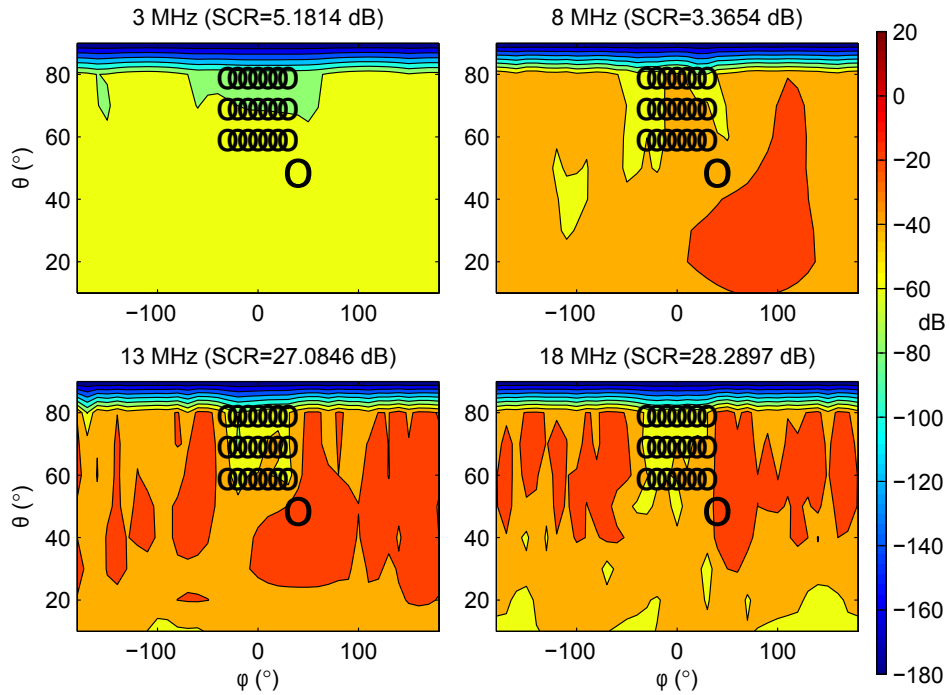

(a)

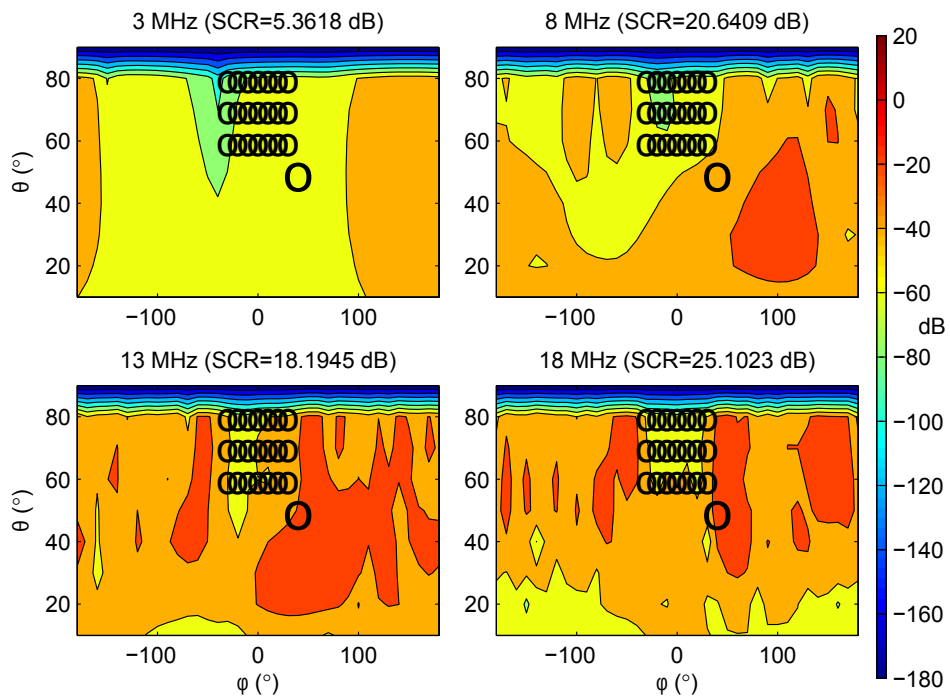

(b)

Figure 12: *Radiation patterns with the 32 radial ground system for each element over arctic land calibrated with (a) the model of Section 2.2 (ignoring the soil) and (b) the model of Section 2.1 (assuming perfect infinite PEC ground).*

affect measurement accuracy. The measurements obtained are valid as long as the ground properties remain constant, and additional factors such as snow cover are likely to require a new manifold measurement. Manifold measurements of OTHR arrays are outside the scope of this report and will be covered in a subsequent report.

2.3.3 Array on good soil

The best achievable performance over a good conductor soil with $\sigma = 0.03$ S/m and $\epsilon = 20\epsilon_o$ is presented in Figure 13(a). With accurate modeling of the soil, reasonable performance is possible, comparable to that of average soil in Figure 9 and of arctic land soil in Figure 11(a). However, Figure 13(b) evaluates the impact of a ground model mismatch where the actual soil is a good soil and the weight vector $\mathbf{w}$ is obtained using the average soil manifold. The SCR performance is observed to drop significantly, in particular at lower frequencies where it is only just over 9 dB at 3 MHz. It is seen in Figure 14 that better performance can be obtained at 8 MHz using the perfect ground model. At higher frequencies, it appears that the average soil model is still the best.

2.4 Analysis based on elevation

The contribution of the currents on the radials to the radiated fields is highly dependent on the elevation angle θ. It is observed in (11) and (18) that the two submatrices associated with the x-directed and y-directed currents in (10) are scaled by $\cos\theta$ in the manifold of (17). For this reason, it is possible that the manifold is less sensitive to the soil properties at low elevations above the ground (high values of θ). This is evaluated in this section for three different elevations: low, medium and high elevation relative to the ground. The findings are summarized in Tables 1-2.

The same signal scenario as that of Section 2.3 is considered for low elevation and the results of that section are compiled in Tables 1-2. For medium and high elevation, only the elevation of the 21 nulls and the target elevation are changed. The medium elevation scenario has nulls that are equally distributed over $35° \leq \theta \leq 55°$ and a target at $\theta = 25°$, while the high elevation scenario has nulls that are equally distributed over $10° \leq \theta \leq 30°$ and a target at $\theta = 40°$ so that the angular separation between the target and clutter remains 10°. The various calibration models are summarized below:

- Average Soil: excitations are determined using the full-wave antenna model operating over an average soil with $\sigma = 0.005$ S/m and $\epsilon_r = 13$;
- Ignoring Soil: excitations are determined using the numerical model in the absence of soil, i.e. free-space;
- Perfect Ground: excitations are determined using the numerical model of monopoles on infinite perfect electric conductor (PEC) ground plane;
- Ideal: excitations assume point sources, i.e. uncalibrated;

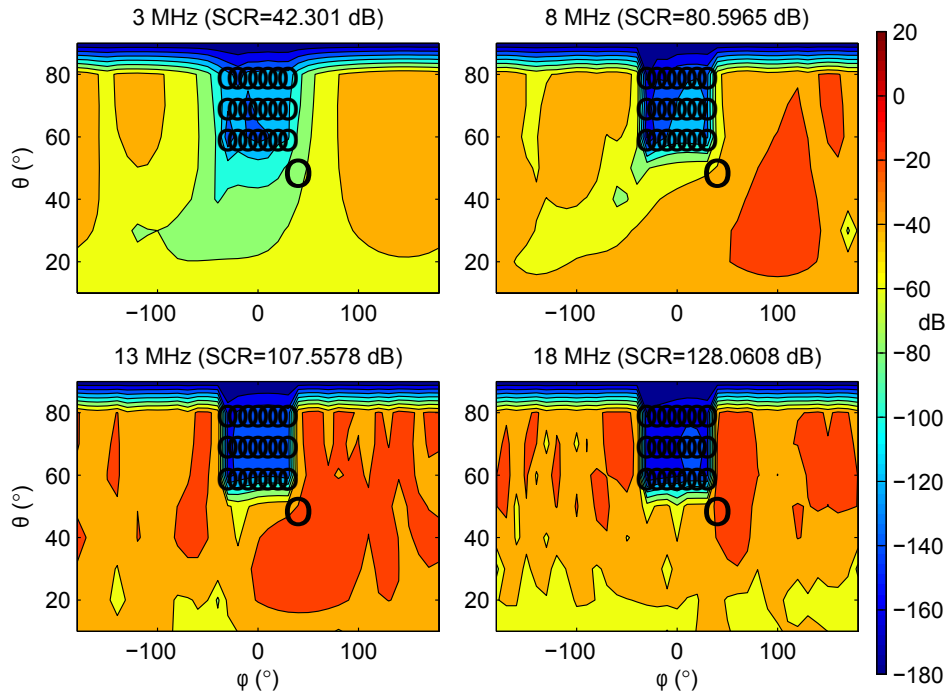

(a)

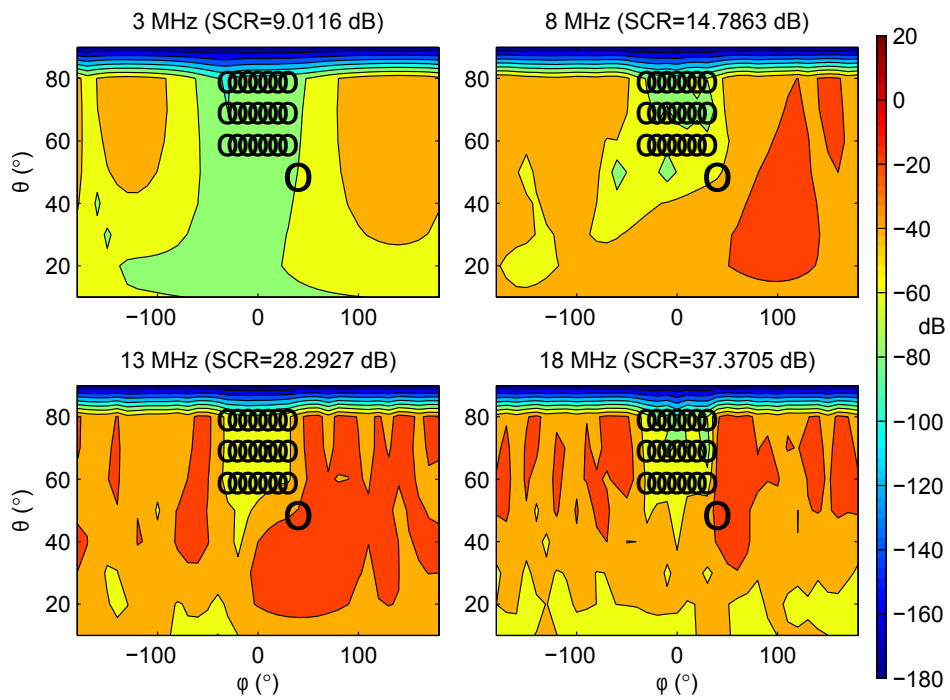

(b)

Figure 13: *Radiation patterns with the 32 radial ground system for each element over good conductor soil calibrated with (a) accurate manifold and (b) average soil manifold.*

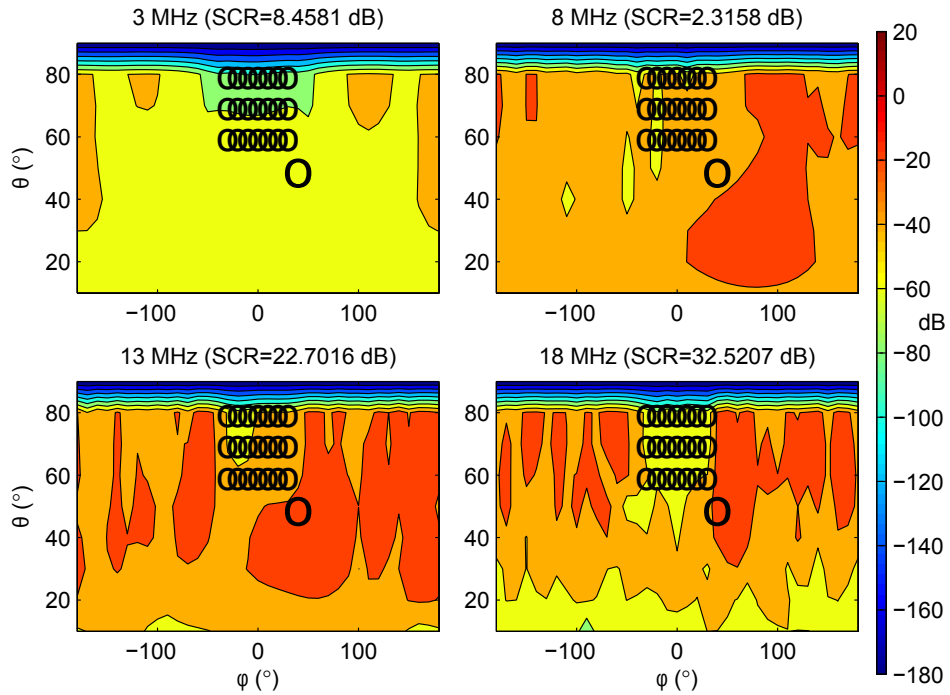

(a)

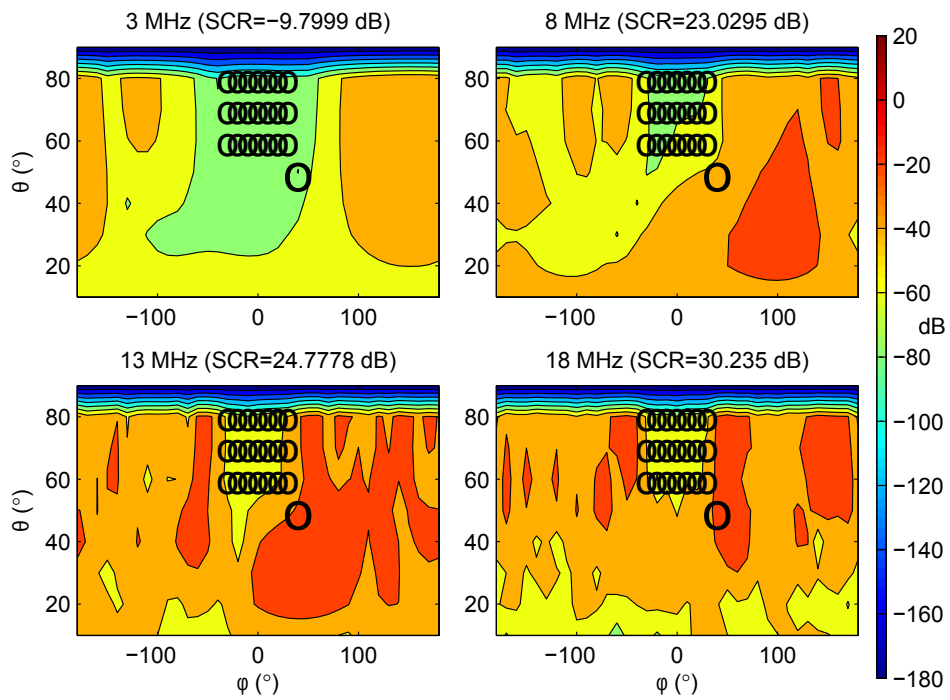

(b)

Figure 14: *Radiation patterns with the 32 radial ground system for each element over good conductor soil calibrated with (a) the model of Section 2.2 (ignoring the soil) and (b) the model of Section 2.1 (assuming perfect infinite PEC ground).*

Table 1: *Summary of the beamformer SCR performance in decibels based on elevation for the 32 radial array on arctic land (poor conductor). The best SCR value is indicated in bold for each elevation and frequency.*

Elevation	**Frequency**	**Accurate Model**	**Model**				
			Average Soil	**Ignoring Soil**	**Perfect Ground**	**Ideal**	**Impedance Matrix**
Low	3 MHz	41.2	**6.7**	5.2	5.4	4.4	3.2
	8 MHz	81.5	15.2	3.4	**20.6**	6.8	15.1
	13 MHz	105.3	22.0	**27.1**	18.2	14.9	4.4
	18 MHz	126.7	**32.4**	28.3	25.1	24.9	21.9
Medium	3 MHz	44.4	-13.3	-0.6	**0.2**	0.0	-0.2
	8 MHz	92.8	**9.6**	9.5	6.9	-0.9	-5.0
	13 MHz	115.6	12.6	**16.7**	7.1	10.5	1.0
	18 MHz	128.7	**20.1**	-13.6	8.4	11.9	6.5
High	3 MHz	47.8	**7.4**	0.8	-7.2	-2.0	-12.4
	8 MHz	85.9	7.5	8.0	**10.2**	1.6	8.4
	13 MHz	100.6	17.5	**19.6**	11.4	15.3	6.5
	18 MHz	113.0	**30.7**	24.9	26.1	20.7	25.2

Table 2: *Summary of the beamformer SCR performance in decibels based on elevation for the 32 radial array on good conductor soil. The best SCR value is indicated in bold for each elevation and frequency.*

Elevation	**Frequency**	**Accurate Model**	**Model**				
			Average Soil	**Ignoring Soil**	**Perfect Ground**	**Ideal**	**Impedance Matrix**
Low	3 MHz	42.3	**9.0**	8.5	-9.8	8.9	0.7
	8 MHz	80.6	14.8	2.3	**23.0**	1.4	10.6
	13 MHz	107.6	**28.3**	22.7	24.8	15.2	2.6
	18 MHz	128.1	**37.4**	32.5	30.2	22.9	19.9
Medium	3 MHz	38.7	-1.2	-6.5	1.7	**3.1**	0.8
	8 MHz	81.4	11.2	10.2	**18.1**	2.0	7.9
	13 MHz	105.3	**29.3**	13.8	22.4	14.0	11.0
	18 MHz	117.3	**21.4**	11.0	12.6	11.7	8.3
High	3 MHz	54.2	**7.0**	2.3	-0.1	-1.5	5.6
	8 MHz	90.9	2.5	2.8	**15.0**	8.5	11.9
	13 MHz	98.4	**27.5**	15.4	20.7	20.7	16.3
	18 MHz	112.2	**43.6**	26.6	31.5	25.8	25.3

- Impedance Matrix: excitations use the mutual impedance matrix to attempt mutual coupling compensation (equation (9)); this is a popular approach but inaccurate in general [3].

The uncalibrated performance based on the ideal model and the performance of the mutual impedance matrix model approach discussed in Section 2.1.2 are compared in Tables 1-2 although their plots were not shown in Section 2.3. Note that the mutual impedance matrix model approach assumes that the impedance matrix in the presence of the arctic land or good soil is available. This matrix is accurate for the antenna system at hand and could be measured on-site in practice to include all ground effects on port quantities. As discussed in the literature [3], this matrix alone is limited since it only characterizes the antenna system at the circuit level and unfortunately is insufficient in correcting mutual coupling effects completely. The full radiation patterns are necessary, and this can be verified by examining the results of the last column in Tables 1-2.

The average soil model is seen to outperform other models at a majority of elevation and frequency combinations on arctic land. On good soil, the average soil model appears to outperform other models in general as well. Unlike the arctic ground results of Table 1, ignoring the soil never gives better performance on good soil. An interesting observation is that the array behaves more like a perfect monopole array at resonance around 8 MHz for all elevations in Table 2, with the perfect ground model always exceeding other models at that frequency. However, at other frequencies, better performance is generally obtained with the average soil model.

2.5 Impact of adding more and longer radials

The high sensitivity of null-steering performance to ground properties is due to the restricted size of the ground plane and empty space existing between the radials. While it is impractical to aim for a ground plane that can be considered approximately infinite, variations on the design studied in the previous sections are worth exploring.

Two other designs are considered in this section. The first design uses the same design of 32 radials per monopole, with the exception that the 12 outermost radials (pointing away from the array center) of the edge monopoles are 42 feet long instead of 32 feet. There are 28 edge monopoles around the array. This constitutes an additional 28 x 12 x 10 = 3,360 feet of radial wires. The second design uses 48 radials for every monopole and each radial is 42 feet long. This is an additional 16 radials per monopole and all radials are 10 feet longer, for a total additional radial length of 64(32 x 10 + 16 x 42) = 63,488 feet. This is almost twice the total radial length of the initial design.

The results for these two new designs are compared against those of the initial one in Tables 3-4. Performance improvements can be observed in particular for the 48 radial monopole array operating over arctic land. The improvement is more evident at low elevations where the SCR is better than the other arrays at all frequencies. At higher elevations, its performance is not as dominant and the other two arrays can give better SCR values depending

Table 3: *Comparison of beamformer SCR performance in decibels based on elevation for the different arrays made of different radials on arctic land. The best achievable SCR is shown along with the SCR obtained using the average soil model calibration. The best SCR values are indicated in bold for each elevation and frequency.*

Elevation	**Frequency**	**Accurate Model**			**Average Soil Model**		
		32 Radials	**12 Longer**	**48 Radials**	**32 Radials**	**12 Longer**	**48 Radials**
Low	3 MHz	41.2	42.0	**42.1**	6.7	7.0	**8.0**
	8 MHz	**81.5**	79.4	79.8	15.2	12.6	**16.3**
	13 MHz	105.3	107.0	**108.8**	22.0	16.1	**25.8**
	18 MHz	126.7	128.0	**128.4**	32.4	31.6	**33.6**
Medium	3 MHz	44.4	**46.2**	45.4	-13.3	-14.5	**2.7**
	8 MHz	**92.8**	88.1	91.3	**9.6**	8.4	8.3
	13 MHz	115.6	118.7	**126.7**	12.6	8.4	**16.3**
	18 MHz	**128.7**	126.4	127.2	**20.1**	17.5	19.8
High	3 MHz	47.8	**53.6**	52.7	7.4	**8.8**	7.6
	8 MHz	85.9	83.6	**89.3**	7.5	**10.3**	7.5
	13 MHz	100.6	106.4	**109.6**	17.5	17.7	**24.7**
	18 MHz	113.0	**114.4**	109.4	30.7	31.0	**33.3**

on frequency. On good conductor soil in Table 4, the 48 radial array is not as advantageous

Table 4: *Comparison of beamformer SCR performance in decibels based on elevation for the different arrays made of different radials on good soil. The best achievable SCR is shown along with the SCR obtained using the average soil model calibration. The best SCR values are indicated in bold for each elevation and frequency.*

Elevation	**Frequency**	**Accurate Model**			**Average Soil Model**		
		32 Radials	**12 Longer**	**48 Radials**	**32 Radials**	**12 Longer**	**48 Radials**
Low	3 MHz	42.3	**43.1**	42.1	**9.0**	7.7	7.3
	8 MHz	**80.6**	80.3	80.5	14.8	**23.0**	14.9
	13 MHz	107.6	108.5	**109.8**	28.3	27.8	**29.3**
	18 MHz	**128.1**	126.3	127.4	37.4	37.4	**38.3**
Medium	3 MHz	38.7	**49.1**	41.1	-1.2	**1.9**	-3.2
	8 MHz	81.4	**87.0**	82.7	11.2	15.6	**20.4**
	13 MHz	105.3	**110.1**	107.9	**29.3**	23.9	24.5
	18 MHz	117.3	**122.0**	115.9	**21.4**	21.3	21.2
High	3 MHz	54.2	**55.7**	52.8	7.0	**16.8**	5.2
	8 MHz	**90.9**	90.3	90.5	2.5	6.9	**8.3**
	13 MHz	98.4	98.2	**101.5**	27.5	**30.0**	29.6
	18 MHz	**112.2**	109.2	108.0	**43.6**	38.3	40.5

with SCR values often below those of the other two arrays even at low elevations.

From this analysis, it appears that small modifications to the monopole ground systems do not improve performance in a systematic way. Even doubling the amount of radial wire did not succeed in this endeavor. Much larger ground planes would likely be required, but are unfortunately impractical.

2.6 Radial orientation mismatch

The radial ground plane model used in previous sections assumed a constant orientation of the radials from element to element. For the 32 radial ground system, the radials of an element were uniformly separated by 11.25° around the monopole. In practice, it is possible that differences exist from element to element. To determine the impact of a possible mismatch, we model the same array on average soil, but with all radials rotated by 2.8125°. Then the manifold previously calculated in Section 2.3.1 is used for calibrating this array in a medium elevation signal scenario where the target is below the clutter. The resulting SCR performance is shown in Figure 15. The impact appears not to be catastrophic except

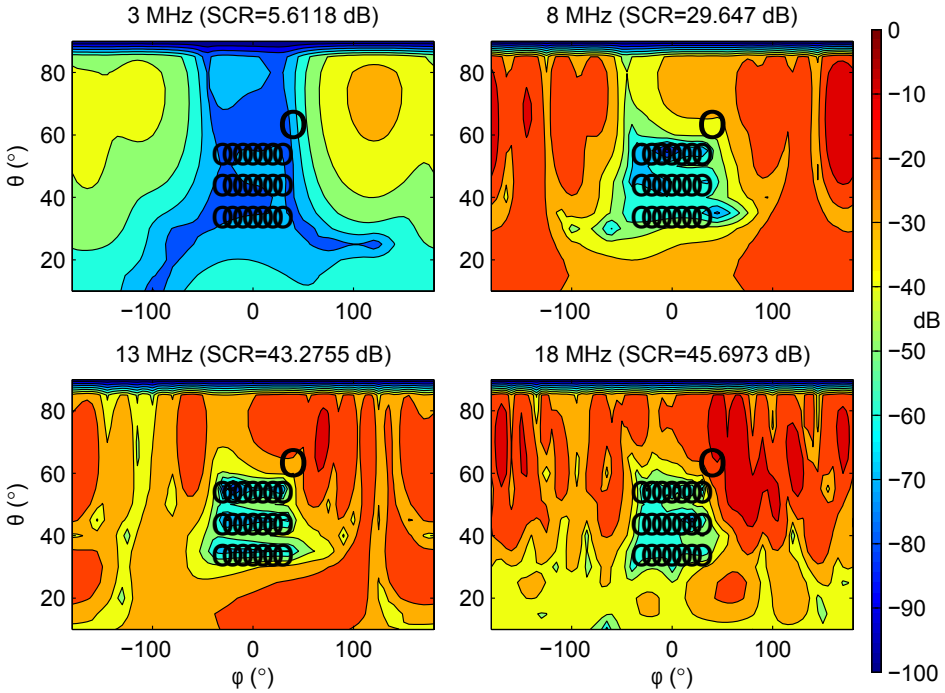

Figure 15: *Radiation patterns for desired radiation at* $(\theta, \phi) = (65°, 40°)$ *and* 21 *nulls equally spaced over* $35° \leq \theta \leq 55°$ *and* $-30° \leq \phi \leq 30°$ *with 32 radial ground system for each element over average soil with radial orientation mismatch.*

for low frequencies where the SCR only reaches approximately 5.6 dB at 3 MHz. It is important to note that in practical situations, the radial orientation mismatch tends to be random between elements and the impact on performance can be less severe than the presented case here where all radials have exactly the same deviation.

3 Cross-polarization considerations in beamforming

As discussed in Section 2.2, horizontal currents need to be taken into account when dealing with finite ground planes. Not only these currents radiate vertically polarized signals at higher elevations, but they also radiate horizontally polarized signals at all elevations. The latter cross-polarized signals can potentially affect the performance of the beamformer if not accurately accounted for [3, 14].

3.1 Cross-polarization radiation mechanism

As illustrated in Figure 16 in the simplified case of a single vertical monopole centered on a four radial ground system, the radial current I is equal at locations $(x_1, y_1) = (x, 0)$, $(x_2, y_2) = (-x, 0)$, $(x_3, y_3) = (0, x)$ and $(x_4, y_4) = (0, -x)$ on the radials. Taking into consideration the different orientations of this current at the four locations, the radial current contribution to the cross-polarized field can be expressed:

$$\begin{aligned} E_\phi(\theta,\phi) &= -I\sin\phi e^{j\frac{2\pi}{\lambda}x\sin\theta\cos\phi} + I\sin\phi e^{-j\frac{2\pi}{\lambda}x\sin\theta\cos\phi} \\ &\quad +I\cos\phi e^{j\frac{2\pi}{\lambda}x\sin\theta\sin\phi} - I\cos\phi e^{-j\frac{2\pi}{\lambda}x\sin\theta\sin\phi} \\ &= -I\sin\phi\left(e^{j\frac{2\pi}{\lambda}x\sin\theta\cos\phi} - e^{-j\frac{2\pi}{\lambda}x\sin\theta\cos\phi}\right) \\ &\quad +I\cos\phi\left(e^{j\frac{2\pi}{\lambda}x\sin\theta\sin\phi} - e^{-j\frac{2\pi}{\lambda}x\sin\theta\sin\phi}\right) \\ &= -j2I\sin\phi\sin\left(\frac{2\pi}{\lambda}x\sin\theta\cos\phi\right) + j2I\cos\phi\sin\left(\frac{2\pi}{\lambda}x\sin\theta\sin\phi\right) \end{aligned} \tag{20}$$

If $\frac{2\pi}{\lambda}x << 1$, (20) reduces to:

$$E_\phi(\theta,\phi) \approx -jI\frac{4\pi}{\lambda}x\sin\theta\sin\phi\cos\phi + jI\frac{4\pi}{\lambda}x\sin\theta\sin\phi\cos\phi = 0 \tag{21}$$

Since stronger currents are close to the monopole, the small angle approximation holds and the contributions of the radial currents to the cross-polarized fields tend to cancel due to symmetry. This can be extended in a straightforward manner to larger numbers of radials arranged symmetrically around a vertical monopole, and the same observation can be made.

Unfortunately, when placed in an array configuration, monopoles are no longer symmetrical with respect to the ground plane. With the addition of mutual coupling, strong cross-polarized fields can develop and need to be carefully considered.

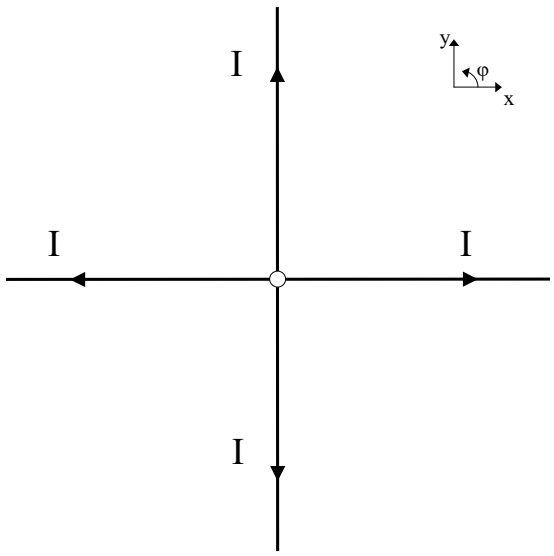

Figure 16: *Illustration of symmetric radial current in a single vertical monopole at the center of a radial ground plane. The current I flows on the radials away from the monopole.*

3.2 Cross-polarization modeling

In the context of the monopole array, the cross-polarized signal can be expressed as:

$$\mathbf{E}_{\phi}(\theta,\phi) = C\left(\mathbf{v}^{\phi}_{ideal}\left(\theta,\phi\right) + \Gamma_{\phi}\mathbf{v}^{\phi}_{ideal}\left(\theta,\phi\right)'\right) \tag{22}$$

where

$$\Gamma_{\phi} = \frac{\eta_1\cos\theta - \eta_0\cos\theta_t}{\eta_1\cos\theta + \eta_0\cos\theta_t} \tag{23}$$

$$\mathbf{v}^{\phi}_{ideal}(\theta,\phi) = \begin{bmatrix} -\sin\phi \begin{bmatrix} e^{j\frac{2\pi}{\lambda}(\sin\theta(x_1\cos\phi+y_1\sin\phi)+z_1\cos\theta)} \\ \vdots \\ e^{j\frac{2\pi}{\lambda}(\sin\theta(x_M\cos\phi+y_M\sin\phi)+z_M\cos\theta)} \end{bmatrix} \\ \cos\phi \begin{bmatrix} e^{j\frac{2\pi}{\lambda}(\sin\theta(x_1\cos\phi+y_1\sin\phi)+z_1\cos\theta)} \\ \vdots \\ e^{j\frac{2\pi}{\lambda}(\sin\theta(x_M\cos\phi+y_M\sin\phi)+z_M\cos\theta)} \end{bmatrix} \\ 0 \begin{bmatrix} e^{j\frac{2\pi}{\lambda}(\sin\theta(x_1\cos\phi+y_1\sin\phi)+z_1\cos\theta)} \\ \vdots \\ e^{j\frac{2\pi}{\lambda}(\sin\theta(x_K\cos\phi+y_K\sin\phi)+z_K\cos\theta)} \end{bmatrix} \end{bmatrix} \tag{24}$$

$$\mathbf{v}^{\phi}_{ideal}(\theta,\phi)' = \begin{bmatrix} -\sin\phi \begin{bmatrix} e^{j\frac{2\pi}{\lambda}(\sin\theta(x_1\cos\phi+y_1\sin\phi)-z_1\cos\theta)} \\ \vdots \\ e^{j\frac{2\pi}{\lambda}(\sin\theta(x_M\cos\phi+y_M\sin\phi)-z_M\cos\theta)} \end{bmatrix} \\ \cos\phi \begin{bmatrix} e^{j\frac{2\pi}{\lambda}(\sin\theta(x_1\cos\phi+y_1\sin\phi)-z_1\cos\theta)} \\ \vdots \\ e^{j\frac{2\pi}{\lambda}(\sin\theta(x_M\cos\phi+y_M\sin\phi)-z_M\cos\theta)} \end{bmatrix} \\ 0 \begin{bmatrix} e^{j\frac{2\pi}{\lambda}(\sin\theta(x_1\cos\phi+y_1\sin\phi)-z_1\cos\theta)} \\ \vdots \\ e^{j\frac{2\pi}{\lambda}(\sin\theta(x_K\cos\phi+y_K\sin\phi)-z_K\cos\theta)} \end{bmatrix} \end{bmatrix} \tag{25}$$

Note that the third sub-matrix in (24)-(25) is a null vector since the currents on the vertical monopoles do not contribute to cross-polarized radiation. Using this formulation, the same matrix C can be used to calculate both vertically and horizontally polarized radiation patterns which fully characterize the array manifold.

Unlike (8), we now consider cross-polarization in the total radiated field magnitude:

$$E_{total}(\theta,\phi) = \sqrt{\left|\mathbf{w}^H\mathbf{E}(\theta,\phi)\right|^2 + \left|\mathbf{w}^H\mathbf{E}_{\phi}(\theta,\phi)\right|^2} \tag{26}$$

The signal-to-clutter ratio is then given by:

$$SCR = \frac{\mathbf{w}^H\mathbf{E}\left(\theta_s,\phi_s\right)\mathbf{E}\left(\theta_s,\phi_s\right)^H\mathbf{w}}{\frac{1}{L}\sum\limits_{l=1}^{L}\left|\mathbf{w}^H\mathbf{E}\left(\theta_l,\phi_l\right)\right|^2 + \left|\mathbf{w}^H\mathbf{E}_{\phi}\left(\theta_l,\phi_l\right)\right|^2} \tag{27}$$

3.3 Null-steering performance analysis

The null-steering performance is evaluated when cross-polarization is ignored and when it is considered in Sections 3.3.1 and 3.3.2 respectively.

3.3.1 Null-steering performance ignoring cross-polarization

The scenario of Section 2.3.1 is considered here where the same array weights are used without consideration to cross-polarization. The resulting null-steering performance obtained with (26)-(27) is presented in Figure 17(a). Compared to Figure 9, dramatically low performance is observed, in particular at lower frequencies where the SCR reaches below 0 dB at 3 MHz. This is explained by the power in the target direction in Figure 9, which is only approximately -80 dB due to the close electrical proximity to the nulls. This is approximately equal to the cross-polarized signal magnitude in the directions of the nulls. As a result, the SCR is close to 0 dB. This strongly suggests that cross-polarization should not be overlooked.

3.3.2 Null-steering performance considering cross-polarization

Thankfully, it is very straightforward to properly consider cross-polarization in beamformers. This is done by computing a new array correlation matrix as follows:

$$R_{xx} = \sum_{l=1}^{L} \left(\mathbf{E}(\theta_l, \phi_l)\mathbf{E}(\theta_l, \phi_l)^H + \mathbf{E}_\phi(\theta_l, \phi_l)\mathbf{E}_\phi(\theta_l, \phi_l)^H \right) + \sigma_o^2 I \tag{28}$$

Substituting (28) into (7) and then (7) into (26)-(27) gives the results shown in Figure 17(b). The improvement in performance is significant compared to Figure 17(a) with SCR gains exceeding 38 dB at all frequencies.

3.4 Analysis based on elevation

Similar to Section 2.4, the performance is evaluated here for different elevation angles but this time taking into consideration the cross-polarized signal component. The results using the different calibration models are presented in Tables 5-6 for the array operating on arctic land and good soil respectively. Again, significant performance degradations are observed due to calibration model mismatches. The average soil model appears to be better in general as in Section 2.4. Ignoring soil turns out never to be better than using other models even when operating over poor conductor soil. On good conductor soil, the array tends to be closer to an ideal array of monopoles and the perfect ground model can outperform the average soil model in particular around resonant frequencies of the monopoles.

3.5 Impact of adding more and longer radials

Similar to Section 2.5, the null-steering performance is compared here for longer and more radials in the ground systems. Unlike Section 2.5, the cross-polarized signal is considered

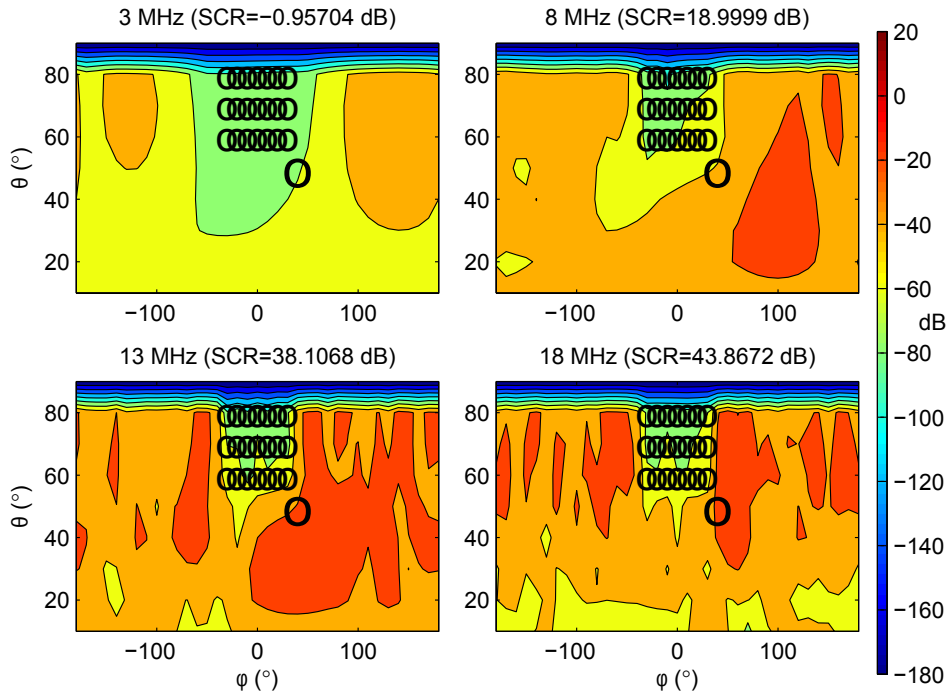

(a)

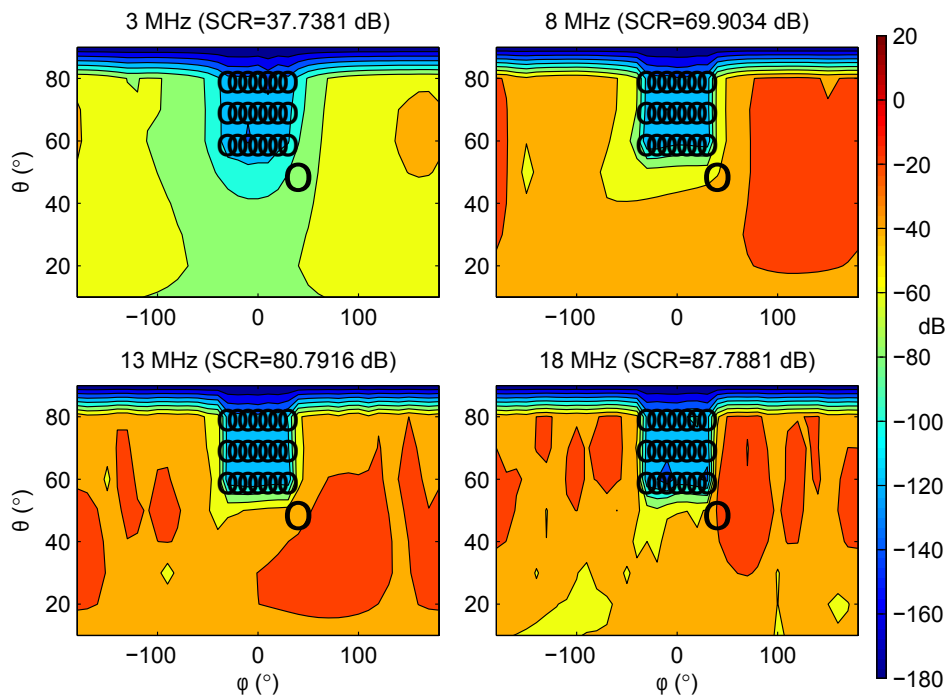

(b)

Figure 17: *Total gain patterns for low elevation signal scenario with the 32 radial ground system over average soil when cross-polarization is (a) ignored and (b) considered.*

Table 5: *Summary of the beamformer SCR performance in decibels based on elevation for the 32 radial array on arctic land (poor conductor) when cross-polarization is considered. The best SCR value is indicated in bold for each elevation and frequency.*

Elevation	**Frequency**	**Accurate Model**	**Model**				
			Average Soil	**Ignoring Soil**	**Perfect Ground**	**Ideal**	**Impedance Matrix**
Low	3 MHz	36.4	1.4	1.7	**4.7**	3.8	2.8
	8 MHz	63.1	**16.4**	15.0	18.1	5.9	14.7
	13 MHz	82.9	**24.1**	18.5	17.9	14.4	4.3
	18 MHz	88.7	**32.8**	26.4	24.8	24.8	21.9
Medium	3 MHz	34.0	-6.4	-2.1	**-0.5**	-0.6	-0.8
	8 MHz	64.5	**9.4**	5.3	5.8	-3.5	-6.7
	13 MHz	81.5	**16.7**	6.9	6.5	10.0	0.7
	18 MHz	91.6	**21.2**	2.8	8.3	11.6	6.4
High	3 MHz	41.1	**2.8**	0.3	-8.4	-2.8	-13.2
	8 MHz	64.1	-3.3	5.2	**7.9**	0.2	7.1
	13 MHz	79.1	**20.2**	15.7	10.2	14.3	4.4
	18 MHz	93.2	**27.1**	22.3	25.0	18.7	24.4

Table 6: *Summary of the beamformer SCR performance in decibels based on elevation for the 32 radial array on good conductor soil when cross-polarization is considered. The best SCR value is indicated in bold for each elevation and frequency.*

Elevation	**Frequency**	**Accurate Model**	**Model**				
			Average Soil	**Ignoring Soil**	**Perfect Ground**	**Ideal**	**Impedance Matrix**
Low	3 MHz	38.2	8.1	3.5	-10.6	**8.8**	0.7
	8 MHz	72.0	16.3	13.0	**22.5**	1.4	10.6
	13 MHz	84.3	**26.2**	16.2	24.7	15.2	2.6
	18 MHz	88.1	**40.4**	28.3	30.1	22.9	19.9
Medium	3 MHz	36.1	-0.3	-3.0	0.0	**2.5**	0.3
	8 MHz	69.6	15.4	5.8	**17.3**	1.9	7.4
	13 MHz	87.6	19.8	9.1	**22.1**	14.0	11.0
	18 MHz	93.7	**25.0**	10.7	12.6	11.7	8.3
High	3 MHz	41.6	**5.7**	0.7	-3.5	-2.5	3.3
	8 MHz	66.2	0.3	6.4	**13.2**	8.2	11.0
	13 MHz	80.7	**24.6**	8.1	20.0	20.5	15.4
	18 MHz	94.7	**41.6**	24.3	31.3	25.2	25.2

here. The results are presented in Tables 7-8 for operation on poor and good conductor grounds respectively.

Table 7: *Comparison of beamformer SCR performance in decibels based on elevation for the different arrays made of different radials on arctic land when cross-polarization is considered. The best achievable SCR is shown along with the SCR obtained using the average soil model calibration. The best SCR values are indicated in bold for each elevation and frequency.*

Elevation	**Frequency**	**Accurate Model**			**Average Soil Model**		
		32 Radials	**12 Longer**	**48 Radials**	**32 Radials**	**12 Longer**	**48 Radials**
Low	3 MHz	36.4	**38.3**	37.5	1.4	**6.6**	5.2
	8 MHz	63.1	67.5	**68.1**	**16.4**	16.2	5.4
	13 MHz	82.9	85.6	**94.4**	**24.1**	16.5	21.9
	18 MHz	88.7	98.4	**98.9**	**32.8**	27.6	32.5
Medium	3 MHz	34.0	**36.4**	34.2	-6.4	-4.0	**-2.5**
	8 MHz	64.5	**70.2**	69.2	**9.4**	5.0	7.8
	13 MHz	81.5	**91.8**	89.6	**16.7**	7.2	13.2
	18 MHz	91.6	**102.9**	101.7	**21.2**	16.0	20.5
High	3 MHz	**41.1**	**41.1**	40.5	2.8	**8.9**	6.1
	8 MHz	64.1	**68.0**	65.1	-3.3	**3.0**	-7.2
	13 MHz	79.1	85.3	**87.9**	**20.2**	14.2	18.5
	18 MHz	93.2	93.8	**94.3**	27.1	22.9	**33.0**

As in Section 2.5, there is no systematic improvement in performance with the ground system modification. Perhaps one observation can be made at medium elevations over good conductor soil where the 48 radial system appears to outperform other systems at all frequencies.

3.6 Radial orientation mismatch

Similar to Section 2.6, the radial orientation mismatch is evaluated here with all radials rotated by 2.8125° on average soil. This time, the cross-polarized signal is taken into consideration in the beamformer. The results are presented in Figure 18 for the medium elevation signal scenario of Section 2.6. Similar to Section 2.6, low frequencies suffer from the radial orientation mismatch with the SCR only reaching approximately 5.4 dB at 3 MHz. It is important to note here that unlike Section 3.3.1 where cross-polarized radiation was simply overlooked, it is duly considered in this example but the resulting performance is

Table 8: *Comparison of beamformer SCR performance in decibels based on elevation for the different arrays made of different radials on good conductor soil when cross-polarization is considered. The best achievable SCR is shown along with the SCR obtained using the average soil model calibration. The best SCR values are indicated in bold for each elevation and frequency.*

Elevation	**Frequency**	**Accurate Model**			**Average Soil Model**		
		32 Radials	**12 Longer**	**48 Radials**	**32 Radials**	**12 Longer**	**48 Radials**
Low	3 MHz	38.2	**40.8**	39.0	8.1	3.7	**8.4**
	8 MHz	72.0	**74.1**	70.6	16.3	**23.5**	7.2
	13 MHz	84.3	83.7	**85.1**	26.2	**29.7**	26.5
	18 MHz	**88.1**	87.1	86.8	**40.4**	37.3	38.6
Medium	3 MHz	36.1	**37.8**	36.3	-0.3	-4.7	**0.1**
	8 MHz	69.6	**71.1**	69.4	15.4	16.8	**18.4**
	13 MHz	**87.6**	82.1	82.3	19.8	19.4	**20.6**
	18 MHz	**93.7**	88.9	83.9	25.0	21.0	**29.2**
High	3 MHz	41.6	**45.4**	41.9	5.7	**6.4**	2.7
	8 MHz	66.2	**69.4**	67.6	0.3	**3.5**	0.1
	13 MHz	80.7	**83.5**	81.2	24.6	23.5	**28.5**
	18 MHz	94.7	**98.7**	94.3	41.6	39.0	**44.8**

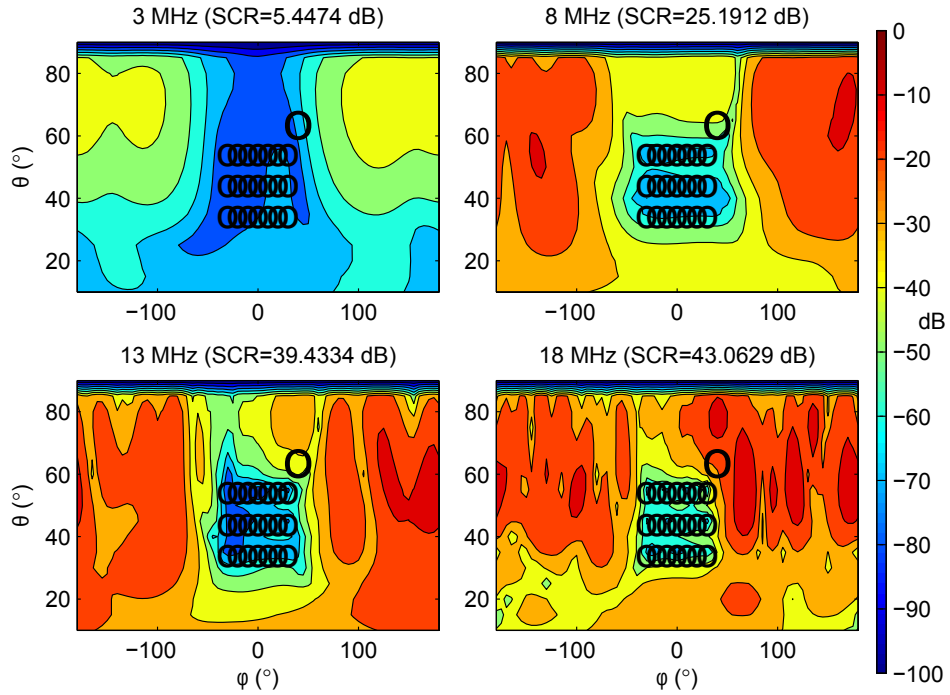

Figure 18: *Total gain patterns for desired radiation at* $(\theta, \phi) = (65°, 40°)$ *and* 21 *nulls equally spaced over* $35° \leq \theta \leq 55°$ *and* $-30° \leq \phi \leq 30°$ *with 32 radial ground system for each element over average soil with radial orientation mismatch when both vertical and horizontal polarizations are considered.*

poor at lower frequencies. This highlights the importance of having a model that matches the actual configuration of the radials, and making sure that radials do not move after installation. Again, as discussed in Section 2.6, radials in practical situations tend to have random deviations yielding less severe performance deteriorations.

4 Robust beamforming

The uncertainty on the manifold over practical grounds motivates the use of robust beamforming techniques which are less sensitive to model mismatches. These have been widely documented in the literature in [15–21]. They are generally employed in an adaptive beamformer where signal statistics in a receiver array are used to optimize performance. In the case of a transmit array, which is the case studied in previous sections, received statistics are generally not available and beamforming needs to be performed deterministically.

Multiple-input-multiple-output (MIMO) radar techniques have been developed [22–28], which can potentially perform transmit beamforming a posteriori using data statistics at the radar receiver array. Unlike traditional transmit beamformers where all array elements transmit the same signal and only change their relative amplitudes and phases, the array elements of a transmit MIMO radar transmit distinct waveforms that can be separated at the receiver. The two approaches are very different in that the first one actively attempts to focus energy toward a target and suppress energy toward the clutter while the second simply radiates energy in all directions. There is still much debate in the literature as to which one is better [24, 28], and their comparison is outside the scope of this report and will be left as future work. However, MIMO radar is based on adaptive processing which is covered in Section 5. Section 5 can therefore provide some insights on the performance of a MIMO radar.

Although robust beamforming techniques are generally used adaptively, there is no reason that they should not be used in a deterministic beamformer to try mitigating the effects of a calibration model mismatch. This is evaluated in this section. Different approaches exist to make the beamformer more robust, the majority of which simply consist in adding uncorrelated noise at each of the array elements. This is generally referred to as diagonal loading and is simply implemented by increasing the value of σ_o^2 in (6) and (28). This was shown to be optimal in [15], but an apparent open research problem with this approach remains as to how to determine the optimal value of σ_o^2. Many techniques have been reported, but they appear to be highly dependent on a user-selected parameter, such as a manifold uncertainty, that is generally unknown in practice. Notable exceptions are [19–21], but they require signal statistics and are therefore suitable only in the context of adaptive processing.

Based on these limitations, null-steering performance is evaluated in Section 4.1 in an ad hoc fashion for different diagonal loading values, and an example is presented in Section 4.2 where a value of diagonal loading is judiciously selected to potentially improve SCR

performance. Finally, improving beamformer robustness to radial orientation mismatches is examined in Section 4.3.

4.1 Null-steering performance as a function of diagonal loading for different elevations

The SCR performance is evaluated in Figures 19-21 for the low, medium and high elevation cross-polarized signal scenarios considered previously in Section 3.4, when the diagonal loading value σ_o^2 in (28) is varied from -60 dB to 20 dB. These values are relative to the target and clutter signal power levels used in the determination of the correlation matrix, which are assumed to be of unitary value in (28).

The solid curves are those of the accurate manifold and are seen to decrease dramatically with higher diagonal loading values. This is the penalty incurred due to manifold uncertainty. If one had excellent confidence in the manifold, then there would be no reason to add diagonal loading. However, in practical situations there remains uncertainty on the manifold since it is difficult to model the ground accurately. The dashed curves are those of the average soil model and show that a reasonable amount of diagonal loading can offer significant performance gains. But this comes at the expense of a reduced achievable SCR if the actual manifold were more accurate than expected.

Figure 20(a) in particular highlights the importance of a good choice for the diagonal loading parameter. A significant performance degradation is seen at 3 MHz with $\sigma_o^2 \approx -25$ dB. In this case, instead of improving performance, diagonal loading degrades it unless a better value is chosen. Figures 19-21 suggest that diagonal loading can be more helpful at low frequencies where performance gains upward of 10 dB are possible. In particular, the average soil manifold model curves at 18 MHz are observed to be more constant with more moderate possible performance gains.

4.2 Null-steering performance example for a judiciously selected diagonal loading value

The total gain patterns for the low elevation cross-polarized signal scenario are shown in Figures 22-23 for the array operating on arctic land and good soil respectively. The top plots (a) are those without diagonal loading, i.e. $\sigma_o^2 = -60$ dB, and the bottom plots (b) use the following diagonal loading values:

- $\sigma_o^2 = 0$ dB at 3 MHz;
- $\sigma_o^2 = -10$ dB at 8 MHz;
- $\sigma_o^2 = -10$ dB at 13 MHz;
- $\sigma_o^2 = -20$ dB at 18 MHz.

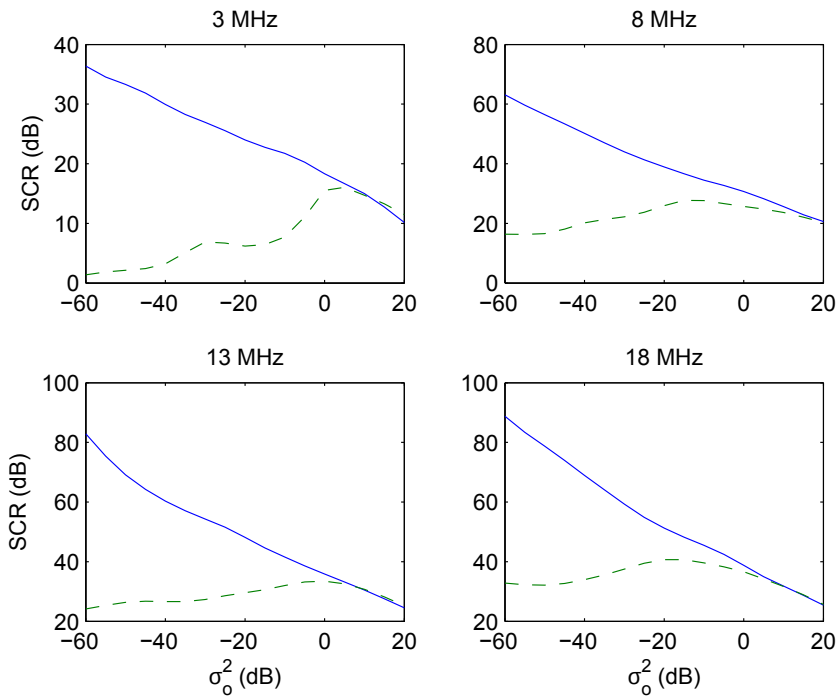

(a)

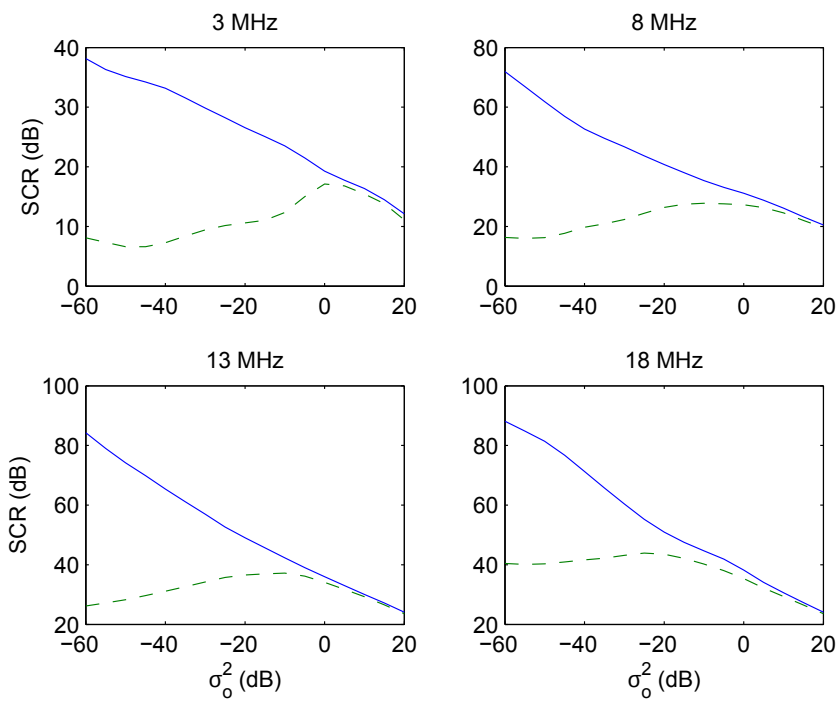

(b)

Figure 19: *SCR vs. diagonal loading value in the low elevation cross-polarized signal scenario on (a) arctic land and (b) good soil. Both the accurate calibration model performance (–) and the average soil model performance (- -) are shown.*

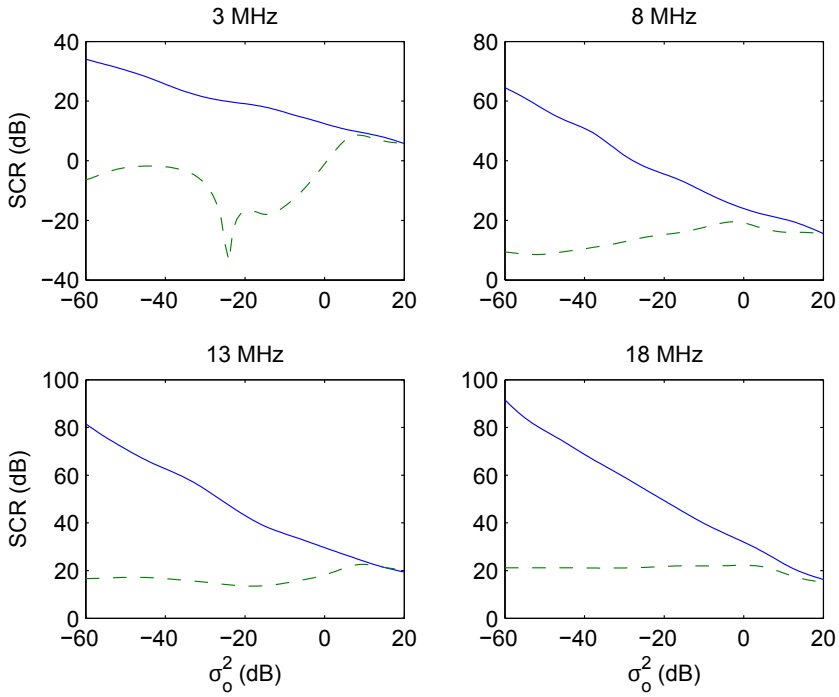

(a)

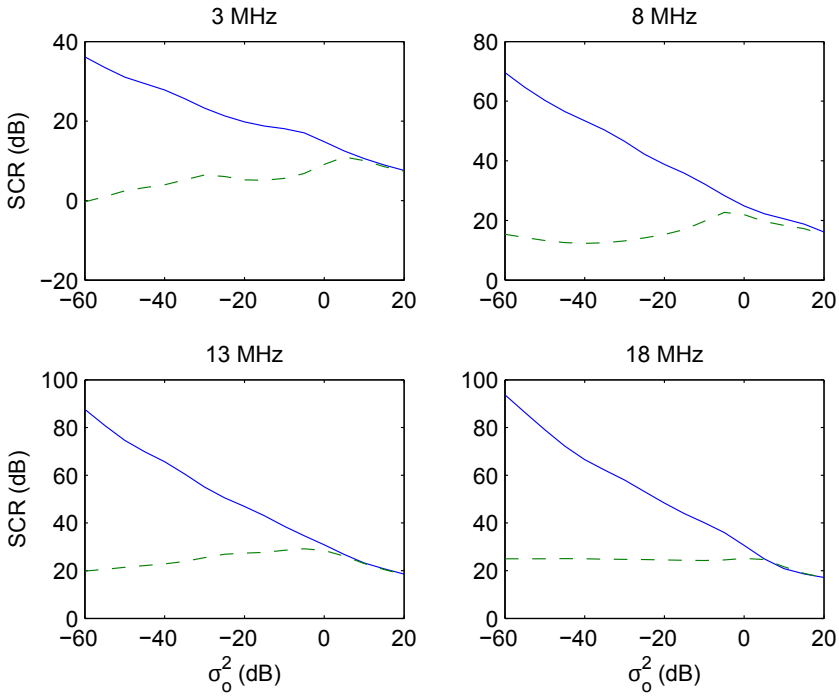

(b)

Figure 20: *SCR vs. diagonal loading value in the medium elevation cross-polarized signal scenario on (a) arctic land and (b) good soil. Both the accurate calibration model performance (–) and the average soil model performance (- -) are shown.*

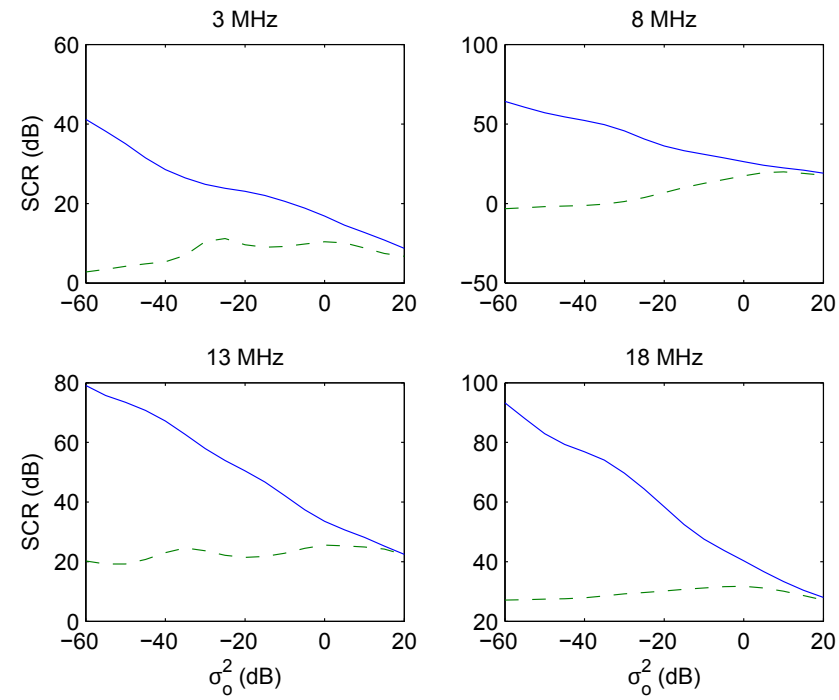

(a)

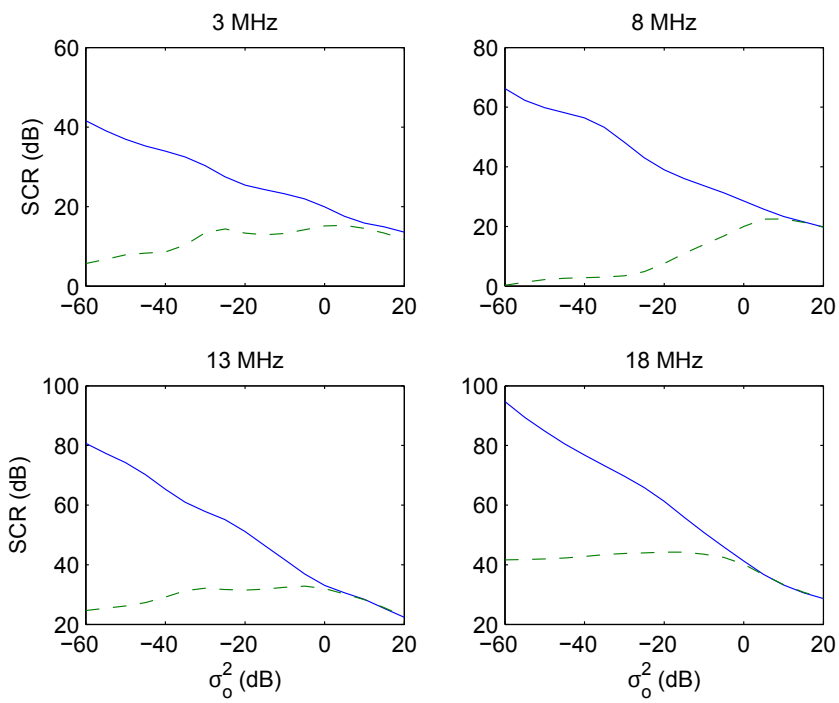

(b)

Figure 21: *SCR vs. diagonal loading value in the high elevation cross-polarized signal scenario on (a) arctic land and (b) good soil. Both the accurate calibration model performance (–) and the average soil model performance (- -) are shown.*

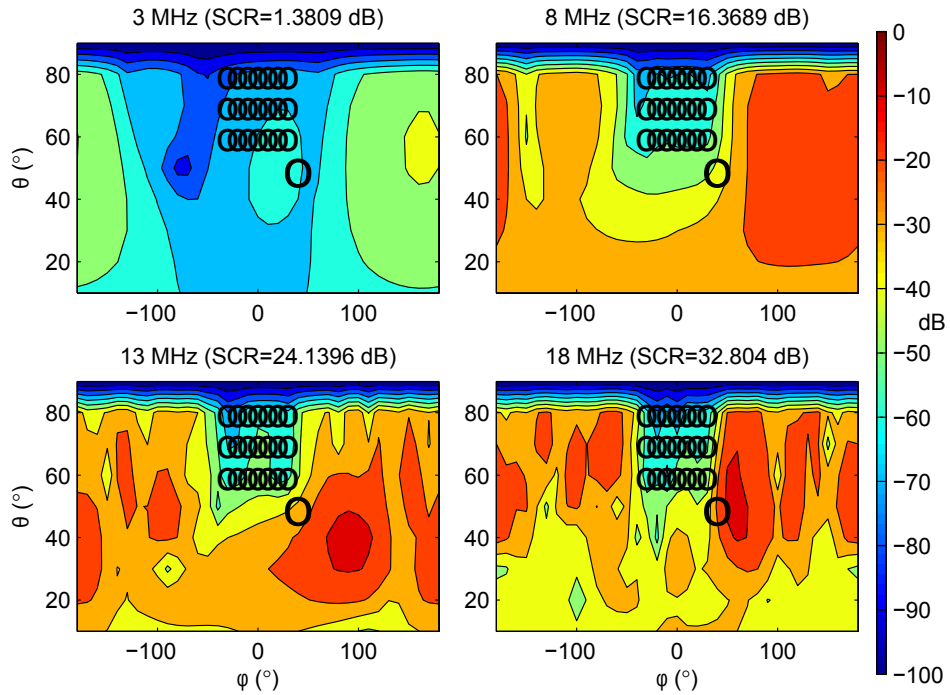

(a)

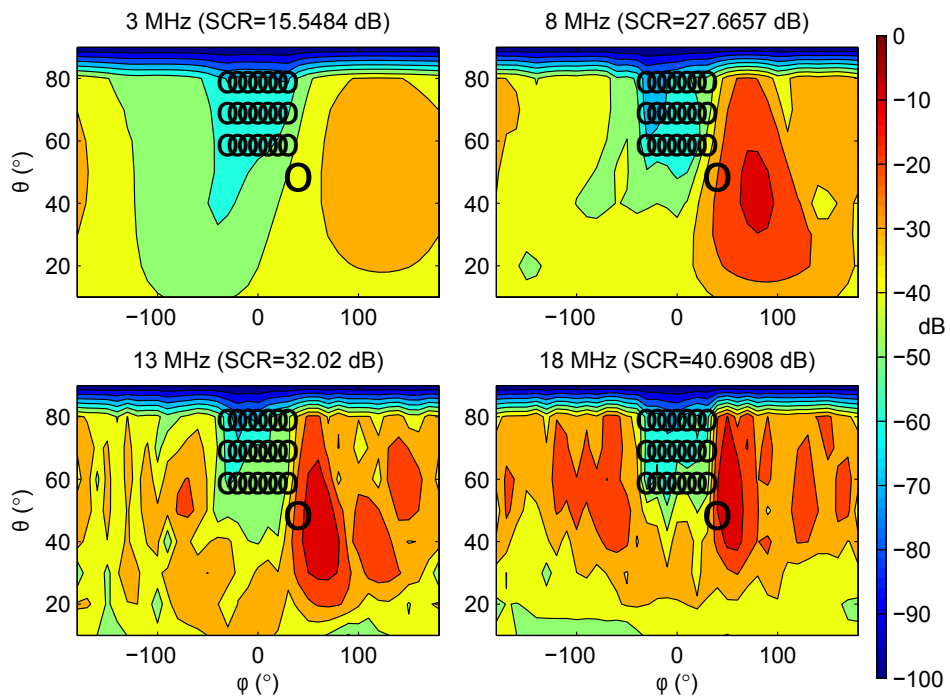

(b)

Figure 22: *Comparison of beamforming performance (a) without diagonal loading and (b) with diagonal loading for the low elevation cross-polarized signal scenario on poor soil using the average soil calibration model.*

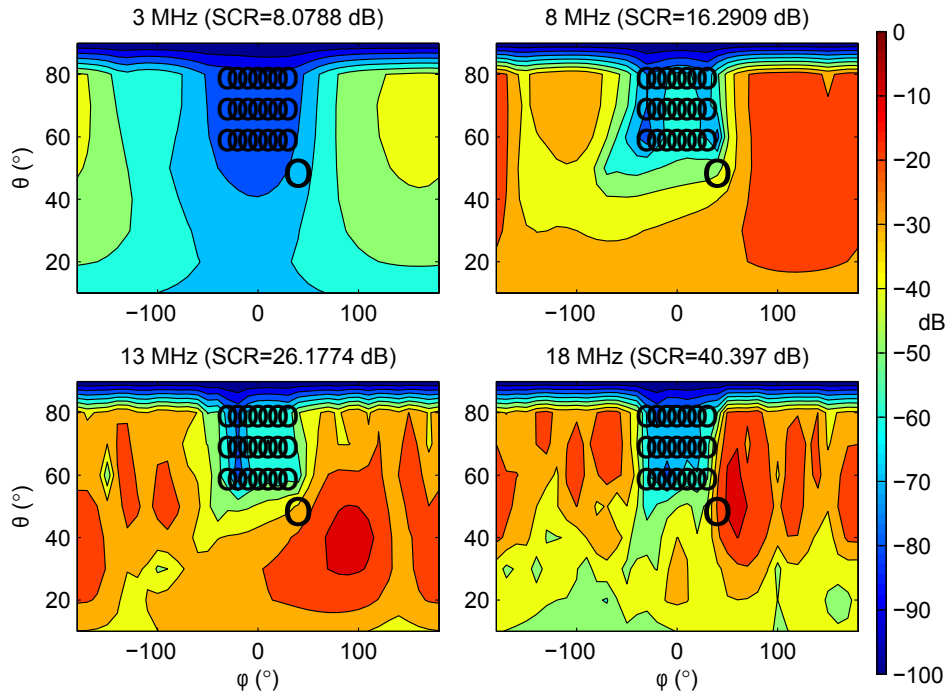

(a)

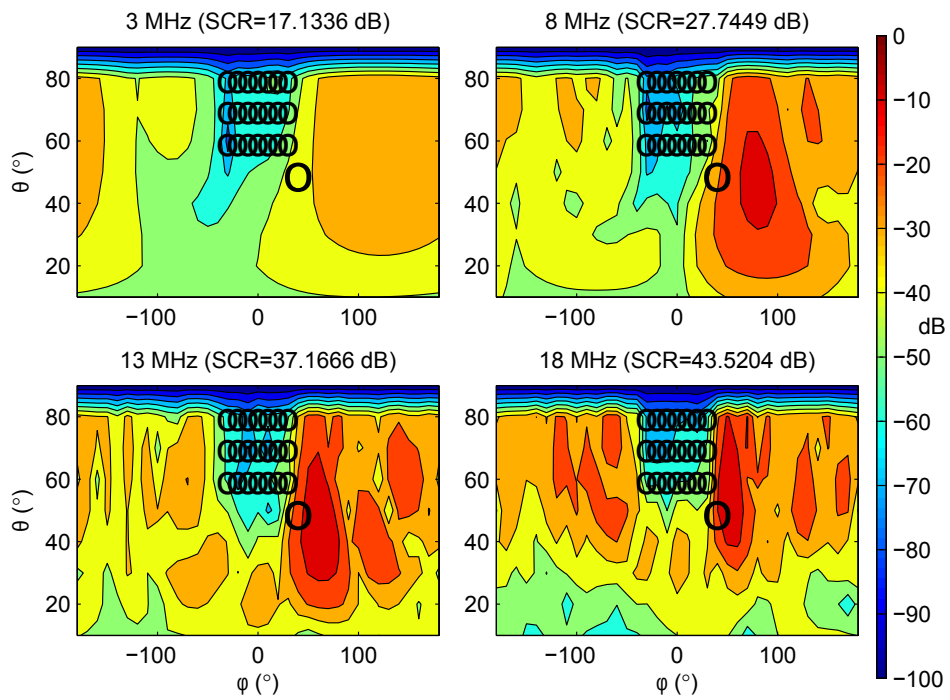

(b)

Figure 23: *Comparison of beamforming performance (a) without diagonal loading and (b) with diagonal loading for the low elevation cross-polarized signal scenario on good soil using the average soil calibration model.*

With these choices, the SCR is seen to improve at all frequencies. This is very noticeable at 3 MHz on arctic land where performance without diagonal loading was just below 1.4 dB, but improves to over 15.5 dB with 0 dB of loading. At all frequencies, the main beam is also seen to be closer to the target angle.

4.3 Radial orientation mismatch

The radial orientation mismatch studied in Section 3.6 is considered here. It was shown that null-steering performance dropped significantly at low frequencies due to the radial orientation mismatch in the low elevation cross-polarized signal scenario. We now want to determine whether diagonal loading can improve performance. The SCR is plotted as a function of diagonal loading value σ_o^2 in Figure 24. Interestingly, it is seen that modest

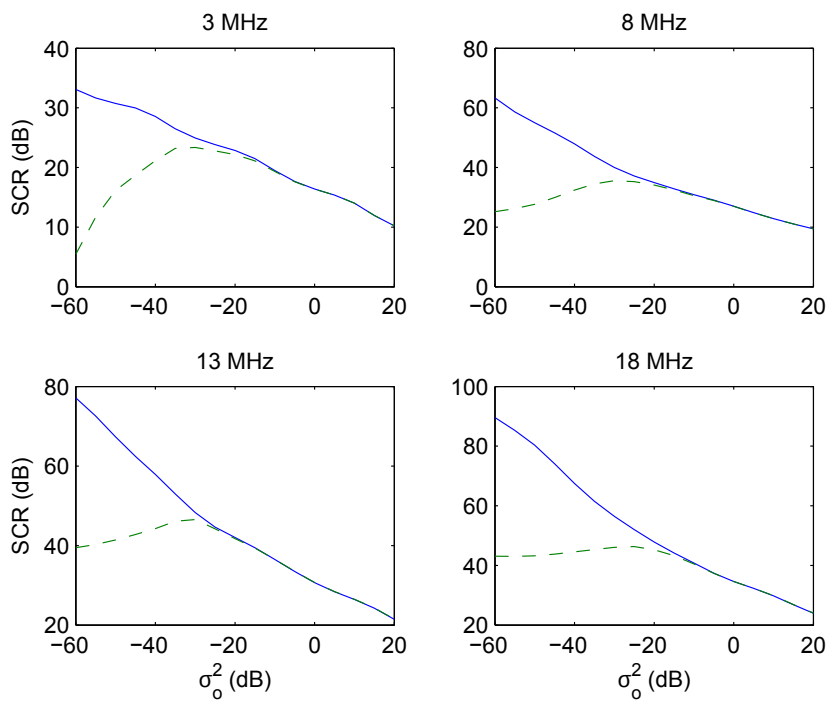

Figure 24: *SCR vs. diagonal loading value in the low elevation cross-polarized signal scenario on average soil with radial orientation mismatch. Both the accurate calibration model performance (–) and the performance with mismatch (- -) are shown.*

values of diagonal loading can increase the SCR very significantly at 3 MHz. In fact, using $\sigma_o^2 = -30$ dB at all frequencies yields the total gain patterns shown in Figure 25. Compared to Figure 18, this is an improvement of 18 dB at 3 MHz. Performance at other frequencies also improves, but to a smaller extent. Again, the drawback is that the achievable performance is reduced. But in the presence of radial orientation uncertainty, these results suggest that a minimal diagonal loading of -40 dB should be helpful.

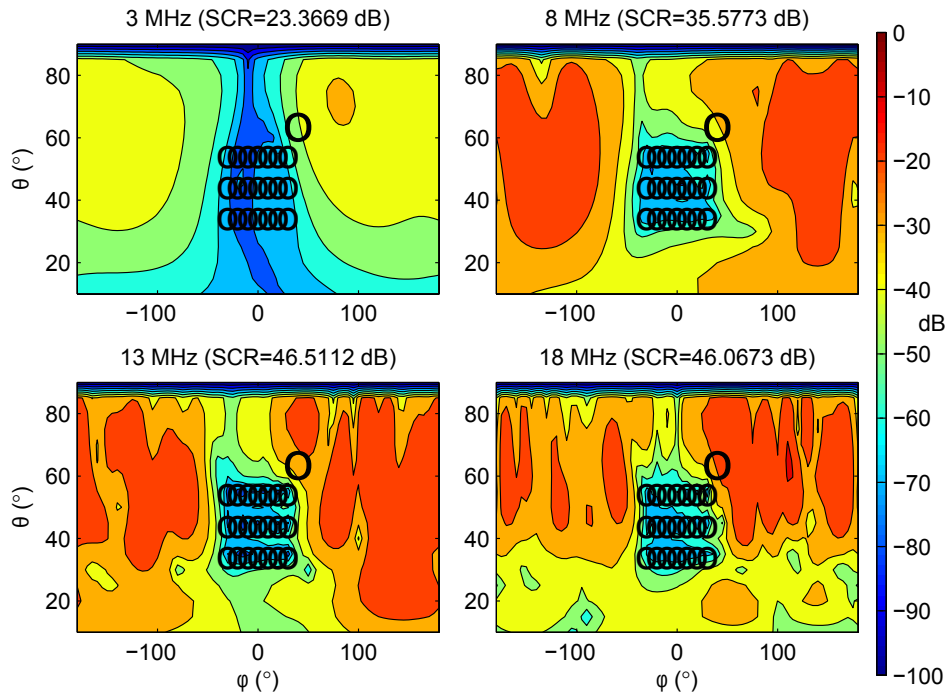

Figure 25: *Beamforming performance with $\sigma_o^2 = -30$ dB diagonal loading for the low elevation cross-polarized signal scenario on average soil with with radial orientation mismatch.*

5 Adaptive processing

As discussed earlier, transmit beamforming is often performed in a deterministic fashion since no signal statistics are available to help shape the radiation beam pattern. Due to reciprocity [3], it is possible to design a radar network where the receiver would also transmit pilot signals for the transmitter to use for forming its transmit beam pattern. However, radar transmitters and receivers are often limited to a single function, either transmit or receive, but not both. This is true for the case at hand, and we do not have the advantage of dual-function radar systems. However, it is relevant to study what would happen if this option were available. In addition, this can provide some insight into the performance of a receiving radar, including a MIMO radar, having a similar antenna array.

In an adaptive array, the correlation matrix is estimated over time using received signals as follows:

$$\hat{R}_{xx} = E\left(\mathbf{v}\mathbf{v}^H\right) \tag{29}$$

where $E(\cdot)$ denotes the expectation over time and $\mathbf{v}$ is a column vector whose entries are the received signals at each of the array elements. Assuming ergodicity and stationarity, the estimate $\hat{R}_{xx}$ approaches the actual correlation matrix as the observation time increases. The optimal weight vector can then be determined using:

$$\mathbf{w} = \hat{R}_{xx}^{-1}\mathbf{v}(\theta_s, \phi_s) \tag{30}$$

where $\mathbf{v}(\theta_s, \phi_s)$ is the steering vector or manifold in the target direction defined by elevation and azimuth angles θ_s and ϕ_s respectively.

In communication applications, it is often possible to determine weights adaptively using a known training sequence. However, this potentially forms multiple beams in directions that include multipath directions in order to optimize the gain of the array. In radar applications, this is generally not an option since we need to avoid receiving signals other than the target signal. Therefore, unlike communication systems where it is possible to ignore antenna calibration imperfections, a well-calibrated antenna array is required in radar to steer in the direction of the target using $\mathbf{v}(\theta_s, \phi_s)$. On the other hand, this is the only requirement in a receive array. Unlike the deterministic case where the calibrated array is required for forming nulls as well, it can be done automatically in a receive array simply using the estimate $\hat{R}_{xx}$. As discussed in previous sections, nulls are very sensitive to calibration errors. It is therefore expected that adaptive processing in a receive array yields better results.

A well-known issue with adaptive beamformers is that, in the presence of the target signal in the training data used to obtain $\hat{R}_{xx}$, the steering vector $\mathbf{v}(\theta_s, \phi_s)$ needs to be very accurate otherwise important performance degradations are expected. In this case, the beamformer treats the target as an interferer and simply attempts to suppress its signal. This can motivate the estimation of the correlation matrix in the absence of targets, but it is not always possible due to propagation and signal statistics changing too quickly. Robust

beamforming techniques [15–21] have been developed with this important issue in mind. Similar to Section 4 where robust beamforming was used in the form of diagonal loading in a deterministic fashion, diagonal loading is used in this section to improve performance but this time in a statistical fashion where the target signal is present in the training data of an adaptive beamformer.

Another important issue in adaptive beamformers is the potential correlation between the target signal and other reflected signals. In the presence of the target signal in the training data, correlation can degrade performance significantly even with a very accurate manifold [29]. The beamformer then treats the interference as the target signal and does not suppress it. Since it is the same signal in the OTHR that reflects off the target and the auroral clutter, it is possible that they are correlated to some extent. However, factors such as spatial separation and motion can contribute to the reduction in signal correlation. Other forms of multipath propagation are also susceptible to being highly correlated with the target signal and it appears to be worth studying. This is done in Section 5.2.

5.1 Adaptive beamforming performance with target signal in training data

The performance improvement in adaptive beamforming when the target signal is present in the training data is evaluated with a fixed diagonal loading value in Section 5.1.1 and a variable diagonal loading value in Section 5.1.2. Finally, a beamforming example is presented in Section 5.1.3.

5.1.1 Fixed diagonal loading value

The performance degradation due to the presence of the target signal in the training data is dependent on the strength of the target signal. Hence we evaluate the adaptive SCR performance here as a function of the target signal power denoted by σ_s^2. The presence of the target signal is then included using the following correlation matrix expression:

$$\begin{aligned}\hat{R}_{xx} &= \sigma_s^2 \mathbf{v}(\theta_s, \phi_s)\mathbf{v}(\theta_s, \phi_s)^H \\ &\quad + \sum_{l=1}^{L} \left(\mathbf{v}(\theta_l, \phi_l)\mathbf{v}(\theta_l, \phi_l)^H + \mathbf{v}_\phi(\theta_l, \phi_l)\mathbf{v}_\phi(\theta_l, \phi_l)^H \right) + \sigma_o^2 I \end{aligned} \tag{31}$$

The interferers at angles (θ_l, ϕ_l) are seen to have unity power in this expression and only the target and noise signal powers σ_s^2 and σ_o^2 vary. Note that σ_o^2 is also the diagonal load that can be artificially increased to make the beamformer more robust to manifold mismatches.

The adaptive SCR performance on arctic land as a function of σ_s^2 is shown in Figure 26 (a) and (b) for $\sigma_o^2 = -60$ dB and $\sigma_o^2 = 0$ dB respectively. These decibel values are relative to the interference unity power. Similarly, the same scenario is evaluated for the array operating over good conductor soil in Figure 27. Without surprise, the accurate manifold yields a constant SCR performance irrespective of the target signal strength. In practice, manifold

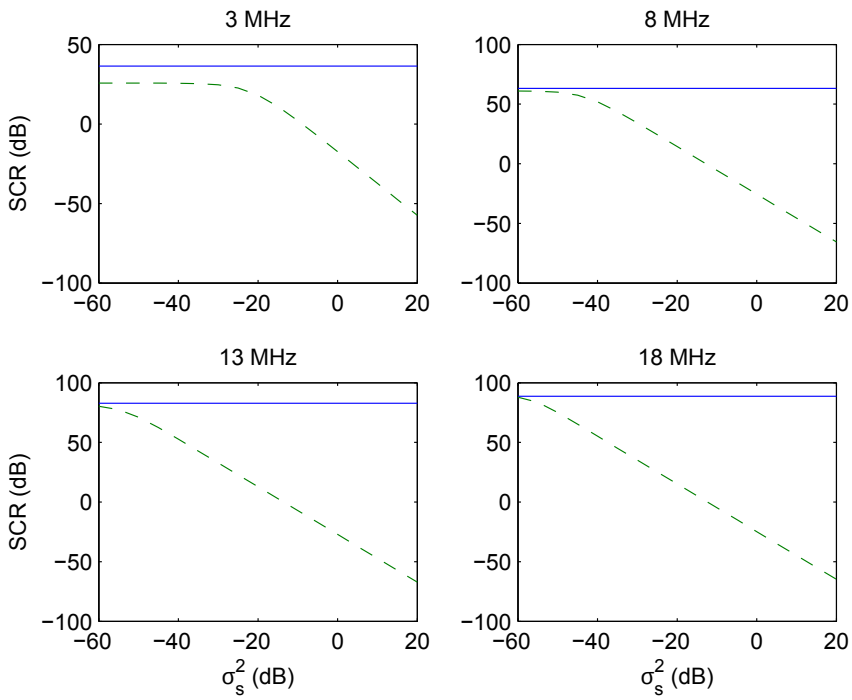

(a)

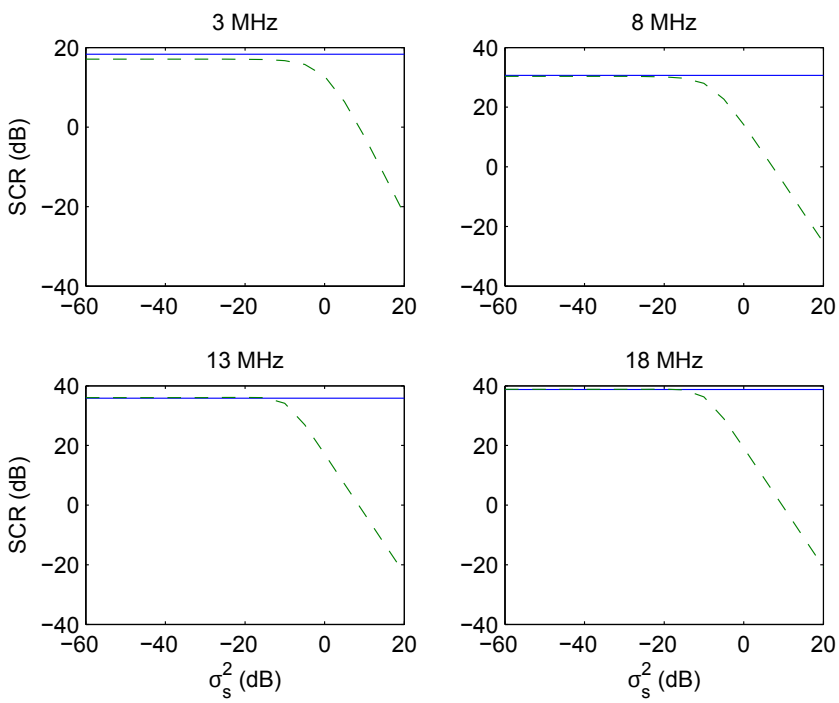

(b)

Figure 26: *Adaptive SCR vs. target signal power in the low elevation cross-polarized signal scenario on arctic land with (a) $\sigma_o^2 = -60$ dB and (b) $\sigma_o^2 = 0$ dB. Performance of accurate (–) and average soil (- -) models are shown.*

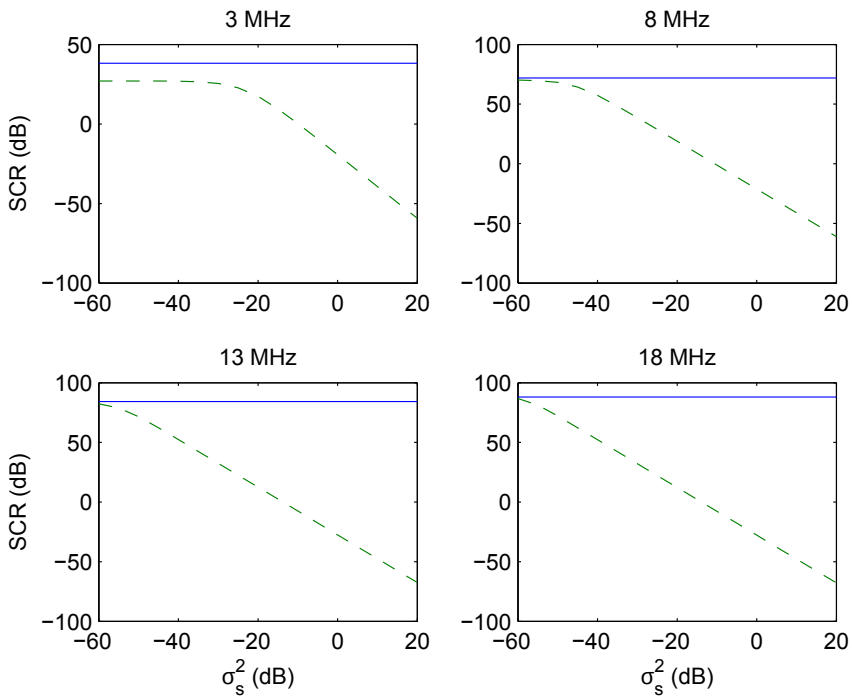

(a)

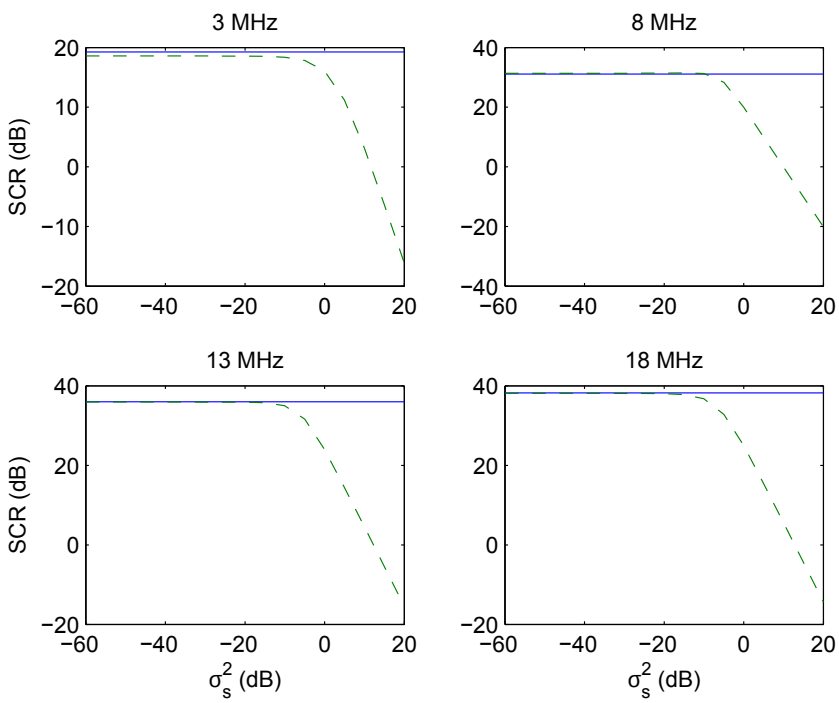

(b)

Figure 27: *Adaptive SCR vs. target signal power in the low elevation cross-polarized signal scenario on good soil with (a) $\sigma_o^2 = -60$ dB and (b) $\sigma_o^2 = 0$ dB. Performance of accurate (–) and average soil (- -) models are shown.*

errors are expected and the SCR performance using the average soil manifold model is of interest. Using this model, it is observed in Figures 26-27(a) that significant performance degradations can occur when the desired signal strength exceeds approximately -40 dB without diagonal loading applied. Lower frequencies are more tolerant where $\sigma_s^2 \approx -30$ dB still yields approximately the same performance as without diagonal loading at 3 MHz. However, beyond this value the SCR degrades rapidly. It is interesting to note that for very low values of target signal strength, or in the absence of the target signal, the achievable adaptive performance can be reduced by as much as 10 dB at lower frequencies due to the manifold mismatch. This is a result of the inaccuracy in determining the target manifold $\mathbf{v}(\theta_s, \phi_s)$. Although adaptive processing is more robust to manifold mismatches, because nulls are placed automatically using the estimated array correlation matrix, it ultimately can suffer from inaccuracies in its main beam especially at lower frequencies. The impact of diagonal loading can be appreciated in Figures 26-27(b) where a value of $\sigma_o^2 = 0$ dB is employed. The unavoidable consequence of diagonal loading is that the accurate manifold SCR decreases significantly. The average soil model SCR is also much closer to the accurate manifold SCR and over a larger range of target signal strengths. In fact, the two are seen to be approximately the same up to $\sigma_s^2 = -10$ dB at all frequencies.

5.1.2 Variable diagonal loading value

In order not to over-penalize the beamformer by using a diagonal loading value that is much stronger than the target signal, it may be more judicious to select σ_o^2 closer to σ_s^2. The results of Section 5.1.1 suggest that using $\sigma_o^2 = \sigma_s^2 + 10$ dB may be a good choice. This is evaluated in Figure 28 over (a) poor conductor and (b) good conductor soils. This approach appears to yield good results at most frequencies except at 3 MHz in particular over poor conductor soil where the SCR can drop to approximately 3 dB with $\sigma_s^2 = -60$ dB and $\sigma_o^2 = -50$ dB using the average soil model. Over good soil, performance is satisfactory at 3 MHz with a SCR close to 30 dB. These results suggest that it could be preferable to only use diagonal loading at lower frequencies when the target signal strength exceeds approximately -30 dB. At higher frequencies, it appears beneficial to use $\sigma_o^2 = \sigma_s^2 + 10$ dB for very low target signal strength as well. It is observed that using this approach yields SCR values always better than 0 dB at all frequencies for target signal strengths up to $\sigma_s^2 = 20$ dB.

On a practical note, it may very difficult to estimate the target signal strength accurately. An alternative is a search for the best diagonal loading value. This can be done by adding various values of σ_o^2 to the correlation matrix estimate and comparing all the beamformer results. This can be computationally intensive unfortunately, but it appears that no alternative exists since the manifold uncertainty is unknown in practice.

5.1.3 Example

Figures 29-30 present an adaptive beamforming example for the low elevation cross-polarized signal scenario studied in previous sections where the target signal is present in the beam-

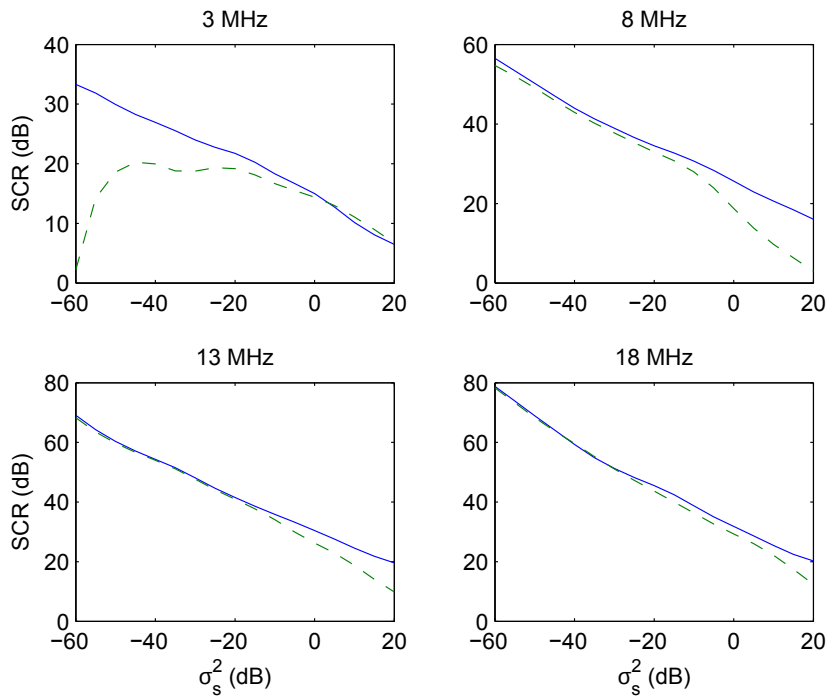

(a)

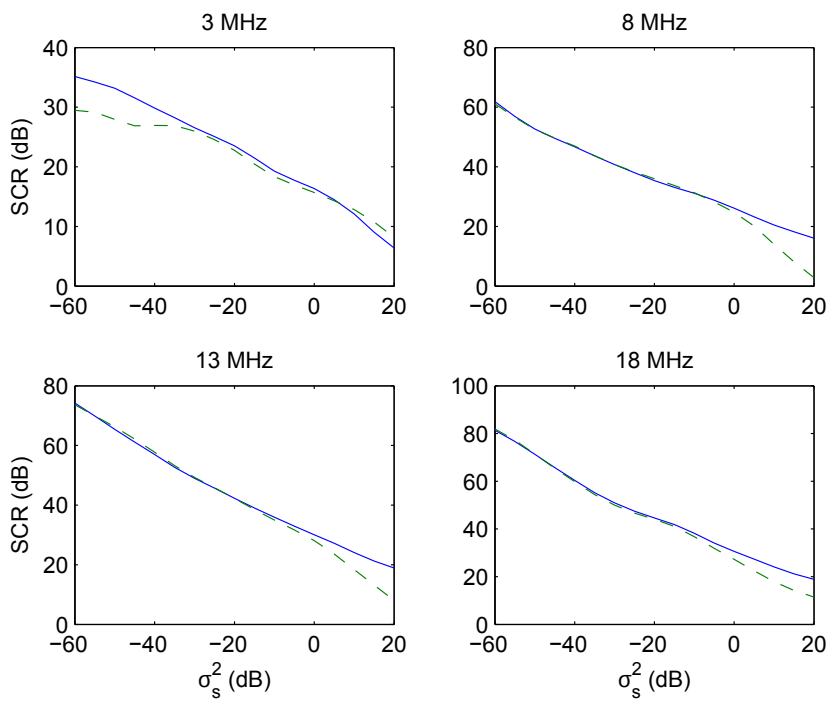

(b)

Figure 28: *Adaptive SCR vs. target signal power in the low elevation cross-polarized signal scenario for $\sigma_o^2 = \sigma_s^2 + 10$ dB on (a) arctic land and (b) good soil. Performance of accurate (–) and average soil (- -) models are shown.*

former training data at $\sigma_s^2 = -10$ dB. No diagonal loading is applied in Figures 29-30(a) while diagonal loading $\sigma_o^2 = 0$ dB is applied in Figures 29-30 (b). In both Figure 29(a) on poor conductor soil and Figure 30(a) on good conductor soil, the beamformer is seen to attempt suppressing the target signal instead of maximizing its reception, leading to very low SCR results often below 0 dB. This is due to the manifold mismatch in the presence of the target signal in the training data. Using $\sigma_o^2 = 0$ dB in Figures 29-30 (b), the beamformer performance increases significantly by at least 14 dB at all frequencies. A null no longer forms in the target direction, and the main beam is clearly seen to be much closer to the target.

5.2 Adaptive beamforming performance with target signal in training data and correlation between signals

Similar to Section 5.1, the adaptive beamforming performance in the presence of the target signal in the training data is evaluated in this section as a function of target signal strength, but with the addition of signal correlation between the target signal and interferers. Signal correlation is modeled by:

$$\begin{aligned}\hat{R}_{xx} &= \sigma_s^2 \mathbf{v}(\theta_s,\phi_s)\mathbf{v}(\theta_s,\phi_s)^H + \sigma_s\left(\rho\mathbf{v}(\theta_s,\phi_s)\mathbf{v}(\theta_L,\phi_L)^H + \rho^*\mathbf{v}(\theta_L,\phi_L)\mathbf{v}(\theta_s,\phi_s)^H\right) \\ &\quad + \sum_{l=1}^{L}\left(\mathbf{v}(\theta_l,\phi_l)\mathbf{v}(\theta_l,\phi_l)^H + \mathbf{v}_\phi(\theta_l,\phi_l)\mathbf{v}_\phi(\theta_l,\phi_l)^H\right) + \sigma_o^2 I \qquad (32)\end{aligned}$$

where ρ is the correlation value, ρ^* is the complex conjugate of ρ, and θ_L and ϕ_L are the elevation and azimuth angles of the closest interferer to the target. Fixed diagonal loading is studied in Section 5.2.1 and variable diagonal loading is studied in Section 5.2.2.

5.2.1 Fixed diagonal loading value

The signal correlation magnitude ρ in (32) can be anywhere between 0 and 1, with a value of 0 being uncorrelated and 1 being fully correlated or coherent. A value of $\rho = 0.5$ is evaluated here in Figures 31-32 over poor and good conductor soils respectively for a target signal strength varying from -60 dB to 20 dB. Unlike Figures 26-27, the accurate manifold SCR is seen to degrade as the target signal strength increases due to the correlation between the target signal and the interferer. Adding diagonal loading is seen to improve performance for target signal strengths up to -20 dB using $\sigma_o^2 = 0$ dB. This comes again at the expense of reduced achievable performance with an accurate manifold when the target signal is weak.

5.2.2 Variable diagonal loading value

Using diagonal loading $\sigma_o^2 = \sigma_s^2 + 10$ dB as in Section 5.1.2 yields the performance shown in Figure 33. Compared to Figure 28, the accurate manifold performance is seen to be lower and closer to the average soil model performance as the target signal strength becomes very large. In all cases, the SCR remains better than 0 dB up to $\sigma_s^2 = 20$ dB. As in Section 5.2.2,

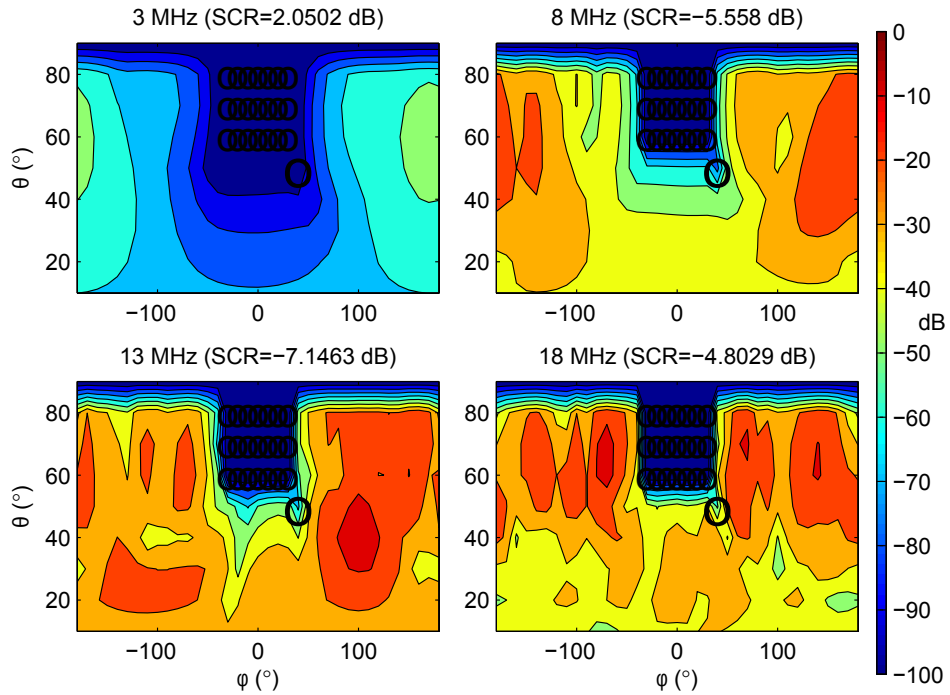

(a)

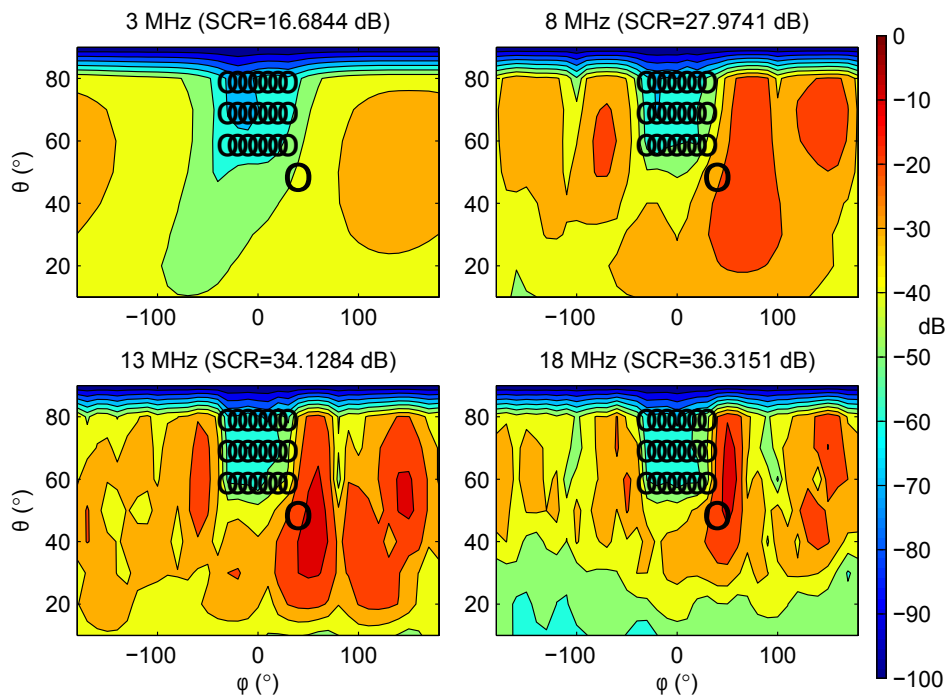

(b)

Figure 29: *Comparison of adaptive beamforming performance with target power $\sigma_s^2 = -10$ dB (a) without diagonal loading and (b) with $\sigma_o^2 = 0$ dB for the low elevation cross-polarized signal scenario on poor soil using the average soil calibration model.*

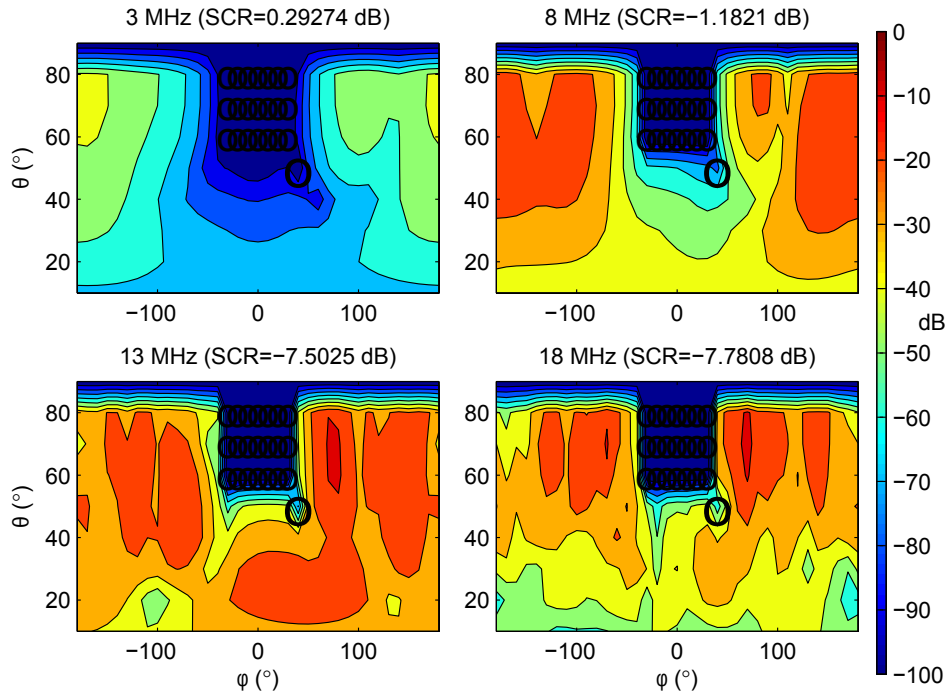

(a)

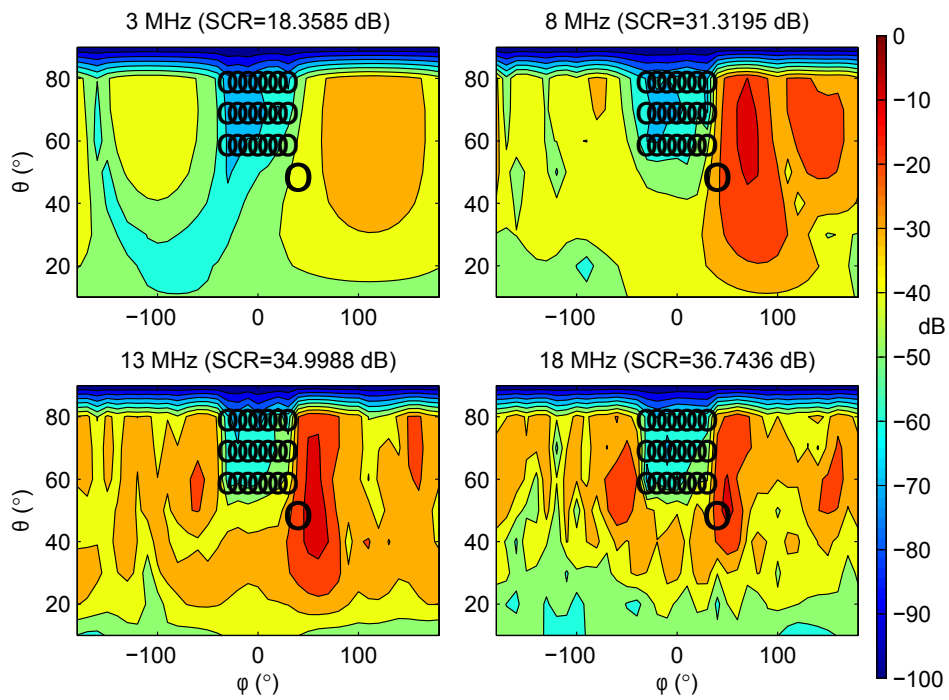

(b)

Figure 30: *Comparison of adaptive beamforming performance with target power $\sigma_s^2 = -10$ dB (a) without diagonal loading and (b) with $\sigma_o^2 = 0$ dB for the low elevation cross-polarized signal scenario on good soil using the average soil calibration model.*

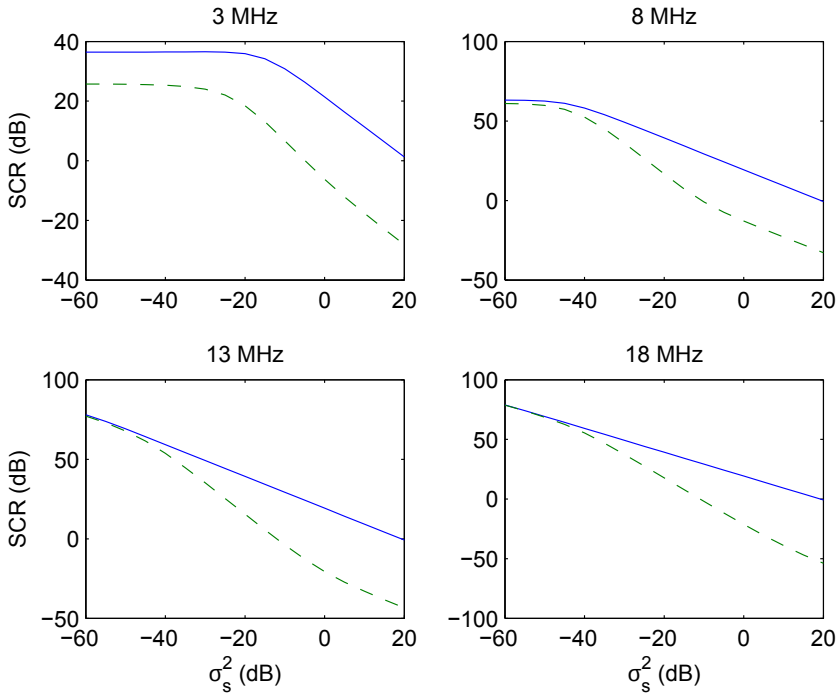

(a)

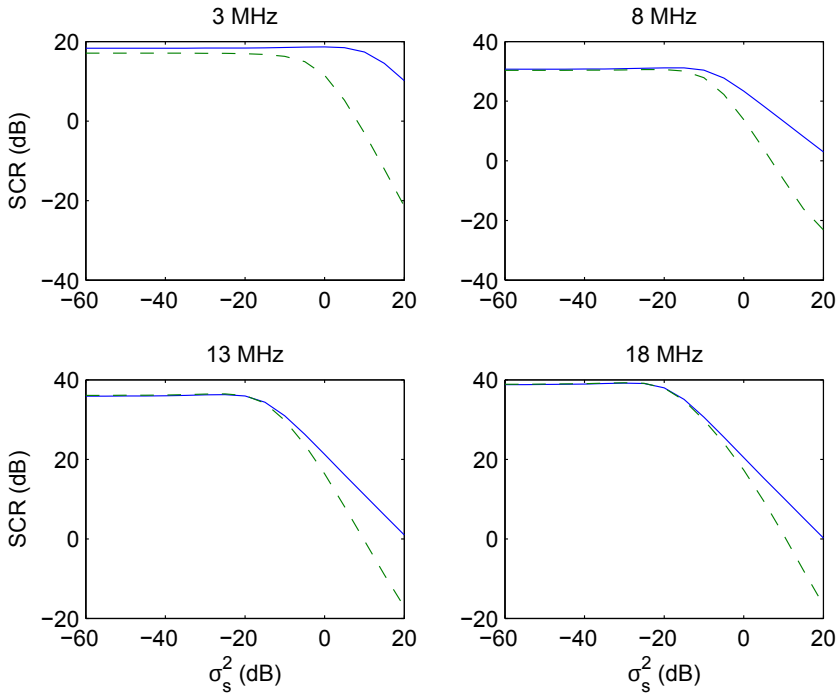

(b)

Figure 31: *Adaptive SCR vs. target signal power with correlation in the low elevation cross-polarized signal scenario on arctic land with (a) $\sigma_o^2 = -60$ dB and (b) $\sigma_o^2 = 0$ dB. Performance of accurate (–) and average soil (- -) models are shown.*

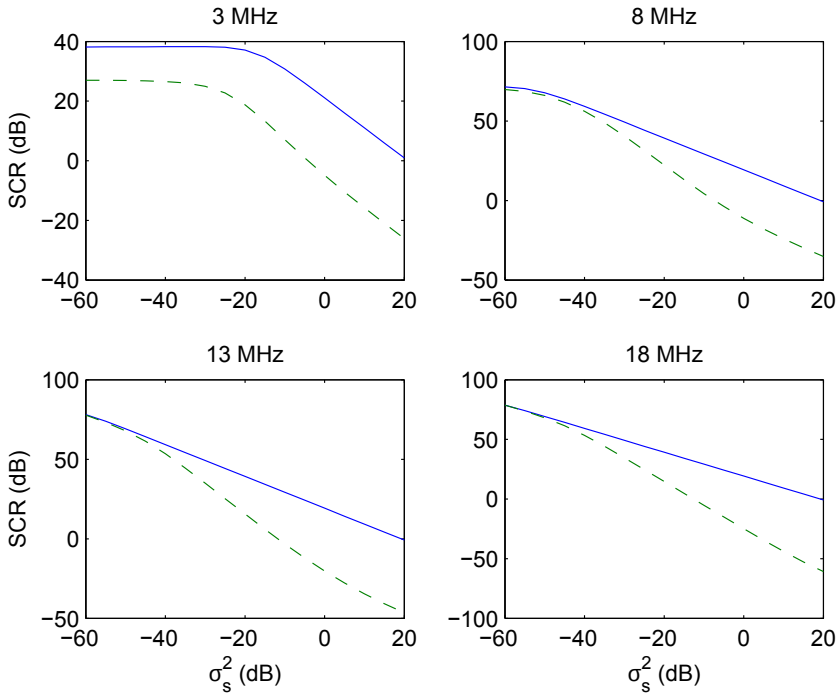

(a)

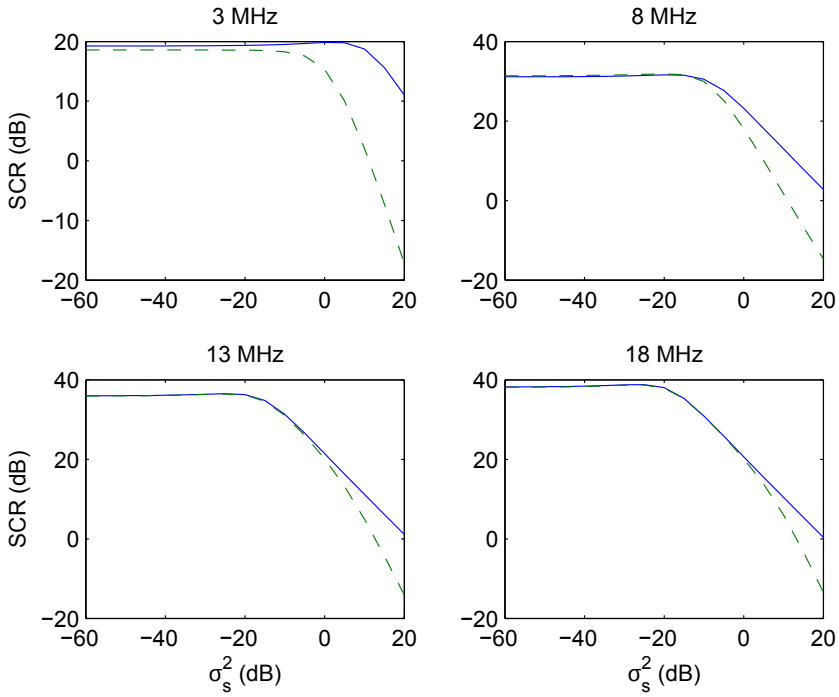

(b)

Figure 32: *Adaptive SCR vs. target signal power with correlation in the low elevation cross-polarized signal scenario on good soil with (a) $\sigma_o^2 = -60$ dB and (b) $\sigma_o^2 = 0$ dB. Performance of accurate (–) and average soil (- -) models are shown.*

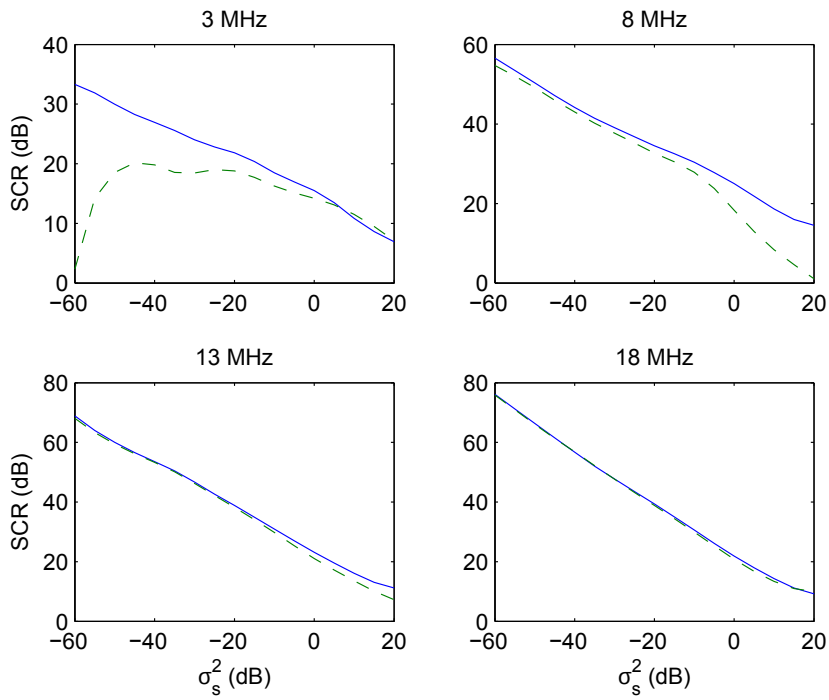

(a)

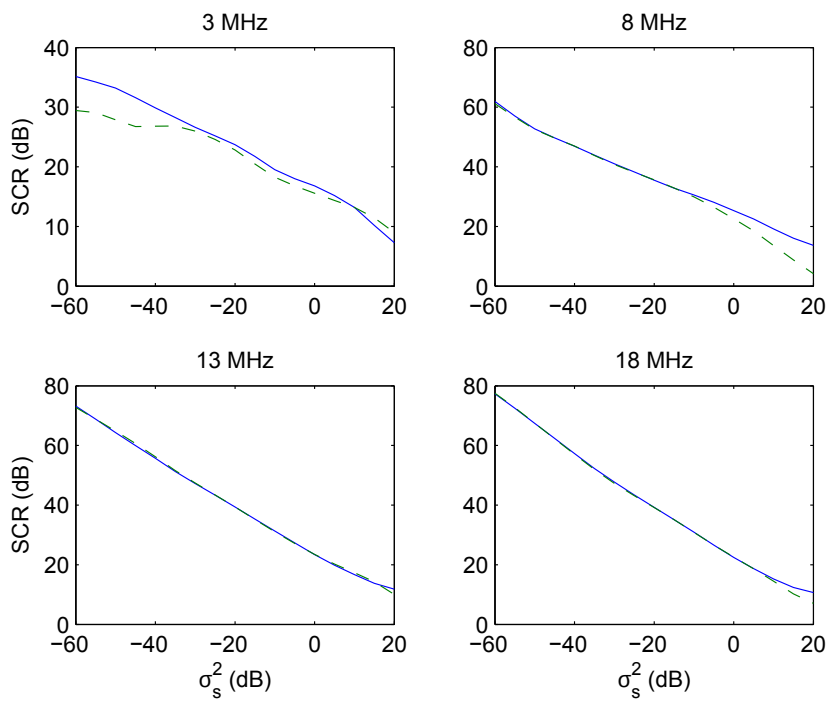

(b)

Figure 33: *Adaptive SCR vs. target signal power with correlation in the low elevation cross-polarized signal scenario for* $\sigma_o^2 = \sigma_s^2 + 10$ *dB on (a) arctic land and (b) good soil. Performance of accurate (–) and average soil (- -) models are shown.*

lower frequencies on poor conductor soil are seen to have poor performance for weaker target signal strengths when this variable diagonal loading scheme is used. With the additional signal correlation it is therefore still preferable that no diagonal loading be applied at lower frequencies up to $\sigma_s^2 = -30$ dB on poor conductor soils.

6 Determination of high power amplifier backoff

A very important practical consideration in a transmit array concerns the reflected signals due to the unavoidable impedance mismatch between the array elements and the transmit circuit. High power amplifiers have a limited tolerance to reflected power, and to avoid damaging them or render them unusable, we may have to apply a proportional reduction to the array weights. This procedure is referred to here as high power amplifier backoff.

Determining the required amplifier backoff is not trivial since weights and their reflections are dependent on the signal scenario, the array manifold and other factors such as diagonal loading. Amplifier specifications are also determining factors in the required backoff. It is important to note that the beamforming SCR performance is not affected by amplifier backoff because weights are only scaled down proportionally. However, the total radiated power is reduced and this can make a difference whether a target can be detected at the radar receiver.

Different methods are available to determine the required backoff. The first one is very crude and can work if a mechanism is in place to detect faults with the amplifiers. For example, some amplifiers can simply shut down if the reflected power is too strong. By trial and error, it is possible to begin with a large backoff and slowly decrease it until a fault is detected. The second method is more elaborate and requires additional sensors at each array element to measure the mutual impedance matrix of the array. Once this matrix is known, reflected signals can be predicted for any excitation weight vector. The third method is based on theoretical calculations of the mutual impedance matrix. In fact, this matrix was used throughout this report, but as discussed previously, there can be inaccuracies due to a ground model mismatch.

High power amplifiers are nonlinear devices and generate harmonics when strong signals are applied at their inputs. This behavior is governed by the class and output saturation specifications of the amplifiers. Harmonics can technically be eliminated using filters at the amplifier outputs to prevent the array elements from radiating them, which otherwise could create unintentional interference and possibly violate spectrum regulations. However, reflective filters are often used since they can be less bulky and more economical than absorptive filters. In turn, all the harmonics generated by the amplifiers are reflected back as well. Not only the reflections from the antennas have to be accounted for in the amplifier backoff calculations, but also the reflected harmonics.

In this section, the theoretical method is studied to determine the required backoff and the possible errors due to a ground model mismatch. The required backoff due solely to antenna

impedance mismatches is first calculated in Section 6.1. The additional backoff due to the nonlinear effects in amplifiers is calculated in Section 6.2. Finally, the total required backoff when diagonal loading is employed is evaluated in Section 6.3.

6.1 Required backoff due to mutual coupling and impedance mismatches

Reflected signals due to impedance mismatches can be calculated using:

$$\mathbf{V}^- = S\mathbf{w}^* \tag{33}$$

where $\mathbf{w}^*$ is the complex conjugate of the weight vector, and S is the array scattering matrix which can be obtained by:

$$S = (Z + Z_L)^{-1} (Z - Z_L) \tag{34}$$

where Z is the array mutual impedance matrix and Z_L is a diagonal matrix whose entries are the transmitter load impedances. These are the same matrices that were used in (10). Let V^-_{max} be the largest reflected signal magnitude in $\mathbf{V}^-$ and w_{max} the largest weight magnitude in $\mathbf{w}$. The required amplifier backoff is given by:

$$B = \frac{V^-_{max}}{w_{max}\sqrt{R_T}} \tag{35}$$

where R_T is the amplifier reflection tolerance. It is the fraction of power that is allowed to reflect back to the amplifier. If $B < 1$, no backoff is required. Otherwise, the backoff given by (35) is required. The parameter w_{max} corresponds to the maximum forward power allowed by the amplifiers. A lower value of w_{max} relative to the amplifier specification would generally increase the reflection tolerance, but for the purpose of this analysis w_{max} is always the maximum magnitude allowed, in order to maximize transmit power. Using the weight vectors calculated in Section 3.4 in the low elevation signal scenario, the required amplifier backoff B is evaluated in Figure 34 for all possible values of reflection tolerance R_T. The results indicate that the required backoff does not have a strong dependence on the ground type, especially at 3 and 13 MHz. Stronger dependence is observed at 8 and 18 MHz. Differences of over 2 dB can be observed at 18 MHz between the average and arctic grounds. Note that due to mutual coupling, it is possible that reflected signals exceed 100%. This phenomenon can be observed at 8 MHz in the case of the arctic soil. The results of Figure 34 are those obtained when the accurate manifold is used in the determination of the weight vector. In case of a manifold mismatch due to ground model uncertainty, the resulting reflection exceeding the amplifier tolerance is plotted in Figure 35 for arctic land and good conductor soil when the average soil manifold is used. Note that these results are not obtained simply by comparing the different curves of Figure 34. They require a backoff value to be determined using (35) for the average soil model, scaling the same weights in (33) using B, multiplying them with the arctic or good soil model S matrix, and finally verifying whether the resulting reflected signals exceed the tolerance. In some cases such as

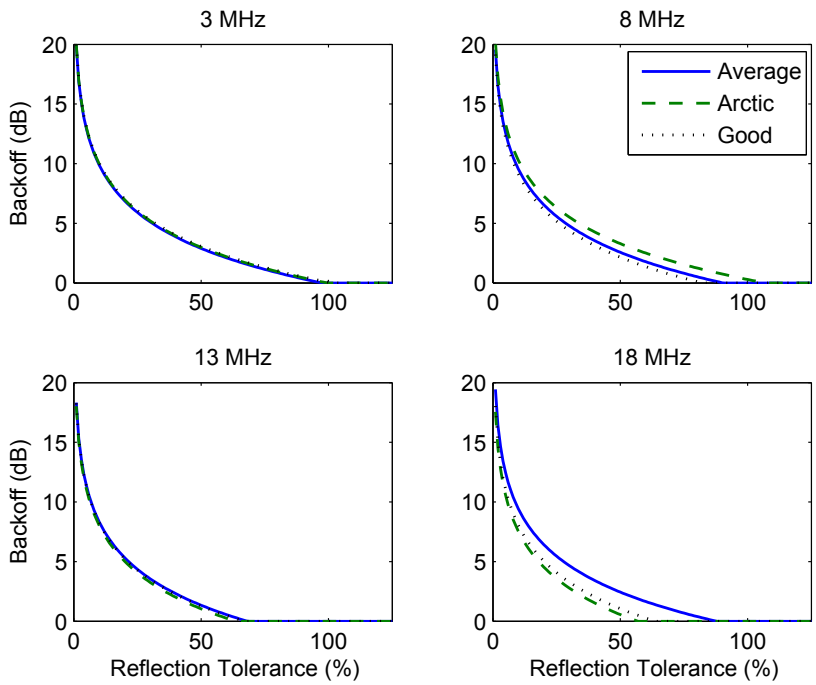

Figure 34: *Required amplifier backoff as a function of reflection tolerance in the low elevation cross-polarized signal scenario for various ground types when the accurate manifold is used.*

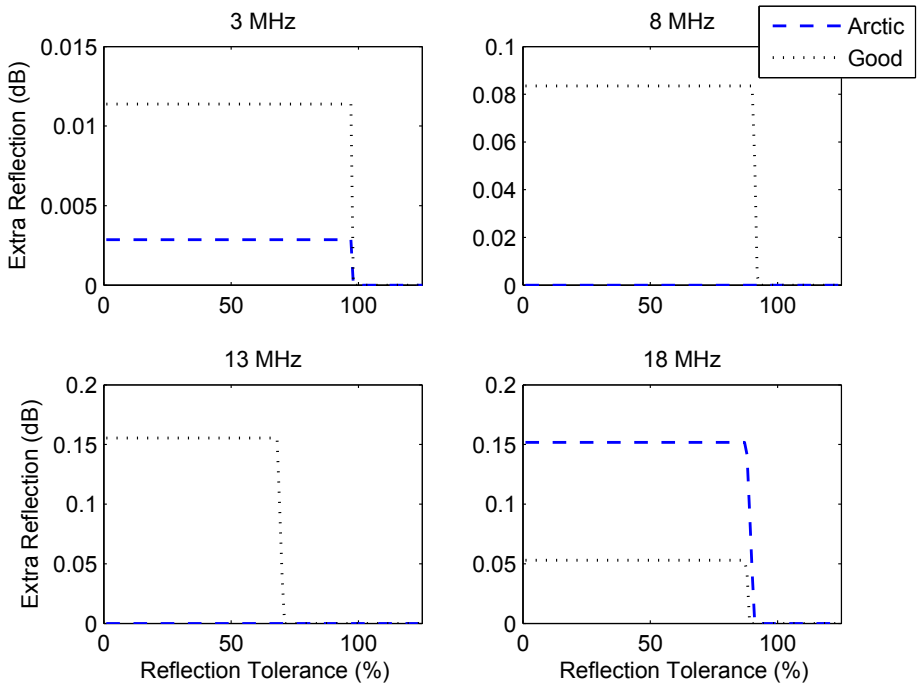

Figure 35: *Additional reflection due to the use of the average soil model manifold in the determination of the amplifier backoff, as a function of reflection tolerance in the low elevation cross-polarized signal scenario for various ground types.*

at 8 and 13 MHz on arctic soil, the backoff value is sufficient and actual reflections do not exceed the tolerance. When extra reflections are present, they are seen to be independent of reflection tolerance until $B = 0$ in (35). Beyond this point, they quickly drop to 0 dB with increasing R_T. Although there can be reflections exceeding the tolerance, these results indicate that they are relatively small with less than 0.2 dB at all frequencies. A small safety margin can be added to the amplifier backoff to address the model mismatch issue.

6.2 Required backoff due to nonlinear effects

The power transfer function of a power amplifier with gain G in decibels is shown in Figure 36. Three straight lines with slopes 1:1, 2:1 and 3:1 are shown. The first one describes the

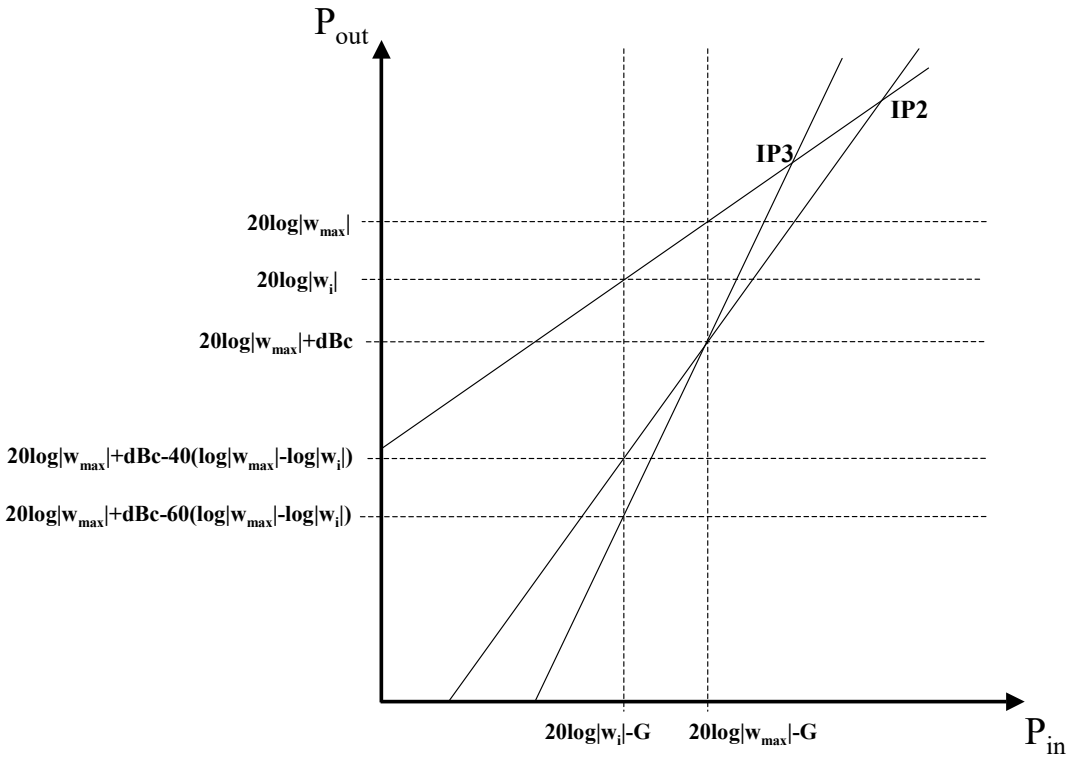

Figure 36: *Amplifier output power as a function of input power with gain G in decibels and the same harmonic specification dBc applying to both second and third order harmonics. The second and third order intercept points IP2 and IP3 are also indicated.*

main amplifying function, and in the linear regime is simply described by $P_{out} = P_{in} + G$, with P_{in} and P_{out} on a logarithmic scale. The second and third ones are the second and third order harmonic lines and intersect the first line at second and third order intercept points IP2 and IP3 respectively. These are undesired but always present in amplifiers. The amplifier specification dBc is assumed to be the same here for both second and third order harmonics, and determines the harmonic levels when the input and output powers are at their nominal value. Lower input powers simply yield weaker harmonics. To maximize output power, the weight with the largest amplitude w_{max} is made equal to the amplifier nominal output power and all the other weights are scaled proportionally. The second and third order harmonics at element i can be determined using:

$$P_{2i} = dBc - 40\left(\log|w_{max}| - \log|w_i|\right) \tag{36}$$

$$P_{3i} = dBc - 60\left(\log|w_{max}| - \log|w_i|\right) \tag{37}$$

where w_i is the weight at element i. Assuming that these harmonics are completely reflected by the filters, making their way back to the amplifiers unfiltered, and ignoring higher order harmonics, the total reflected power at element i relative to the maximum output power is given by:

$$P_i^- = \frac{{V_i^-}^2 + 10^{P_{2i}/10} + 10^{P_{3i}/10}}{{w_{max}}^2} \tag{38}$$

where V_i^- is the i-th element of $\mathbf{V}^-$ in (33). The new total required amplifier backoff is then given by:

$$B_T = \sqrt{\frac{P_{max}^-}{R_T}} \tag{39}$$

where P_{max}^- is the largest value of P_i^- for $1 \leq i \leq N$. It should be noted that the element with the largest weight w_{max} will have the strongest harmonics but not necessarily the largest impedance mismatch reflected signal V_{max}^-. Therefore it is possible that no additional backoff is required to account for nonlinear effects depending on the amplifier reflection tolerance.

The additional backoff required due to nonlinear effects is obtained by dividing (39) by (35), and is plotted in Figure 37 for average, arctic and good conductor ground types as a function of reflection tolerance for an amplifier specification of -10 dBc. The additional backoff is seen to be independent of reflection tolerance until $B = 0$ in (35). Beyond this point, it quickly drops to 0 with increasing R_T. The additional backoff required due to harmonics appears to be relatively small compared to the backoff due to impedance mismatch of Figure 34. All values in Figure 37 are in fact less than 1 dB. These results are for accurate modeling of the ground. In case there are ground model mismatches, reflections exceeding the tolerance are plotted in Figure 38. Similar to Figure 35, the extra reflections are seen to be relatively low and always less than 0.2 dB. The same additional margin could be added to the total backoff B_T to address potential ground model mismatch issues.

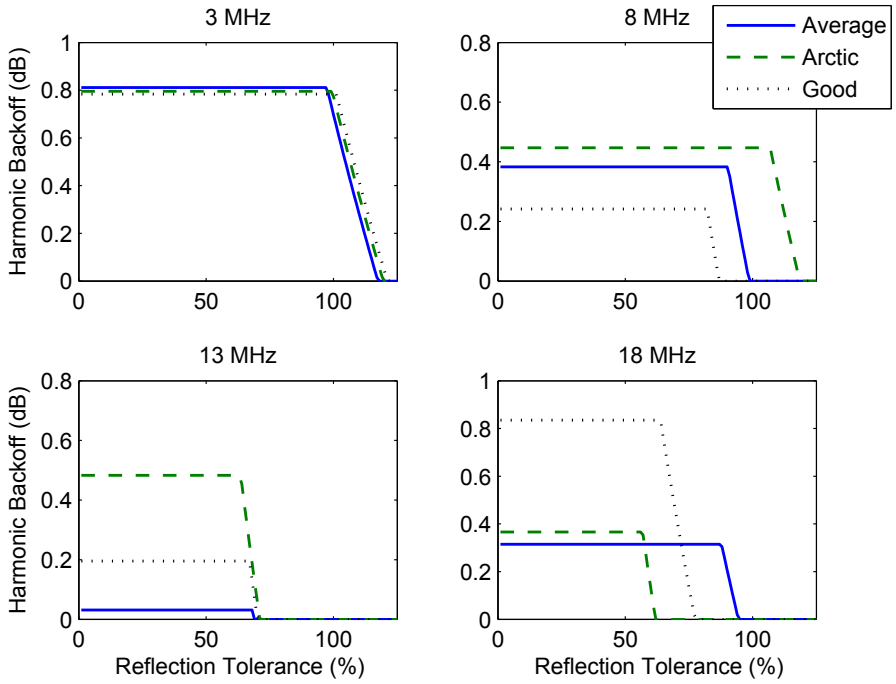

Figure 37: *Additional amplifier backoff required due to harmonic reflections as a function of reflection tolerance in the low elevation cross-polarized signal scenario for various ground types when the accurate manifold is used. The second and third order harmonic specification is* -10 *dBc.*

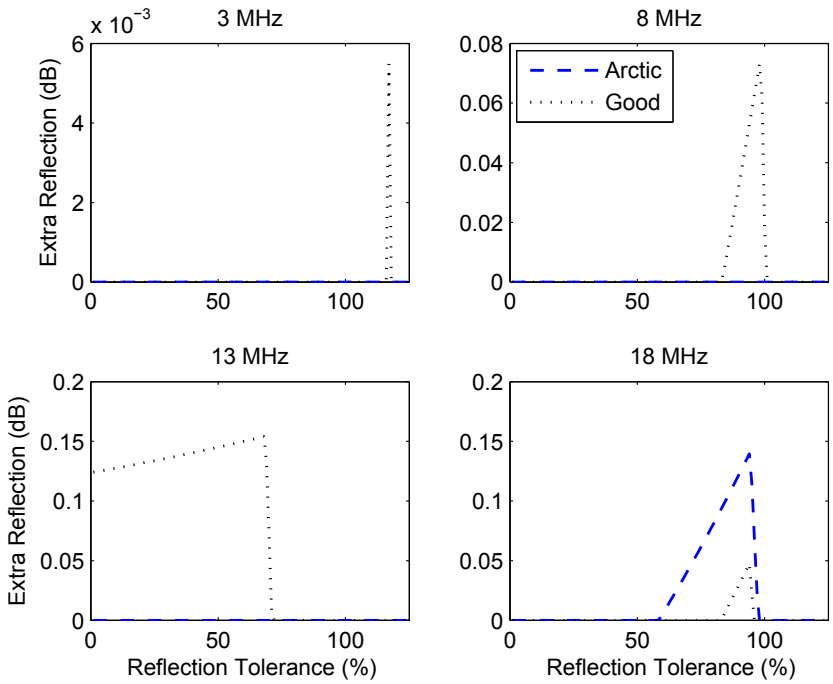

Figure 38: *Additional reflections including harmonic reflections due to the use of the average soil model manifold in the determination of the amplifier backoff and expected harmonic reflections, as a function of reflection tolerance in the low elevation cross-polarized signal scenario for various ground types. The second and third order harmonic specification is* -10 *dBc.*

A similar analysis is performed in Figures 39-40, but this time as a function of the dBc amplifier specification for a fixed reflection tolerance of 25%. It is clear in Figure 39 that

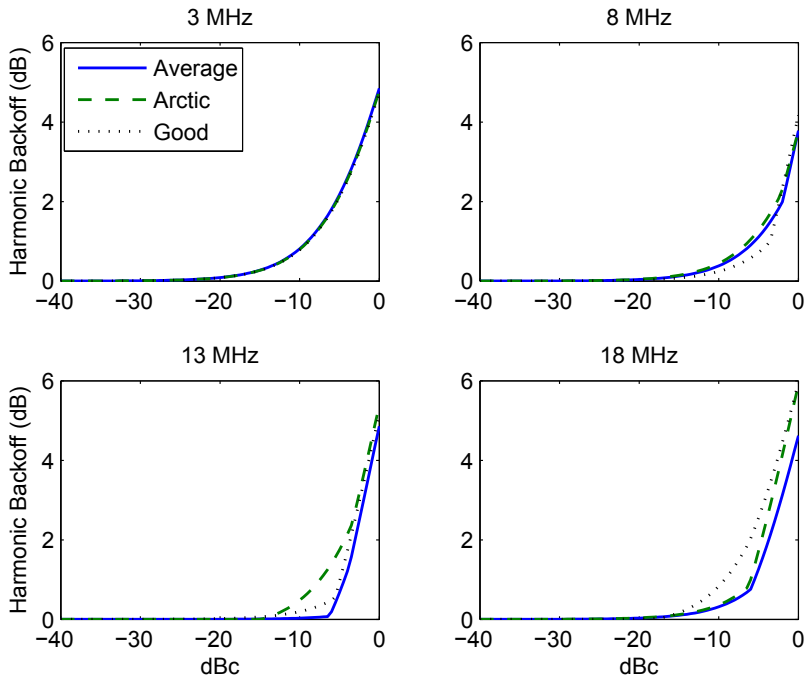

Figure 39: *Additional amplifier backoff required due to harmonic reflections as a function of amplifier specification in dBc in the low elevation cross-polarized signal scenario for various ground types when the accurate manifold is used. The reflection tolerance is 25%.*

the dBc specification can make a big difference, and it appears that using amplifiers with specifications lower than −20 dBc can eliminate the requirement for additional backoff. The reflections exceeding the tolerance in the presence of ground model mismatches in Figure 40 are again relatively small and less than 0.2 dB at all frequencies and dBc values. Therefore it appears that no additional backoff margin is necessary to account for amplifiers with different nonlinear specifications in the presence of ground model uncertainties.

6.3 Total required backoff with diagonal loading

The results of Sections 6.1-6.2 were obtained with weights calculated without diagonal loading. As discussed in Sections 4-5, diagonal loading can improve beamforming performance when there are manifold uncertainties. This is likely the case in the OTHR monopole array. To evaluate the impact of diagonal loading on the required amplifier backoff, the amplifier specification and reflection tolerance are fixed at −10 dBc and 25% respectively. The total backoff is calculated with (39) using various values of σ_o^2 in (28) to determine the beamformer weights in (7). The resulting total required backoff is plotted in Figure 41 for the

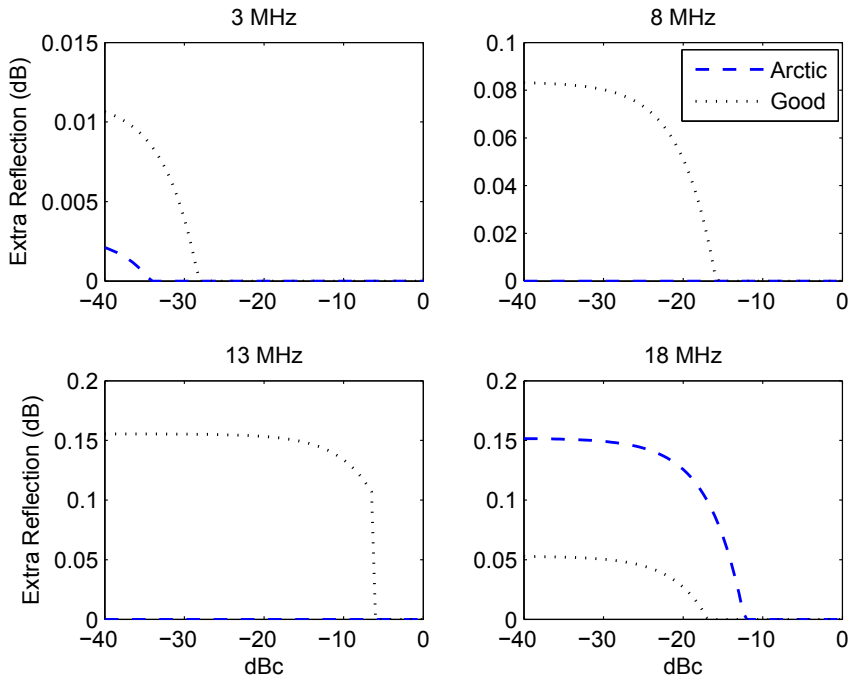

Figure 40: *Additional reflections including harmonic reflections due to the use of the average soil model manifold in the determination of the amplifier backoff and expected harmonic reflections, as a function of amplifier specification in dBc in the low elevation cross-polarized signal scenario for various ground types. The reflection tolerance is 25%.*

low elevation cross-polarized signal scenario. The backoff fluctuations can be significant

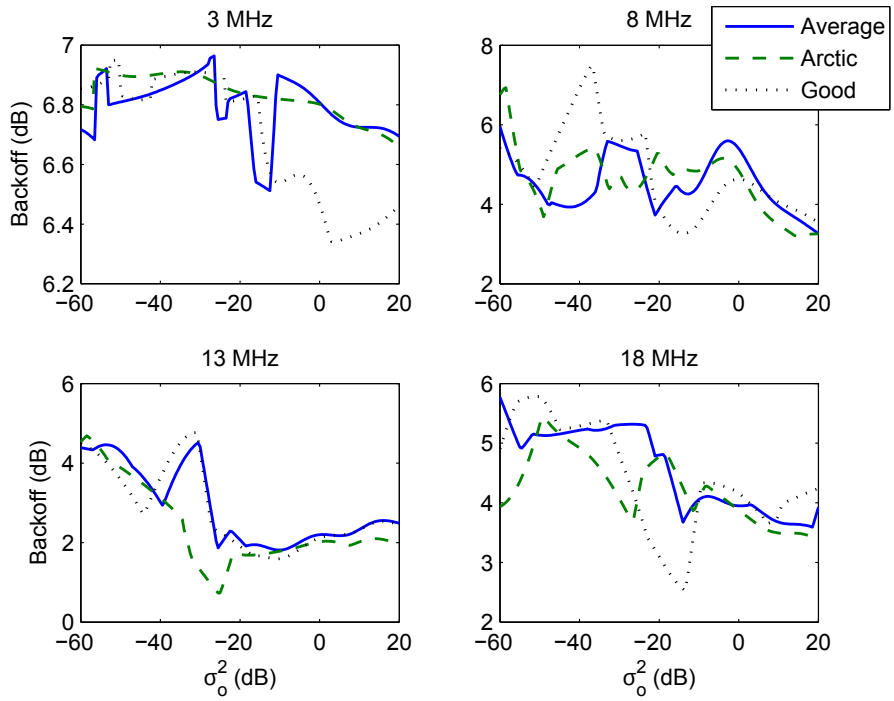

Figure 41: *Total amplifier backoff required as a function of diagonal loading in the low elevation cross-polarized signal scenario for various ground types when the accurate manifold is used. The amplifier harmonic specification is* -10 *dBc and the reflection tolerance is 25%.*

depending on frequency. In particular, the results at higher frequencies are interesting. At 13 MHz, a value of $\sigma_o^2 = -10$ dB was selected in Section 4.2 to significantly improve beamforming SCR performance. This same value is seen to lower the required backoff by over 2 dB for any ground type. Another example is at 18 MHz on good conductor soil where a value of $\sigma_o^2 = -20$ was selected in Section 4.2 and here also lowers the required backoff by over 2 dB. The reflections exceeding the tolerance with ground model mismatches as a function of diagonal loading are shown in Figure 42. With this signal scenario and amplifier specifications, only on good conductor soil do reflections exceed the tolerance, but again only by magnitudes lower than 0.2 dB, which can be prevented by a small margin added to the backoff.

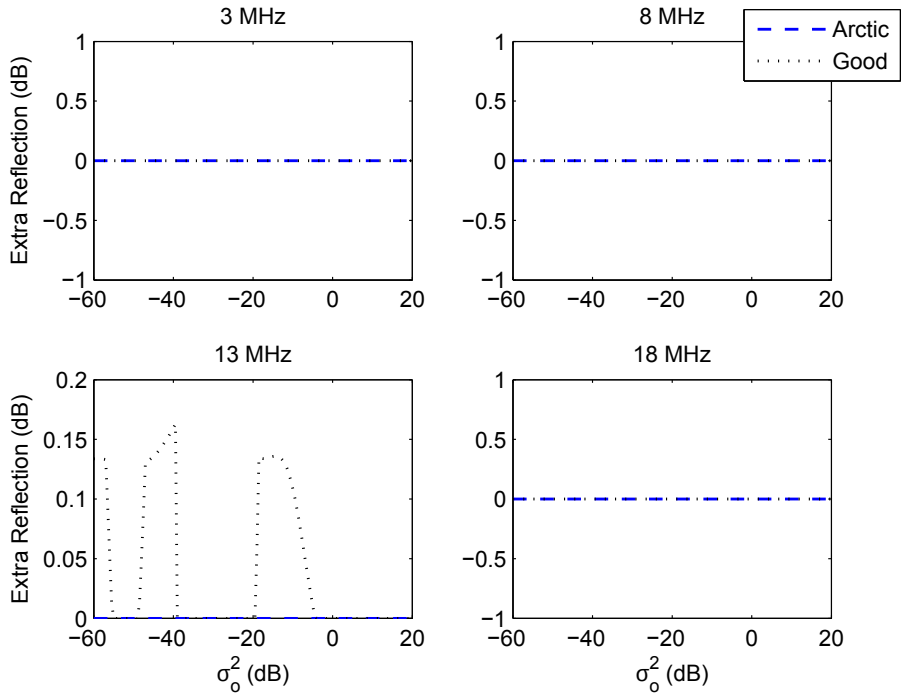

Figure 42: *Additional reflections including harmonic reflections due to the use of the average soil model manifold in the determination of the amplifier backoff and expected harmonic reflections, as a function of diagonal loading in the low elevation cross-polarized signal scenario for various ground types. The amplifier harmonic specification is* -10 *dBc and the reflection tolerance is 25%.*

7 Conclusions

The challenges of monopole arrays operating close to the ground in an OTHR radar were demonstrated in this report. A comprehensive methodology was presented to calculate the monopole array manifold for arbitrary azimuth, elevation and polarization. Results were discussed for a 64 element regular planar monopole array, and the calculated manifold obtained by this work can be used to calibrate the experimental OTHR array. They were used for theoretically predicting auroral clutter suppression performance with several error mechanisms. In particular, performance was shown to be very sensitive to ground properties. This is an important conclusion because it is very difficult to accurately model the ground in practice, and ground model mismatches are unavoidable. The assumptions of ideal antennas or perfect monopoles were determined to be very poor approximations, and using the average ground model may be a good tradeoff to mitigate ground model uncertainties. Notwithstanding these conclusions, it may be reassuring to know that clutter suppressions exceeding 40 dB are possible with an accurate ground model and these numbers increase with frequency.

Based on the results presented in this report, it is recommended that cross-polarization be always considered in clutter suppression since cross-polarized radiation in the clutter direction can be at levels similar to those in the target direction. This is particularly true at lower frequencies where proximity between target and clutter directions is more challenging due to longer wavelengths.

It was determined that small modifications to the monopole ground system, such as adding radials or making them longer, does not improve performance systematically. However, care must be taken to orient radials correctly and ensure that they do not move after installation, otherwise important performance deteriorations are possible at lower frequencies. These can be mitigated to some extent by diagonal loading, a process where noise is artificially added to the array correlation matrix that is used in beamforming. This makes the array more robust to model uncertainties and was shown to potentially improve performance significantly with uncertainties on ground properties as well. However, the amount of diagonal loading needs to be judiciously selected and the main drawback is that the achievable performance in case the ground model is accurate decreases.

When adaptive array processing is used, it was shown that one should aim at estimating the correlation matrix in the absence of the target signal in the training data. Otherwise, diagonal loading should be employed with a level approximately 10 dB higher than the target signal. At lower frequencies, it was observed that diagonal loading should be avoided for a target signal less than 30 dB lower than the clutter in the presence of ground model uncertainties. In practice, these relative levels are difficult to estimate. Therefore, a search for the best diagonal loading level could be performed using the received signals but this is a computationally intensive procedure. Correlation between target and clutter signals was shown to potentially degrade performance even more. Unlike the uncorrelated case where the achievable performance with an accurate manifold remains constant with an increasing

target signal level, the achievable performance degrades when the target and clutter signals are correlated and the performance is only worse with ground model mismatches. It was also observed that even in the absence of the target signal in the training data, the adaptive clutter suppression can drop by 10 dB at lower frequencies due to a ground model mismatch. All these results on adaptive processing are not only insightful with respect to a receive OTHR beamforming array, but also to a MIMO radar, as well as a transmit OTHR array that could also estimate signal statistics.

It was determined that high power amplifier backoff seems to be unavoidable due to mutual coupling and impedance mismatches unless the amplifier can sustain more than 100% reflection. A ground model mismatch only adds a relatively small reflection that exceeds tolerance and a small additional backoff margin can be used to address ground model mismatch issues. To prevent nonlinear effects from affecting OTHR performance, the additional backoff required was found to be relatively small as well and rapidly decreases with better amplifier specifications. With harmonic specifications less than -20 dBc, almost no additional backoff is necessary. Significant amplifier backoff variations were observed with diagonal loading. When the diagonal loading level is judiciously selected, not only can clutter suppression improve but also the radiated power level. It should be noted that this all depends on the amplifier specifications, the ground and also the signal scenario. An idea to find the best diagonal loading level is to use feedback from the receiver to make adjustments at the transmitter.

Finally, future work in this research involves similar manifold calculations and performance analysis for a 256 monopole array. Manifold measurements are also planned using drones. Overall radar performance will then be compared using calculated and measured manifolds.

References

[1] Riddolls, R. J. (2010), Auroral clutter mitigation in an over-the-horizon radar using joint transmit-receive adaptive beamforming, (DRDC Ottawa 2010-265) Defence Research and Development Canada – Ottawa Research Centre.

[2] Chiu, S., Yasotharan, A., and Riddolls, R. (2017), A US-Canada over-the-horizon radar experiment: Auroral clutter mitigation via minimum variance adaptive beamforming, (DRDC-RDDC-2017-R046) Defence Research and Development Canada – Ottawa Research Centre.

[3] Henault, S. and Antar, Y. M. M. (2015), Unifying the theory of mutual coupling compensation in antenna arrays, *IEEE Antennas and Propagation Magazine*, 57(2), 104–122.

[4] Voors, A. (2018), 4NEC2 – NEC Based Antenna Modeler and Optimizer (online), http://www.qsl.net/4nec2.

[5] Burke, G. J. and Poggio, A. J., Numerical Electromagnetics Code (NEC-2) User's Manual.

[6] Dawson, B. F. and Lockwood, S. S. (2008), Revisiting medium-wave ground-system requirements, *IEEE Antennas and Propagation Magazine*, 50(4), 111–114.

[7] Brown, G. H., Lewis, R. F., and Epstein, J. (1937), Ground systems as a factor in antenna efficiency, *Proceedings of the IRE*, 25(6), 753–787.

[8] A. Christman, K. (2004), Maximum-gain radial ground systems for vertical antennas, *National Contest Journal*, Vol. March/April.

[9] (2018), FEKO – EM Simulation Software (online), https://www.feko.info.

[10] Lindell, I. V. and Alanen, E. (1984), Exact image theory for the Sommerfeld half-space problem, Part I: Vertical magnetic dipole, *IEEE Transactions on Antennas and Propagation*, 32(2), 126–133.

[11] Lindell, I. V. and Alanen, E. (1984), Exact image theory for the Sommerfeld half-space problem, Part II: Vertical electric dipole, *IEEE Transactions on Antennas and Propagation*, 32(8), 841–847.

[12] Lindell, I. V. and Alanen, E. (1984), Exact image theory for the Sommerfeld half-space problem, Part III: General formulation, *IEEE Transactions on Antennas and Propagation*, 32(10), 1027–1032.

[13] Riddolls, R. (2017), Comparison of linear and planar arrays for auroral clutter control in an over-the-horizon radar, In *Radar Conference (RadarConf), 2017 IEEE*, pp. 1153–1158, IEEE.

[14] Henault, S., Antar, Y. M. M., Rajan, S., Inkol, R., and Wang, S. (2009), Impact of a finite ground plane on the accuracy of conventional wideband direction finding systems for signals of unknown polarization, In *Electrical and Computer Engineering, 2009. CCECE'09. Canadian Conference on*, pp. 1111–1116, IEEE.

[15] Cox, H., Zeskind, R., and Owen, M. (1987), Robust adaptive beamforming, *IEEE Transactions on Acoustics, Speech, and Signal Processing*, 35(10), 1365–1376.

[16] Vorobyov, S. A., Gershman, A. B., and Luo, Z.-Q. (2003), Robust adaptive beamforming using worst-case performance optimization: A solution to the signal mismatch problem, *IEEE Transactions on Signal Processing*, 51(2), 313–324.

[17] Li, J., Stoica, P., and Wang, Z. (2003), On robust Capon beamforming and diagonal loading, *IEEE Transactions on Signal Processing*, 51(7), 1702–1715.

[18] Lorenz, R. G. and Boyd, S. P. (2005), Robust minimum variance beamforming, *IEEE Transactions on Signal Processing*, 53(5), 1684–1696.

[19] Du, L., Li, J., and Stoica, P. (2010), Fully automatic computation of diagonal loading levels for robust adaptive beamforming, *IEEE Transactions on Aerospace and Electronic Systems*, 46(1).

[20] Gu, Y. and Leshem, A. (2012), Robust adaptive beamforming based on interference covariance matrix reconstruction and steering vector estimation, *IEEE Transactions on Signal Processing*, 60(7), 3881–3885.

[21] Huang, L., Zhang, J., Xu, X., and Ye, Z. (2015), Robust adaptive beamforming with a novel interference-plus-noise covariance matrix reconstruction method, *IEEE Transactions on Signal Processing*, 63(7), 1643–1650.

[22] Fishler, E., Haimovich, A., Blum, R., Chizhik, D., Cimini, L., and Valenzuela, R. (2004), MIMO radar: An idea whose time has come, In *Radar Conference, 2004. Proceedings of the IEEE*, pp. 71–78, IEEE.

[23] Li, J. and Stoica, P. (2007), MIMO radar with colocated antennas, *IEEE Signal Processing Magazine*, 24(5), 106–114.

[24] Daum, F. and Huang, J. (2008), MIMO radar: Snake oil or good idea?, In *Signals, Systems and Computers, 2008 42nd Asilomar Conference on*, pp. 183–187, IEEE.

[25] Frazer, G., Abramovich, Y., and Johnson, B. A. (2009), Multiple-input multiple-output over-the-horizon radar: experimental results, *IET radar, sonar & navigation*, 3(4), 290–303.

[26] Hassanien, A. and Vorobyov, S. A. (2010), Phased-MIMO radar: A tradeoff between phased-array and MIMO radars, *IEEE Transactions on Signal Processing*, 58(6), 3137–3151.

[27] Abramovich, Y. I., Frazer, G. J., and Johnson, B. A. (2013), Principles of mode-selective MIMO OTHR, *IEEE Transactions on Aerospace and Electronic Systems*, 49(3), 1839–1868.

[28] Brookner, E. (2014), MIMO radar demystified and where it makes sense to use, In *Radar Conference (Radar), 2014 International*, pp. 1–6, IEEE.

[29] Reddy, V., Paulraj, A., and Kailath, T. (1987), Performance analysis of the optimum beamformer in the presence of correlated sources and its behavior under spatial smoothing, *IEEE Transactions on Signal Processing*, 35(7), 927–936.

This page intentionally left blank.

Annex A NEC2 input files for 8×8 planar array on infinite PEC ground

A.1 NEC2 input file in transmit-mode when monopole 1 is excited by a voltage source

```
CE
GW 1 5 -28 28 0 -28 28 9 0.0381
GW 2 5 -20 28 0 -20 28 9 0.0381
GW 3 5 -12 28 0 -12 28 9 0.0381
GW 4 5 -4 28 0 -4 28 9 0.0381
GW 5 5 4 28 0 4 28 9 0.0381
GW 6 5 12 28 0 12 28 9 0.0381
GW 7 5 20 28 0 20 28 9 0.0381
GW 8 5 28 28 0 28 28 9 0.0381
GW 9 5 -28 20 0 -28 20 9 0.0381
GW 10 5 -20 20 0 -20 20 9 0.0381
GW 11 5 -12 20 0 -12 20 9 0.0381
GW 12 5 -4 20 0 -4 20 9 0.0381
GW 13 5 4 20 0 4 20 9 0.0381
GW 14 5 12 20 0 12 20 9 0.0381
GW 15 5 20 20 0 20 20 9 0.0381
GW 16 5 28 20 0 28 20 9 0.0381
GW 17 5 -28 12 0 -28 12 9 0.0381
GW 18 5 -20 12 0 -20 12 9 0.0381
GW 19 5 -12 12 0 -12 12 9 0.0381
GW 20 5 -4 12 0 -4 12 9 0.0381
GW 21 5 4 12 0 4 12 9 0.0381
GW 22 5 12 12 0 12 12 9 0.0381
GW 23 5 20 12 0 20 12 9 0.0381
GW 24 5 28 12 0 28 12 9 0.0381
GW 25 5 -28 4 0 -28 4 9 0.0381
GW 26 5 -20 4 0 -20 4 9 0.0381
GW 27 5 -12 4 0 -12 4 9 0.0381
GW 28 5 -4 4 0 -4 4 9 0.0381
GW 29 5 4 4 0 4 4 9 0.0381
GW 30 5 12 4 0 12 4 9 0.0381
GW 31 5 20 4 0 20 4 9 0.0381
GW 32 5 28 4 0 28 4 9 0.0381
GW 33 5 -28 -4 0 -28 -4 9 0.0381
GW 34 5 -20 -4 0 -20 -4 9 0.0381
GW 35 5 -12 -4 0 -12 -4 9 0.0381
GW 36 5 -4 -4 0 -4 -4 9 0.0381
GW 37 5 4 -4 0 4 -4 9 0.0381
GW 38 5 12 -4 0 12 -4 9 0.0381
GW 39 5 20 -4 0 20 -4 9 0.0381
GW 40 5 28 -4 0 28 -4 9 0.0381
GW 41 5 -28 -12 0 -28 -12 9 0.0381
GW 42 5 -20 -12 0 -20 -12 9 0.0381
GW 43 5 -12 -12 0 -12 -12 9 0.0381
GW 44 5 -4 -12 0 -4 -12 9 0.0381
GW 45 5 4 -12 0 4 -12 9 0.0381
```

```
GW 46 5 12 -12 0 12 -12 9 0.0381
GW 47 5 20 -12 0 20 -12 9 0.0381
GW 48 5 28 -12 0 28 -12 9 0.0381
GW 49 5 -28 -20 0 -28 -20 9 0.0381
GW 50 5 -20 -20 0 -20 -20 9 0.0381
GW 51 5 -12 -20 0 -12 -20 9 0.0381
GW 52 5 -4 -20 0 -4 -20 9 0.0381
GW 53 5 4 -20 0 4 -20 9 0.0381
GW 54 5 12 -20 0 12 -20 9 0.0381
GW 55 5 20 -20 0 20 -20 9 0.0381
GW 56 5 28 -20 0 28 -20 9 0.0381
GW 57 5 -28 -28 0 -28 -28 9 0.0381
GW 58 5 -20 -28 0 -20 -28 9 0.0381
GW 59 5 -12 -28 0 -12 -28 9 0.0381
GW 60 5 -4 -28 0 -4 -28 9 0.0381
GW 61 5 4 -28 0 4 -28 9 0.0381
GW 62 5 12 -28 0 12 -28 9 0.0381
GW 63 5 20 -28 0 20 -28 9 0.0381
GW 64 5 28 -28 0 28 -28 9 0.0381
GE 1
EK
EX 0 1 1 0 1 0
GN 1
FR 0 16 0 0 3 1
XQ
EN
```

A.2 NEC2 input file in receive-mode for signal arriving from (θ,ϕ)=(60°,60°)

```
CE
GW 1 5 -28 28 0 -28 28 9 0.0381
GW 2 5 -20 28 0 -20 28 9 0.0381
GW 3 5 -12 28 0 -12 28 9 0.0381
GW 4 5 -4 28 0 -4 28 9 0.0381
GW 5 5 4 28 0 4 28 9 0.0381
GW 6 5 12 28 0 12 28 9 0.0381
GW 7 5 20 28 0 20 28 9 0.0381
GW 8 5 28 28 0 28 28 9 0.0381
GW 9 5 -28 20 0 -28 20 9 0.0381
GW 10 5 -20 20 0 -20 20 9 0.0381
GW 11 5 -12 20 0 -12 20 9 0.0381
GW 12 5 -4 20 0 -4 20 9 0.0381
GW 13 5 4 20 0 4 20 9 0.0381
GW 14 5 12 20 0 12 20 9 0.0381
GW 15 5 20 20 0 20 20 9 0.0381
GW 16 5 28 20 0 28 20 9 0.0381
GW 17 5 -28 12 0 -28 12 9 0.0381
GW 18 5 -20 12 0 -20 12 9 0.0381
GW 19 5 -12 12 0 -12 12 9 0.0381
GW 20 5 -4 12 0 -4 12 9 0.0381
GW 21 5 4 12 0 4 12 9 0.0381
```

```
GW 22 5 12 12 0 12 12 9 0.0381
GW 23 5 20 12 0 20 12 9 0.0381
GW 24 5 28 12 0 28 12 9 0.0381
GW 25 5 -28 4 0 -28 4 9 0.0381
GW 26 5 -20 4 0 -20 4 9 0.0381
GW 27 5 -12 4 0 -12 4 9 0.0381
GW 28 5 -4 4 0 -4 4 9 0.0381
GW 29 5 4 4 0 4 4 9 0.0381
GW 30 5 12 4 0 12 4 9 0.0381
GW 31 5 20 4 0 20 4 9 0.0381
GW 32 5 28 4 0 28 4 9 0.0381
GW 33 5 -28 -4 0 -28 -4 9 0.0381
GW 34 5 -20 -4 0 -20 -4 9 0.0381
GW 35 5 -12 -4 0 -12 -4 9 0.0381
GW 36 5 -4 -4 0 -4 -4 9 0.0381
GW 37 5 4 -4 0 4 -4 9 0.0381
GW 38 5 12 -4 0 12 -4 9 0.0381
GW 39 5 20 -4 0 20 -4 9 0.0381
GW 40 5 28 -4 0 28 -4 9 0.0381
GW 41 5 -28 -12 0 -28 -12 9 0.0381
GW 42 5 -20 -12 0 -20 -12 9 0.0381
GW 43 5 -12 -12 0 -12 -12 9 0.0381
GW 44 5 -4 -12 0 -4 -12 9 0.0381
GW 45 5 4 -12 0 4 -12 9 0.0381
GW 46 5 12 -12 0 12 -12 9 0.0381
GW 47 5 20 -12 0 20 -12 9 0.0381
GW 48 5 28 -12 0 28 -12 9 0.0381
GW 49 5 -28 -20 0 -28 -20 9 0.0381
GW 50 5 -20 -20 0 -20 -20 9 0.0381
GW 51 5 -12 -20 0 -12 -20 9 0.0381
GW 52 5 -4 -20 0 -4 -20 9 0.0381
GW 53 5 4 -20 0 4 -20 9 0.0381
GW 54 5 12 -20 0 12 -20 9 0.0381
GW 55 5 20 -20 0 20 -20 9 0.0381
GW 56 5 28 -20 0 28 -20 9 0.0381
GW 57 5 -28 -28 0 -28 -28 9 0.0381
GW 58 5 -20 -28 0 -20 -28 9 0.0381
GW 59 5 -12 -28 0 -12 -28 9 0.0381
GW 60 5 -4 -28 0 -4 -28 9 0.0381
GW 61 5 4 -28 0 4 -28 9 0.0381
GW 62 5 12 -28 0 12 -28 9 0.0381
GW 63 5 20 -28 0 20 -28 9 0.0381
GW 64 5 28 -28 0 28 -28 9 0.0381
GE 1
EK
LD 1 1 1 1 200 0
LD 1 2 1 1 200 0
LD 1 3 1 1 200 0
LD 1 4 1 1 200 0
LD 1 5 1 1 200 0
LD 1 6 1 1 200 0
LD 1 7 1 1 200 0
LD 1 8 1 1 200 0
LD 1 9 1 1 200 0
```

```
LD 1 10 1 1 200 0
LD 1 11 1 1 200 0
LD 1 12 1 1 200 0
LD 1 13 1 1 200 0
LD 1 14 1 1 200 0
LD 1 15 1 1 200 0
LD 1 16 1 1 200 0
LD 1 17 1 1 200 0
LD 1 18 1 1 200 0
LD 1 19 1 1 200 0
LD 1 20 1 1 200 0
LD 1 21 1 1 200 0
LD 1 22 1 1 200 0
LD 1 23 1 1 200 0
LD 1 24 1 1 200 0
LD 1 25 1 1 200 0
LD 1 26 1 1 200 0
LD 1 27 1 1 200 0
LD 1 28 1 1 200 0
LD 1 29 1 1 200 0
LD 1 30 1 1 200 0
LD 1 31 1 1 200 0
LD 1 32 1 1 200 0
LD 1 33 1 1 200 0
LD 1 34 1 1 200 0
LD 1 35 1 1 200 0
LD 1 36 1 1 200 0
LD 1 37 1 1 200 0
LD 1 38 1 1 200 0
LD 1 39 1 1 200 0
LD 1 40 1 1 200 0
LD 1 41 1 1 200 0
LD 1 42 1 1 200 0
LD 1 43 1 1 200 0
LD 1 44 1 1 200 0
LD 1 45 1 1 200 0
LD 1 46 1 1 200 0
LD 1 47 1 1 200 0
LD 1 48 1 1 200 0
LD 1 49 1 1 200 0
LD 1 50 1 1 200 0
LD 1 51 1 1 200 0
LD 1 52 1 1 200 0
LD 1 53 1 1 200 0
LD 1 54 1 1 200 0
LD 1 55 1 1 200 0
LD 1 56 1 1 200 0
LD 1 57 1 1 200 0
LD 1 58 1 1 200 0
LD 1 59 1 1 200 0
LD 1 60 1 1 200 0
LD 1 61 1 1 200 0
LD 1 62 1 1 200 0
LD 1 63 1 1 200 0
```

```
LD 1 64 1 1 200 0
EX 1 1 1 0 60 60 0 5 5 0
GN 1
FR 0 16 0 0 3 1
XQ
EN
```

A.3 NEC2 input file in beamforming example for desired radiation towards (θ,ϕ)=(45°,60°) and 15 nulls equally spaced by 10° over 60$^\circ \leq \theta \leq$80° and $-$20$^\circ \leq \phi \leq$20°

```
CE
GW 1 5 -28 28 0 -28 28 9 0.0381
GW 2 5 -20 28 0 -20 28 9 0.0381
GW 3 5 -12 28 0 -12 28 9 0.0381
GW 4 5 -4 28 0 -4 28 9 0.0381
GW 5 5 4 28 0 4 28 9 0.0381
GW 6 5 12 28 0 12 28 9 0.0381
GW 7 5 20 28 0 20 28 9 0.0381
GW 8 5 28 28 0 28 28 9 0.0381
GW 9 5 -28 20 0 -28 20 9 0.0381
GW 10 5 -20 20 0 -20 20 9 0.0381
GW 11 5 -12 20 0 -12 20 9 0.0381
GW 12 5 -4 20 0 -4 20 9 0.0381
GW 13 5 4 20 0 4 20 9 0.0381
GW 14 5 12 20 0 12 20 9 0.0381
GW 15 5 20 20 0 20 20 9 0.0381
GW 16 5 28 20 0 28 20 9 0.0381
GW 17 5 -28 12 0 -28 12 9 0.0381
GW 18 5 -20 12 0 -20 12 9 0.0381
GW 19 5 -12 12 0 -12 12 9 0.0381
GW 20 5 -4 12 0 -4 12 9 0.0381
GW 21 5 4 12 0 4 12 9 0.0381
GW 22 5 12 12 0 12 12 9 0.0381
GW 23 5 20 12 0 20 12 9 0.0381
GW 24 5 28 12 0 28 12 9 0.0381
GW 25 5 -28 4 0 -28 4 9 0.0381
GW 26 5 -20 4 0 -20 4 9 0.0381
GW 27 5 -12 4 0 -12 4 9 0.0381
GW 28 5 -4 4 0 -4 4 9 0.0381
GW 29 5 4 4 0 4 4 9 0.0381
GW 30 5 12 4 0 12 4 9 0.0381
GW 31 5 20 4 0 20 4 9 0.0381
GW 32 5 28 4 0 28 4 9 0.0381
GW 33 5 -28 -4 0 -28 -4 9 0.0381
GW 34 5 -20 -4 0 -20 -4 9 0.0381
GW 35 5 -12 -4 0 -12 -4 9 0.0381
GW 36 5 -4 -4 0 -4 -4 9 0.0381
GW 37 5 4 -4 0 4 -4 9 0.0381
GW 38 5 12 -4 0 12 -4 9 0.0381
GW 39 5 20 -4 0 20 -4 9 0.0381
```

```
GW 40 5 28 -4 0 28 -4 9 0.0381
GW 41 5 -28 -12 0 -28 -12 9 0.0381
GW 42 5 -20 -12 0 -20 -12 9 0.0381
GW 43 5 -12 -12 0 -12 -12 9 0.0381
GW 44 5 -4 -12 0 -4 -12 9 0.0381
GW 45 5 4 -12 0 4 -12 9 0.0381
GW 46 5 12 -12 0 12 -12 9 0.0381
GW 47 5 20 -12 0 20 -12 9 0.0381
GW 48 5 28 -12 0 28 -12 9 0.0381
GW 49 5 -28 -20 0 -28 -20 9 0.0381
GW 50 5 -20 -20 0 -20 -20 9 0.0381
GW 51 5 -12 -20 0 -12 -20 9 0.0381
GW 52 5 -4 -20 0 -4 -20 9 0.0381
GW 53 5 4 -20 0 4 -20 9 0.0381
GW 54 5 12 -20 0 12 -20 9 0.0381
GW 55 5 20 -20 0 20 -20 9 0.0381
GW 56 5 28 -20 0 28 -20 9 0.0381
GW 57 5 -28 -28 0 -28 -28 9 0.0381
GW 58 5 -20 -28 0 -20 -28 9 0.0381
GW 59 5 -12 -28 0 -12 -28 9 0.0381
GW 60 5 -4 -28 0 -4 -28 9 0.0381
GW 61 5 4 -28 0 4 -28 9 0.0381
GW 62 5 12 -28 0 12 -28 9 0.0381
GW 63 5 20 -28 0 20 -28 9 0.0381
GW 64 5 28 -28 0 28 -28 9 0.0381
GE 1
LD 1 1 1 1 200 0
LD 1 2 1 1 200 0
LD 1 3 1 1 200 0
LD 1 4 1 1 200 0
LD 1 5 1 1 200 0
LD 1 6 1 1 200 0
LD 1 7 1 1 200 0
LD 1 8 1 1 200 0
LD 1 9 1 1 200 0
LD 1 10 1 1 200 0
LD 1 11 1 1 200 0
LD 1 12 1 1 200 0
LD 1 13 1 1 200 0
LD 1 14 1 1 200 0
LD 1 15 1 1 200 0
LD 1 16 1 1 200 0
LD 1 17 1 1 200 0
LD 1 18 1 1 200 0
LD 1 19 1 1 200 0
LD 1 20 1 1 200 0
LD 1 21 1 1 200 0
LD 1 22 1 1 200 0
LD 1 23 1 1 200 0
LD 1 24 1 1 200 0
LD 1 25 1 1 200 0
LD 1 26 1 1 200 0
LD 1 27 1 1 200 0
LD 1 28 1 1 200 0
```

```
LD 1 29 1 1 200 0
LD 1 30 1 1 200 0
LD 1 31 1 1 200 0
LD 1 32 1 1 200 0
LD 1 33 1 1 200 0
LD 1 34 1 1 200 0
LD 1 35 1 1 200 0
LD 1 36 1 1 200 0
LD 1 37 1 1 200 0
LD 1 38 1 1 200 0
LD 1 39 1 1 200 0
LD 1 40 1 1 200 0
LD 1 41 1 1 200 0
LD 1 42 1 1 200 0
LD 1 43 1 1 200 0
LD 1 44 1 1 200 0
LD 1 45 1 1 200 0
LD 1 46 1 1 200 0
LD 1 47 1 1 200 0
LD 1 48 1 1 200 0
LD 1 49 1 1 200 0
LD 1 50 1 1 200 0
LD 1 51 1 1 200 0
LD 1 52 1 1 200 0
LD 1 53 1 1 200 0
LD 1 54 1 1 200 0
LD 1 55 1 1 200 0
LD 1 56 1 1 200 0
LD 1 57 1 1 200 0
LD 1 58 1 1 200 0
LD 1 59 1 1 200 0
LD 1 60 1 1 200 0
LD 1 61 1 1 200 0
LD 1 62 1 1 200 0
LD 1 63 1 1 200 0
LD 1 64 1 1 200 0
EX 0 1 1 0 0.30343 0.11427
EX 0 2 1 0 0.32618 0.18094
EX 0 3 1 0 0.22859 -0.18839
EX 0 4 1 0 0.099497 -0.42631
EX 0 5 1 0 -0.50791 -0.14102
EX 0 6 1 0 -0.26089 0.25227
EX 0 7 1 0 0.17579 0.40615
EX 0 8 1 0 -0.22209 -0.012554
EX 0 9 1 0 -0.46206 0.12504
EX 0 10 1 0 -0.21774 0.4754
EX 0 11 1 0 0.21858 0.41434
EX 0 12 1 0 0.59883 0.02015
EX 0 13 1 0 0.24681 -0.50701
EX 0 14 1 0 -0.30882 -0.54813
EX 0 15 1 0 -0.60751 0.19269
EX 0 16 1 0 -0.11416 0.25618
EX 0 17 1 0 0.028692 -0.55795
EX 0 18 1 0 -0.33626 -0.6144
```

```
EX 0 19 1 0 -0.78383 0.18862
EX 0 20 1 0 -0.10673 0.79964
EX 0 21 1 0 0.60093 0.35427
EX 0 22 1 0 0.5309 -0.28869
EX 0 23 1 0 0.01104 -0.48603
EX 0 24 1 0 -0.12459 -0.25248
EX 0 25 1 0 0.72752 0.16065
EX 0 26 1 0 0.69289 -0.2323
EX 0 27 1 0 0.045098 -0.77674
EX 0 28 1 0 -0.75715 -0.46404
EX 0 29 1 0 -0.6312 0.54567
EX 0 30 1 0 0.14869 0.7175
EX 0 31 1 0 0.60284 0.1238
EX 0 32 1 0 0.29282 -0.10915
EX 0 33 1 0 -0.47246 0.59777
EX 0 34 1 0 -0.0060431 0.9604
EX 0 35 1 0 0.87219 0.29326
EX 0 36 1 0 0.67071 -0.65688
EX 0 37 1 0 -0.2565 -0.81427
EX 0 38 1 0 -0.81525 -0.1662
EX 0 39 1 0 -0.39064 0.50993
EX 0 40 1 0 -0.068998 0.48891
EX 0 41 1 0 -0.30663 -0.56203
EX 0 42 1 0 -0.74868 -0.53114
EX 0 43 1 0 -0.70991 0.60352
EX 0 44 1 0 0.30062 0.95374
EX 0 45 1 0 0.84542 0.073927
EX 0 46 1 0 0.40675 -0.62797
EX 0 47 1 0 -0.25587 -0.4735
EX 0 48 1 0 -0.3127 -0.17175
EX 0 49 1 0 0.48095 -0.13357
EX 0 50 1 0 0.53752 -0.48703
EX 0 51 1 0 -0.42422 -0.58242
EX 0 52 1 0 -0.69871 0.041258
EX 0 53 1 0 -0.18991 0.69184
EX 0 54 1 0 0.48838 0.31631
EX 0 55 1 0 0.3675 -0.12631
EX 0 56 1 0 0.16364 -0.33826
EX 0 57 1 0 0.26803 0.36356
EX 0 58 1 0 0.69453 0.69892
EX 0 59 1 0 0.70026 -0.47426
EX 0 60 1 0 0.012749 -0.95337
EX 0 61 1 0 -0.87765 -0.24037
EX 0 62 1 0 -0.53709 0.44298
EX 0 63 1 0 0.11217 0.6755
EX 0 64 1 0 0.086198 0.42938
GN 1
FR 0 1 0 0 18 0
RP 0 91 361 0 0 -180 1 1
EN
```

DOCUMENT CONTROL DATA

*Security markings for the title, authors, abstract and keywords must be entered when the document is sensitive

1. ORIGINATOR (Name and address of the organization preparing the document. A DRDC Centre sponsoring a contractor's report, or a tasking agency, is entered in Section 8.) DRDC – Ottawa Research Centre 3701 Carling Avenue, Ottawa ON K1A 0Z4, Canada	2a. SECURITY MARKING (Overall security marking of the document, including supplemental markings if applicable.) CAN UNCLASSIFIED 2b. CONTROLLED GOODS NON-CONTROLLED GOODS DMC A

3. TITLE (The document title and sub-title as indicated on the title page.)

Analysis of planar array of 64 monopoles for over-the-horizon radar: Manifold calculations and null-steering performance study

4. AUTHORS (Last name, followed by initials – ranks, titles, etc. not to be used. Use semi-colon as delimiter)

Henault, S.

5. DATE OF PUBLICATION (Month and year of publication of document.)	6a. NO. OF PAGES (Total pages, including Annexes, excluding DCD, covering and verso pages.)	6b. NO. OF REFS (Total cited in document.)
January 2019	96	29

7. DOCUMENT CATEGORY (e.g., Scientific Report, Contract Report, Scientific Letter)

Scientific Report

8. SPONSORING CENTRE (The name and address of the department project or laboratory sponsoring the research and development.)

DRDC – Ottawa Research Centre
3701 Carling Avenue, Ottawa ON K1A 0Z4, Canada

9a. PROJECT OR GRANT NO. (If appropriate, the applicable research and development project or grant number under which the document was written. Please specify whether project or grant.) 42zz78	9b. CONTRACT NO. (If appropriate, the applicable contract number under which the document was written.)
10a. DRDC DOCUMENT NUMBER DRDC-RDDC-2018-R233	10b. OTHER DOCUMENT NO(s). (Any other numbers which may be assigned this document either by the originator or by the sponsor.)

11a. FUTURE DISTRIBUTION WITHIN CANADA (Approval for further dissemination of the document. Security classification must also be considered.)

Public release

11b. FUTURE DISTRIBUTION OUTSIDE CANADA (Approval for further dissemination of the document. Security classification must also be considered.)

Public release

12. KEYWORDS, DESCRIPTORS or IDENTIFIERS (Use semi-colon as a delimiter.)

DRDC Scientific Report; example document

13. ABSTRACT/RÉSUMÉ (When available in the document, the French version of the abstract must be included here.)

The particular challenges of a 64 planar monopole antenna array used in an over-the-horizon radar (OTHR) and error mechanisms leading to auroral clutter suppression deterioration are evaluated. A comprehensive methodology is presented to calculate the array manifold for arbitrary azimuth, elevation and polarization. The calculated manifold is then available to calibrate the experimental array, and is used in this report to analyze null-steering performance for different ground types and signal scenarios. Clutter rejections exceeding 40 dB are found to be possible in transmission at all frequencies, and increase with frequency, but require a highly accurate manifold. The manifold and performance are found to be very sensitive to ground properties, and techniques are proposed to mitigate the impact of manifold uncertainties. Adaptive array processing is also considered with an emphasis on the presence and strength of the target signal in the training data as well as correlation between the target signal and auroral clutter. Practical considerations relative to power handling and nonlinear effects in high power amplifiers are studied.

Les défis particuliers d'un réseau d'antennes de 64 monopoles utilisé dans un radar transhorizon (OTHR) et les mécanismes d'erreur entraînant une détérioration de la suppression du fouillis auroral sont évalués. Une méthodologie complète est présentée pour calculer les diagrammes de rayonnement pour des azimuth, élevation et polarisation arbitraires. Les diagrammes calculés sont ensuite disponibles pour calibrer le réseau expérimental, et sont utilisés dans ce rapport pour analyser la performance dans la formation de nuls pour différents types de sol et scénarios de signaux. Des rejets du fouillis excédant 40 dB sont déterminés être possibles, et augmente avec la fréquence, mais nécessitent des diagrammes de rayonnement très précis. Les diagrammes et la performance sont très sensibles aux propriétes du sol, et des techniques sont proposées pour réduire les impacts de l'incertitude au sujet des diagrammes de rayonnement. Le traitement réseau adaptatif est aussi considéré avec une attention particulière à la présence et l'amplitude du signal de la cible dans les données d'entraînement, ainsi que la corrélation entre le signal de la cible et le fouillis auroral. Des considérations pratiques relatives à la gestion de la puissance et aux effets non linéaires des amplificateurs à haute puissance sont étudiées.